ISSN 2074-272X

науково-практичний журнал

2018/2

# Електротехніка і Електромеханіка

# Electrical Engineering & Electromechanics

Електротехніка. Визначні події. Славетні імена
Електричні машини та апарати
Електротехнічні комплекси та системи. Силова електроніка
Теоретична електротехніка та електрофізика
Техніка сильних електричних та магнітних полів. Кабельна техніка
Електричний транспорт
Електричні станції, мережі і системи

З 2016р. журнал індексується у міжнародній наукометричній базі Web of Science Core Collection: Emerging Sources Citation Index

# «ELECTRICAL ENGINEERING & ELECTROMECHANICS»

SCIENTIFIC & PRACTICAL JOURNAL

Journal was founded in 2002

**Founders:**

National Technical University «Kharkiv Polytechnic Institute» (Kharkiv, Ukraine)

State Institution «Institute of Technical Problems of Magnetism of the NAS of Ukraine» (Kharkiv, Ukraine)





## ISSUE 2/2018


### TABLE OF CONTENTS




**Editorial office address**: Dept. of Electrical Apparatus, NTU «KhPI», Kyrpychova Str., 2, Kharkiv, 61002, Ukraine

**phones:** +380 57 7076281, +380 67 3594696, **e-mail:** a.m.grechko@gmail.com (**Grechko O.M.)**



**ISSN (print) 2074-272X**

**ISSN (online) 2309-3404**





Printed 10 April 2018. Format 60 x 90 ⅛. Paper – offset. Laser printing. Edition 200 copies.

Printed by Printing house «Madrid Ltd» (11, Maksymilianivska Str., Kharkiv, 61024, Ukraine)

UDC 621.3: 537.8: 910.4 **doi: 10.20998/2074-272X.2018.2.01**

M.I. Baranov

# AN ANTHOLOGY OF THE DISTINGUISHED ACHIEVEMENTS IN SCIENCE AND TECHNIQUE. PART 43: TRADITIONAL POWER ENGINEERING. THERMAL POWER PLANTS: STATE AND PROSPECTS OF THEIR DEVELOPMENT

***Purpose.*** ***Preparation of brief scientific and technical review with an analytical analysis about the state, achievements, problems and prospects of development of world thermal power engineering.*** ***Methodology.*** ***Known scientific methods of collection, analysis and analytical treatment of the opened scientific and technical information, present in scientific monographs, journals and internet reports, world level in area of thermal power engineering.*** ***Results.*** ***A brief analytical scientific and technical review is resulted about the present state, achievements, problem tasks and prospects of development of thermal power engineering in the industrially developed countries of the world. Considerable progress is marked in development and creation of technical base of modern thermal power engineering including such thermal power devices (TPD) as steam generators, steam turbines and turbogenerators. Basic TPDs are described, charts of design and types of the modern thermal power plants (TPP), producing in the world about 70 % annual production electric power are presented. From positions of approach of the systems advantages and lacks of TPPs are described before other types of electric stations, generating heat and electric energy in industrial scales. Basic technical descriptions of largest TPPs of Ukraine are resulted, TPDs of powerful power units of which behave to the morally out-of-date past generation and characterized a large physical wear. Some topical problem tasks and possible ways of their decision are indicated in area of thermal power engineering of Ukraine. In a review an accent is done on the necessity of development and acceptance of strategic plan of development of thermal power engineering of Ukraine on the nearest 10 years. A regard is paid to power engineering experts acceleration of rates of introduction in domestic practice of achievements alternative and ecologically clean power engineering specialists − especially wind energy and sun energy.*** ***Originality.*** ***Systematization of the scientific and technical materials touching functioning of such important sector of world economy as thermal power engineering known from the sources opened in outer informative space is executed. It is shown that for normal development and determination of the nearest prospects for domestic thermal energy the native revision of power politics of Ukraine is needed.*** ***Practical value.*** ***Popularization and deepening for students, engineers and technical specialists and research workers of front-rank scientific and technical knowledge in area of modern thermal energy, extending their scientific range of interests and further development of scientific and technical progress in society.*** References 21, tables 2, figures 7.

*Key words:* **thermal power engineering, thermal power plants, steam generators, turbogenerators, characteristics of thermal power plants, problems and prospects of development of thermal power engineering.**

***Приведен краткий научно-аналитический обзор о современном техническом состоянии и ближайших перспективах развития мировой теплоэнергетики. Рассмотрены основные теплоэнергоустройства, схемы построения и виды тепловых электрических станций (ТЭС). Указаны преимущества и недостатки ТЭС перед другими видами электрических станций, генерирующих тепло и электричество. Приведены основные технические характеристики крупнейших ТЭС Украины. Обозначены существующие проблемные задачи и возможные пути их решения в области теплоэнергетики Украины.*** Библ. 21, табл. 2, рис. 7.

*Ключевые слова:* **теплоэнергетика, тепловые электрические станции, парогенераторы, турбогенераторы, характеристики тепловых электростанций, проблемы и перспективы развития теплоэнергетики.**

**Introduction.** The development of human civilization on planet Earth was impossible without the use of energy by people. Scientists who studied different types of energy (mechanical, thermal, chemical, electrical energy, etc.), in the 18th century, discovered one of the fundamental laws of nature - the law of conservation and transformation of power engineering [1]. In the society, that branch of the national economy, which covers energy resources, production, transformation, transmission, distribution and consumption of various forms of energy, has received the name of energy [2]. In power engineering, five main types of power plants are used: generating, converting, accumulating, transporting and consuming energy. With a fairly large variety in the nature of primary energy resources, at present the main forms of energy used in modern society are *heat* and *electricity*. As is known, these two types of energy, in turn, are used by people also in various forms [2, 3]: thermal energy in the form of water vapor, heated gases, heated water and other liquid heat carriers heated to different temperature levels, and electric energy in the form of alternating, direct and pulsed currents in wires, cables and other conducting structures at different values of electric voltage. The primary sources of thermal energy for earthlings have been and still remain minerals in the form of organic (coal, natural gas, oil, oil shale, etc.) and nuclear (uranium) fuel. The analysis of the interrelationships between energy sources, thermal energy and electricity belongs to the sphere of interests of heat power engineering [2, 3]. Therefore, it can be said that heat power engineering is a branch of the energy industry that is engaged in converting heat into such types of energy as mechanical and electrical. The subject of studying thermal power engineering are thermodynamic cycles, schemes for constructing power plants and their improvement, problems of fuel combustion and heat transfer, thermal properties of working bodies and coolants [2, 3]. The technical basis for modern heat power engineering is thermal power devices (TPDs), used primarily at thermal power plants (TPPs) [4]. The TPDs include boilers and steam turbines that are paired with turbogenerators. Generation of electricity at TPPs is carried out in synchronous turbogenerators. Since TPPs

are one of the main types of power plants in the world, which generate at least half of the total energy consumed by mankind, an analysis of the current state and prospects for the development of TPPs in the developed countries of the world is an urgent task.

**The goal** of the paper is the preparation of a brief scientific and technical review of the extensive material available in information sources for the state and prospects of development in the world of thermal power plants.

**1. General information about thermal power plants, their composition and construction schemes.** TPP is the power plant that generates electricity by converting the chemical energy of the organic fuel first into the thermal energy of water vapor (gas) and then into the mechanical energy of the rotation of the shaft of the steam (gas) turbine and rotor of the turbogenerator, and then converting the latter this mechanical energy into electric energy of its stator [4]. Fig. 1 is a schematic diagram of the construction of a TPP containing such basic devices as [4] boiler-steam generator, steam turbine, synchronous generator, waste steam condenser and circulating pump that provides the closed-loop supply of condensed steam of cooled water back to the boiler-steam generator. The synchronous generator according to Fig. 1 operates only in conjunction with a steam turbine. TPP uses the chemical energy released by burning fuel in the boiler (coal, natural gas, fuel oil, etc.), to convert water into superheated steam (with a temperature of about 540 °C) of high pressure (about 240 atm) [4]. This steam rotates the steam turbine blades and simultaneously the magnetic system located on the rotor shaft of the synchronous generator. The rotating magnetic field of the rotor of this generator due to the phenomenon of electromagnetic induction causes the appearance of electromotive force in the windings of its stator [4, 5].

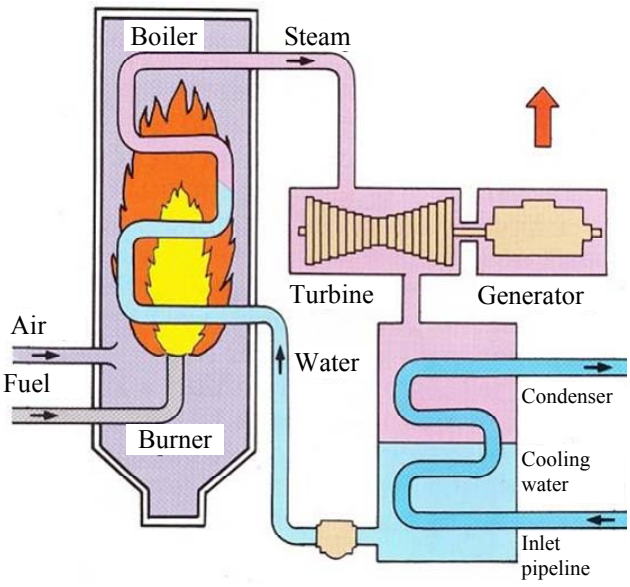


Fig. 1. Schematic diagram of the construction of TPP [4]

Modern TPPs with electrical power of up to several thousand Megawatts convert to electricity up to 50 % of the heat released during the combustion of fuel in their boilers-steam generators [4]. It can be seen that at TPP about 50 % of the generated heat energy is discharged through the boiler and condenser (cooling tower) into the environment. When using waste heat of TPPs for heating residential houses and industrial premises, the energy efficiency can be brought to 80 % [4, 5].

TPPs are subdivided into condensing power plants (CPPs) and heating electric centrals (HECs). CPP produces only electricity [5], and HEC - only heat for heating houses and buildings of enterprises [4]. Earlier in the domestic terminology, CPP was traditionally called as state district power plants (SDPP). Depending on the duration of the TPP operation during the year to cover the graphs of power loads, characterized by the number of hours of use of the installed power $T$, the power stations are classified into basic ($T$>6000 h/year), semi-peak ($T$≈3500 h/year) and peak ($T$<2000 h/year) [4]. The base stations are those that carry the maximum possible constant load during most of the year. In the world power industry, nuclear power plants (NPPs) and CPPs are used as the basic ones. At the same time, peak loads are covered by hydroelectric power plants (HPP), pumped storage plants (PSP) and gas turbine units with high maneuverability and mobility. Peak power plants are switched on at that time of the day when it is required to cover the peak (increased) part of the daily electric load schedule. At present, a gas turbine scheme has become widespread in a number of TPPs, in which the compression mixture of hot gases obtained by burning a gaseous or liquid fuel rotates the impeller of a turbine of a gas turbine plant whose steel axis is connected to the rotor shaft of the generator [4-6]. Such TPPs are called gas turbine power plants (GTPPs) [6]. At the GTPP, after the gas turbine, the exhaust gases remain sufficiently hot. For the useful use of the thermal energy of these gases, they are directed to the recovery boiler (Fig. 2) with further use in combined-cycle plants (engines) and heat supply schemes [7]. The electric power of the GTPP can be from tens of Kilowatts to hundreds of Megawatts [6]. A significant contribution to the creation and practical use of domestic gas turbines was made by the first Head of Department of Turbine Construction of the Kharkiv Polytechnic Institute (KhPI) Professor V.M. Makovsky (1870-1941).

Fig. 2. General view of heat recovery boiler of the GTPP [7]

**1.1. Water tube boilers-steam generators.** In the water-tube boiler of TPP, heat exchange of hot products of fuel burnt in its furnace with boiling steel pipes filled with water takes place [7]. There are direct-flow and

drum-type water tube boilers. Fig. 3 shows the construction of a straight-flow water tube boiler, which is the main component of any steam generator [8]. A straight-flow water tube boiler is, as a rule, a pipe coil with water, placed in a furnace where the fuel burns. Heated water, passing through the evaporative tubes of this coil, gradually turns into steam. After the evaporative tubes, the steam-water mixture enters the boiler superheater. Further, the superheated steam along the steam line is directed to the impellers of the steam turbine.

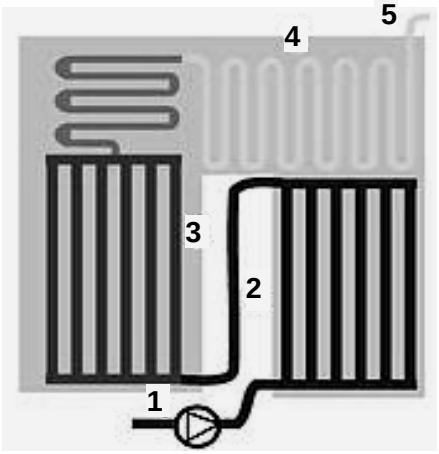


Fig. 3. The scheme of constructing a straight-flow water tube boiler used in the steam generator of TPP
(1 - a feed water pump, 2 - an economizer, 3 - evaporation tubes, 4 - a superheater, 5 - a turbine steam line) [8]

**1.2. Steam turbines.** At TPPs, a steam turbine, in fact, is the thermal engine in which the energy of superheated steam is transformed into mechanical (kinetic) energy of the circular rotation of its impellers with blades and, accordingly, of the axial steel shaft (Fig. 4). For better energy efficiency, this water vapor at the TPP should be dry and not contain microdroplets of water. Curvilinear high-strength turbine blades fixed around the circumference of its rotor are involved in a circular rotation at speed of about 3000 rpm (for bipolar generators) or 1500 rpm (for four-pole generators) by directing nozzles on them with steam from the steam generator [9].

Steam turbines, depending on the direction in which they drive a powerful vapor stream, are distinguished by axial flow (the steam flow in them moves along the longitudinal axis of the turbine, and its working blades are perpendicular to the latter one) and radial (the direction of steam flow in them is perpendicular to the longitudinal axis of the turbine, and its working blades are parallel to the latter one) [10]. Powerful steam turbines can contain high, medium and low pressure steam stages. In this case, the turbine is called a multi-body. This type of steam turbine is mainly used in powerful steam turbine installations. Depending on the purpose, steam turbines, similar to the above classification of TPPs, are divided into basic ones (carry a constant main electric load of consumption), peak (operate during short time to cover the peaks of the electric load of consumption) and auxiliary ones (provide the internal demand of TPPs for electricity).

Fig. 4. General view of the rotor and casing of a modern powerful steam turbine manufactured by Siemens (Germany) in the process of its installation on the TPP site [9]

Depending on the nature of the ongoing thermal process, steam turbines can be divided into three large groups [9]: condensing (without controlled steam extraction with the maximum conversion of its heat into mechanical work and the further release (exhaust) of the exhaust steam into the condenser as shown in Fig. 1); heating (with adjustable steam extraction); special purpose (operating on the waste heat of metallurgical and chemical enterprises). Steam turbines for TPPs have a park life estimated at about 270,000 hours with an overhaul period of 4-5 years [9, 10]. Steam turbines and generators are matched on a power scale. Each steam turbine corresponds to a certain type of electric generator. For block thermal condensation power plants, the turbine power corresponds to the power of the units, and the number of units is determined by the specified power of the TPP. On modern TPP units, ПТ type condensing turbines of power of 160, 200, 220, 300, 500, 800, 1000 and 1200 MW with intermediate steam superheating are used. An important contribution to the development, creation and enhancement of energy efficiency of domestic high-power steam turbines for TPPs and nuclear power plants produced by the Kharkiv-based enterprise Turboatom during the industrial boom of the country was made by the Head of Department of Turbine Construction of the KhPI (1941-1976) Professor Ya.I. Schnee (1902-1977).

**1.3. Turbogenerators.** These power units for TPPs are synchronous generators, working in conjunction with steam (gas) turbines. The main function of the turbogenerator (Fig. 5) is to convert the mechanical

energy of rotation of the steam (gas) turbine into electrical energy. For this purpose, the rotor shaft of synchronous generator in the working zone must create a rotating magnetic field in the air gap between the rotor and the stator of the electric generator. The initial magnetic field of the stationary rotor of the generator is either due to permanent magnets mounted on it (the rotor) or due to the flow of direct current in the copper turns of the excitation winding of the said rotor [11]. The electric potential arising in the three-phase windings of the stator of the generator under consideration and the voltage induced in them will be the greater, the stronger the magnetic field of its rotor, determined by the DC current flowing in its windings. Note that in synchronous turbogenerators with external excitation, the voltage and current in the rotor windings are usually created by a self-excitation thyristor system or a special excitatory generator placed on the shaft of a turbogenerator [10, 11]. The massive steel rotor of the turbogenerator is mounted on two sliding bearings.

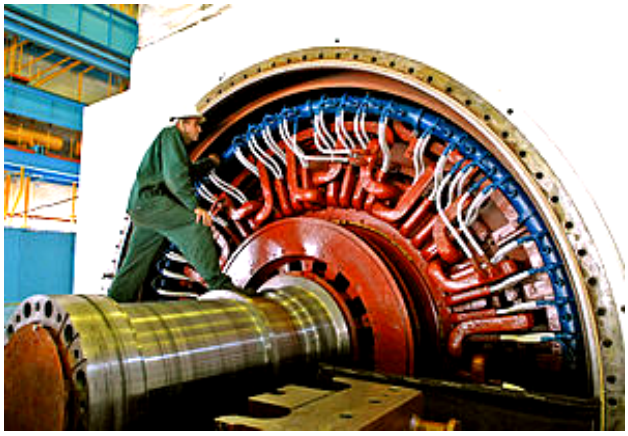

Fig. 5. General view of the fragment of a powerful synchronous turbogenerator of the Balakovo nuclear power plant (RF) after it has been stopped in the course of routine maintenance and repair (in the foreground the steel rotor shaft is seen, and in the background - the elements of its stator) [11]

For the needs of TPPs, the domestic industry produces 2-pole (with speed of rotation $v_{p2}$ 3000 rpm) and 4-pole (with speed of rotation $v_{p4}$ 1500 rpm) synchronous electric generators. Multi-pole turbogenerators can also be manufactured depending on the conditions of their operation. Depending on the cooling methods, the windings of the turbogenerator are distinguished [10]: generators with liquid cooling through the «jacket» of the stator of the turbogenerator; generators with direct liquid cooling of their windings; generators with air cooling of their windings; generators with hydrogen cooling of windings, often used at nuclear power plants. In the course of many years of operation of the TPP it was found that the more power of the turbogenerator, the more economical it is [9, 10]. This leads to a reduction in the cost of 1 kW of installed capacity of TPP. In this connection, turbine generators of high power are installed at the CPP. The rotor speed of the turbogenerator is proportional to the frequency of the current generated by it ($v_{p2} \approx 50$ rpm $\times$ 60 s $\approx$ 3000 rpm), numerically equal to (50±0.1) Hz in accordance with GOST 13109-97. A sharp drop in the electric frequency of the voltage (current) produced by the turbogenerator leads to an emergency stop of the power unit of the TPP and its shutdown from the industrial network [11].

We point out that currently about 86 % of the world's electricity production is produced by turbogenerators driven by steam turbines [10, 11]. These data testify to the important role of the heat and electric power equipment in question when generating electricity in various countries on an industrial scale. Electric power generators of various power at modern TPPs are used [4, 11]: turbogenerators of T series (air-cooled) with power of 2.5, 4, 6, 12 and 20 MW; turbogenerators of ТВФ series (with hydrogen cooling) with power of 63, 110 and 120 MW; turbogenerators of TBB series (with hydrogen-water cooling) with power of 160, 200, 220, 300, 500, 800, 1000 and 1200 MW. We point out that in a TBB series of turbogenerators with efficiency of up to 98.8 %, the stator voltage is up to 24 kV, the stator current is up to 27 kA, and the excitation current is up to 7 kA [11].

**1.4. Advantages and disadvantages of TPPs.** The main advantages of TPP in comparison with other types of power plants are the following [12]:

- organic fuel used at TPP is a relatively cheap raw material;
- for their creation and commissioning TPPs require less capital investment in comparison with such types of power plants as NPPs and HPPs;
- TPPs can be built much faster than NPPs and HPPs and virtually anywhere in the country, regardless of where the fuel source is located;
- for the construction and operation of TPP, the areas of alienation and their withdrawal from the economic turnover of the earth are much less than necessary for nuclear power plants and hydroelectric power plants (in this connection, TPPs occupy less production space and territory than NPPs and HPPs);
- the ability of TPPs to generate electricity without significant seasonal power fluctuations;
- unit cost per unit of installed capacity of TPPs is lower compared to nuclear power plants, and the cost of generating electricity is less than that of such power plants as diesel power plants.

The disadvantages of TPPs in comparison with other types of power plants include the following [12]:

- TPPs are not environmentally friendly sources of electricity and are characterized by high pollution of the environment due to smoke emissions (smoke) and the appearance of ash during their operation;
- higher operating costs compared to similar costs for nuclear power plants and hydroelectric power plants;
- characterized by relatively low efficiency (not more than 40-50 %) of the majority of existing TPPs;
- variability of TPP operation modes reduces their energy efficiency, increases fuel consumption and leads to increased wear of their power units.

**1.5. Ecological aspects of TPPs.** Expert assessments point to the fact that TPPs of the whole world are thrown into the earth's atmosphere every year [13]: about 250 million tons of ash, more than 60 million tons of sulfur dioxide, a large number of nitrogen oxides and carbon dioxide. These emissions lead to a greenhouse effect that causes global and long-term climate change on our planet. It is established that the excess radiation background around TPPs operating on coal is on average 100 times higher in the world than near nuclear power plants of the same power [13]. This is due to the fact that coal as a trace element always contains uranium, thorium and a radioactive isotope of carbon. Despite these negative features, well-developed technologies of construction, equipment and operation of TPPs, as well as a lower cost of their construction, lead to the fact that the TPPs currently account for the bulk of the world's electricity production.

**1.6. The largest thermal power plants in Ukraine.** According to the State Enterprise «National Energy Company «Ukrenergo», as of January 1, 2016, the total installed power of Ukraine's power plants was 54 826.1 MW, of which 34 266 MW (or 62.5 %) accounted for thermal power plants [14]. Electrothermal generation of Ukraine is now provided to six main companies. Five of them are private: DTEK Vostokenergo Ltd, PJSC DTEK Dneproenergo, PJSC DTEK Zapadenergo, PJSC Kyivenergo and Donbassenergo. Privatization of Centrenergo was postponed indefinitely due to a fire at the largest thermal power plant in Ukraine – Uglegorskaya TPP (Fig. 6) in March 2013. We point out that DTEK Vostokenergo Ltd, PJSC DTEK Dneproenergo, PJSC Kyivenergo and DTEK Zapadenergo are part of DTEK, which is the largest energy company of Ukraine, which is part of the financial and industrial group System Capital Management (SCM) [14]. Table 1 on the basis of [14] provides basic information about the largest TPPs in Ukraine.

Fig. 6. General view of the Uglegorskaya TPP with installed power of 3,600 MW with a nearby lake-cooler [4]

At present, the most widespread in the world are thermal power plants of the block type of building their power units. At the same time, each block of such a TPP in one operating mode specified by the operational personnel operates independently of other power plant units. Fig. 7 shows the general view of the control panel of the modern TPP, which serves a 300 MW unit [4, 15].

Table 1

Data on the largest TPPs in Ukraine [14]

| No. | TPP name | Power, MW | Fuel grade | Region |
|---|---|---|---|---|
| 1 | Uglegorskaya (before the fire) | 3600 | Coal ГСШ | Donetsk region |
| 2 | Zaporozhskaya | 2825 | Coal ГСШ | Zaporozh. region |
| 3 | Burshtynskaya | 2334 | Coal Г | I.-Frank. region |
| 4 | Krivorozhskaya | 2328 | Coal Т | Dnipro region |
| 5 | Zmievskaya | 2200 | Coal АШ, Т | Kharkiv region |
| 6 | Starobeshevskaya | 2010 | Coal АШ, Т | Donetsk region |
| 7 | Trypilskaya | 1800 | Coal АШ | Kiev region |
| 8 | Ladyzhynskaya | 1800 | Coal ГСШ | Vinnitsa region |
| 9 | Kurakhovskaya | 1527 | Coal Г | Donetsk region |
| 10 | Zuevskaya | 1270 | Coal Г | Donetsk region |
| 11 | Pridneprovskaya | 1195 | Coal АШ | Dnipro region |
| 12 | Slavianskaya | 800 | Coal АШ, Т | Donetsk region |
| 13 | Dobrotvorskaya | 510 | Coal Г | Lviv region |
| 14 | Myronovskaya | 275 | Coal Г | Donetsk. region |

Fig. 7. General view of the control panel of a modern high-power TPP [15]

**1.7. TPPs generation in the industrialized countries of the world.** A huge amount of electricity is produced and consumed all over the world. So, in 1990 its annual volume was about 11900 billion kWh, and in 2000 - 15100 billion kWh [13]. This electricity has been generated and generated by three traditional types of power plants [13]: TPP, NPP and HPP. It should be noted that in modern conditions the annual volume of electricity generation by non-traditional energy (for example, wind, hydrogen, geothermal and solar power plants) does not exceed 10 % in the world annual electricity production balance [16]. At the same time, in some countries (for example, Denmark) as of 2014, only such a type of alternative energy as wind energy provided electricity

generation up to 40 % in their total annual electricity production balance [16]. As of 2010, about 70 % of the world's annual electricity production was generated by TPPs [13]. For example, in the Russian Federation (RF) about 67 % of electricity is generated at TPPs located in places of organic fuel production (in the central and eastern regions of the country) [13]. In the western and southern regions of the RF, nuclear power plants operating on thermal neutrons are given advantages in the production of electricity. In Table 2, based on the data from [13], the main comparative quantitative indicators of electricity production in the world for 1990 and 2000 are given.

Table 2

The main indicators of electricity generation in the world of thermal power plants, nuclear power plants and hydroelectric power plants [13]

| Indicator | Year | |
|---|---|---|
| | 1990 | 2000 |
| 1. Share of total electricity production by types of power plants in the world, % | | |
| - NPP | 17 | 16 |
| - Natural gas TPP | 14 | 19 |
| - Black oil TPP | 12 | 10 |
| - Coal TPP | 38 | 37 |
| HPP and power plants on renewable energy sources | 19 | 18 |
| 2. Installed power of power plants in the world, GW | 2830 | 3580 |
| - NPP | 340 | 394 |
| - Natural gas TPP | 481 | 716 |
| - Black oil TPP | 424 | 501 |
| - Coal TPP | 934 | 1146 |
| HPP and power plants on renewable energy sources | 651 | 823 |
| 3. Electricity generation by regions of the world, % | | |
| - Western Europe | 20 | 19 |
| - Eastern Europe | 18 | 13 |
| - Americas | 36 | 34 |
| - Asia and Australia | 21 | 28 |
| - Middle East and Africa | 5 | 6 |

**2. Problems of thermal power engineering and prospects of development of thermal power plants in Ukraine.** The basis of modern TPPs and nuclear power plants, as well as HECs is a TPD. In this regard, the technical level of the development of the TPD determines the level of development of technological progress in a particular country in the world as a whole. By the mid-1960s, TPPs using coal in the furnaces of steam generators in a pulverized state had almost reached the limit of perfection in the technology of flare (coal-dust) burning of coal. This made it possible to achieve at these TPPs the conversion factor for the thermal energy of the fuel and steam into electricity at the output of their turbogenerators (efficiency factor) to 40 %. The general crisis in a number of countries (including Ukraine) has led to the fact that they have to spend more money on generating 1 kWh of electricity than in the advanced countries of the world. Thus, in the RF these indicators have increased to 1.5 times [17]. In this regard, in the RF specific consumption of conventional fuel for the generation of 1 kWh of electricity at TPPs is now required to be reduced from 360 to 280 grams [18]. In addition, the greater part of the existing TPDs at TPPs both in the Russian Federation and in Ukraine, built by the end of the 1970s, is worn out and needs to be reconstructed and replaced. Boiler units, steam turbines and turbogenerators of TPPs in Ukraine, which have a design life of 100 thousand hours of operation, have practically exhausted these indicators of their resource [19]. We should be depressed additionally by the fact that the current situation with high depreciation of productive assets concerns all other branches of our economy. For comparison, we note that in the RF approximately 90 % of all operating steam turbines at TPPs have an «age» of at least 20 years [18]. Therefore, one of the most difficult problems (*task No. 1*) for domestic heat power engineering is the decommissioning of the old power equipment from TPPs and replacing it with new and more highly efficient one. Current decisions related to the motivated reasons for the extension of the operational life of the existing TPDs at TPPs (these tasks concern the nuclear power plants, too) do not solve the problem of physical and moral deterioration of the TPD, but only postpone its decision for a certain later time. For this, it is obviously necessary to have a strategic plan for the development of Ukraine's heat and power industry for the next 10 years at least. To my great regret, for the time being, there is no such plan in the energy sector of Ukraine under consideration, in my opinion. Therefore, we are lagging behind the development of new highly efficient TPDs for TPPs. One of the examples of such TPDs is steam and gas installations of power units of TPPs and HECs with efficiency of up to 50 %, actively used in the world practice [19, 20]. Another topical problem (*task No. 2*) in our power engineering is the replacement at the TPPs of the old technology of burning fine-grained coal with a more advanced technology for burning solid fuel in circulating fluidized layer (CFL) at atmospheric pressure [19]. In Western Europe, such advanced technology at TPPs has already been successfully applied in the last 15 years. The use of this technology makes it possible to increase the economy and ecological purity of modern high-power TPPs. In the opinion of authoritative heat-and-power engineers, it is the technology based on the CFL that is the most promising in the reconstruction and construction of new power units of TPPs in Ukraine [19]. By the way, it should be noted that in Ukraine for the past 40 years, due to lack of private investment and due government funding for TPPs, no new power units

have been commissioned. During the years of Ukraine's independence, only one new boiler was built with CFL at the Starobeshevskaya TPP, and only one pulverized coal boiler was reconstructed at Zmievskaya TPP (SDPP) using modern high-efficiency technology [19]. So, one can justifiably say now that even the nearest prospects for the development of TPPs in Ukraine are tightened with «fog» of uncertainty and are covered by a «mountain» of internal problems.

The next problematic task (*task No. 3*) in the heat and power industry of Ukraine is related to the effective solution of the actual environmental aspects arising during the operation of the TPP. Modern power industry including heat and power engineering is causing tangible damage to the environment worsening the living conditions of people on our planet. All technologies for generating electricity at TPPs are associated with a large number of industrial wastes emitted into their environment. Today, the problem of the impact of power industry and especially heat and power engineering on nature becomes particularly acute, as the pollution of the environment (land, air atmosphere and hydrosphere) is increasing every year [21]. Combustion products of organic fuel, getting into the atmosphere, cause the precipitation of acid rains and intensify the greenhouse effect, which has an extremely unfavorable effect on the overall ecological situation. An urgent task for coal-fired TPPs is ash dumps requiring large areas. In addition, they are the centers of accumulation of heavy metals harmful to humans and have increased radioactivity [21]. In this connection, the issues of improving heat and power technologies at TPPs and reducing their negative impact on the environment around the world have been and should continue to be given great attention.

**Conclusions.**

1. The brief scientific and technical review of the development of the global thermal power industry shows that TPPs in the industrialized countries of the world continue to maintain their high positions in industrial power generation. Despite the fact that since the mid-1970s, in the former USSR and in several other countries of the world, the priority in the development of power engineering has been given to the construction of the nuclear power plants with its subsequent rapid «freezing» and, despite the termination since this period of time, real investments in their heat and power engineering and power machinery, TPDs developed and created in those years, having chosen their calculated resource, continue to successfully «work» (for example, in the RF and Ukraine) on many dozens of powerful units of TPPs of the old generation. The countries of Western Europe, in contrast to the above-mentioned countries of Eastern Europe, significantly more successfully modernize their TPDs, increase their energy efficiency and the generation of electricity at the powerful power units of the TPPs of new generation.

2. The normal development of domestic power engineering requires a radical revision of the country's energy policy aimed at ensuring energy saving in all sectors of the economy, training highly qualified electric power professions, supporting relevant research institutes and design bureaus, and developing and creating new heat-resistant materials and technologies for manufacturing and introduction of high-efficiency TPDs on powerful units of the TPPs of new generation TPP. With this new approach, the Ukrainian thermal power industry has a real prospect for its further progress and active participation in the country's energy market.

3. Unconventional (alternative) energy with inexhaustible and renewable energy sources, especially wind power and solar energy, in the coming decade should make up the traditional energy of Ukraine with its powerful TPPs, HECs, NPPs and HPPs, if not a worthy intra-industry competition, then at least a worthy energy supplement in the annual balance of industrial output in Ukraine of heat and electricity.

4. The problem of environmental safety of powerful TPPs in operation in Ukraine for its successful solution requires a new approach and large investments from both private capital and the country's budget. Avoiding its solution only exacerbates the situation of domestic power engineering.

REFERENCES


***1.*** Khramov Yu.A. *Istoriia fiziki* [History of Physics]. Kiev, Feniks Publ., 2006. 1176 p. (Rus).

***2.*** Available at: http://energetika.in.ua/ru/books/book-3/part-1/section-1/1-1 (accessed 22 January 2016). (Rus).

***3.*** Available at: http://elemo.ru/article/teplovye_jelektrostancii.html (accessed 20 May 2015). (Rus).

***4.*** Available at: https://en.wikipedia.org/wiki/Thermal_power_station (accessed 08 August 2016).

***5.*** Available at: https://en.wikipedia.org/wiki/Thermal_power_stations_in_Russia_and_Soviet_Union (accessed 12 June 2016).

***6.*** Available at: https://de.wikipedia.org/wiki/Gasturbinenkraftwerk (accessed 08 April 2015). (Ger).

***7.*** Available at: https://ru.wikipedia.org/wiki/Котёл-утилизатор (accessed 18 September 2013). (Rus).

***8.*** Available at: https://en.wikipedia.org/wiki/Water-tube_boiler (accessed 25 August 2015).

***9.*** Available at: https://en.wikipedia.org/wiki/Steam_turbine (accessed 02 May 2014).

***10.*** Burov V.D., Dorokhov E.V., Elizarov D.P., Lavygin V.M., Sedov V.M., Tsanev S.V. *Teplovye elektricheskie stancii. Uchebnik dlja vuzov* [Thermal electric stations. Textbook for high schools]. Moscow, MEI Publ. House, 2007. 466 p. (Rus).

***11.*** Available at: https://en.wikipedia.org/wiki/Turbo_generator (accessed 12 February 2015).

***12.*** Available at: http://elstan.ru/articles/teplovye-elektrostantsii/10045/ (accessed 28 September 2016). (Rus).

***13.*** Available at: http://www.gigavat.com/tipi_elektrostancij.php (accessed 11 October 2015). (Rus).

***14.*** Available at: https://ru.wikipedia.org/wiki/Список_тепловых_электростанций_Украины (accessed 28 May 2016). (Rus).

***15.*** Available at: http://forca.ru/knigi/arhivy/ustroystvo-i-obsluzhivanie-vtorichnyh-cepey-22.html (accessed 15 March 2016). (Rus).
***16.*** Baranov M.I. An anthology of the distinguished achievements in science and technique. Part 32: Alternative energy: state and prospects of development. *Electrical engineering & electromechanics*, 2016, no.3, pp. 3-16. (Rus). **doi: 10.20998/2074-272X.2016.3.01**.
***17.*** Andryushchenko A.I. Modern problems of thermal energy and the most important ways of their solution. *Vestnik of Saratov State Technical UIniversity*, 2003, no.1, pp. 140-143. (Rus).
***18.*** Available at: http://paes250.ru/ru/pts-problem/index.html (accessed 12 May 2017). (Rus).
***19.*** Kravchenko A.N. Global problems of Ukrainian thermal energy. *Electrician*, 2013, no.9, pp. 38-41. (Rus).
***20.*** Available at: https://en.wikipedia.org/wiki/Combined_cycle (accessed 22 September 2016).
***21.*** Available at: http://www.saveplanet.su/articles_114.html (accessed 15 March 2016). (Rus).

*Received 30.06.2017*

*M.I. Baranov, Doctor of Technical Science, Chief Researcher,*
Scientific-&-Research Planning-&-Design Institute «Molniya»
National Technical University «Kharkiv Polytechnic Institute»,
47, Shevchenko Str., Kharkiv, 61013, Ukraine,
phone +380 57 7076841,
e-mail: baranovmi@kpi.kharkov.ua

*How to cite this article:*
Baranov M.I. An anthology of the distinguished achievements in science and technique. Part 43: Traditional power engineering. Thermal power plants: state and prospects of their development. *Electrical engineering & electromechanics*, 2018, no.2, pp. 3-10. **doi: 10.20998/2074-272X.2018.2.01.**

UDC 621.313:536.2.24:539.2 **doi: 10.20998/2074-272X.2018.2.02**

V.F. Bolyukh, A.I. Kocherga, I.S. Schukin

# ELECTROMECHANICAL PROCESSES IN A LINEAR PULSE-INDUCTION ELECTROMECHANICAL CONVERTER WITH A MOVABLE INDUCTOR AND TWO ARMATURES

***Purpose.*** ***The purpose of the paper is to determine the influence of the height of the mobile and stationary disk electrically conductive armatures covering the movable inductor on the electromechanical processes of linear pulsed-induction electromechanical converter (LPIEC).*** ***Methodology.*** ***With the help of the developed mathematical model that describes electromechanical and thermal processes of LPIEC, the influence of the heights of the armatures on electromechanical processes, the values of the electrodynamic forces acting on the inductor and armature, and the moving speed of the movable armature (MA) is established.*** ***Results.*** ***It is shown that if the height of the stationary armature (SA) is twice the height of the MA, then the inductor at the initial instant of time is acted upon by electrodynamics forces pressing it to the SA, and the displacement of the inductor begins with a delay of 0.35 ms. If the height of the MA is twice the height of the SA, then the electrodynamics forces act on the inductor at the initial instant of time, repelling it from the SA, and its movement begins with a delay of 0.1 ms. If the heights of the SA and the MA are equal, then until the time 0.15 ms on the inductor, the electrodynamics forces practically do not act and the inductor moving relative to the SA begins with a delay of 0.25 ms.*** ***Originality.*** ***The effect of the geometric parameters of the SA and MA on the velocity of the inductor moving relative to the SA, MA relative to the inductor and the MA relative to the SA is established. It has been established that the highest velocity of the MA relative to the SA develops the lowest MA, and the height of the SA does not affect it practically. However, with the increase in the height of the MA, the effect of SA begins to affect. In this case, it is expedient to select the height of the SA to be 0.4-0.42 of the height of the inductor.*** ***Practical value.*** ***It is shown that as the weight of the actuating element increases, the currents in the active elements of the LPIEC increase, the induction velocities of the inductor relative to the SA and the MA decrease relative to the inductor. At the same time, the maximum the electrodynamic forces values acting on the inductor decrease, and the armatures increase. Moreover, the maximum the electrodynamic forces acting on the MA are less than similar forces acting on the SA.*** References 12, figures 7.

*Key words:* **linear pulse-induction electromechanical converter, mathematical model, mobile inductor, stationary armature, movable armature, electromechanical processes.**

***Разработана математическую модель, которая описывает электромеханические процессы в линейном импульсно-индукционном электромеханическом преобразователе с подвижным индуктором, взаимодействующим со стационарным якорем (СЯ) и подвижным якорем (ПЯ), ускоряющим исполнительный элемент. Установлено влияние высот якорей на электромеханические процессы в преобразователе. Если высота СЯ в два раза больше высоты ПЯ, то на индуктор в начальный момент времени действуют электродинамические усилия (ЭДУ), прижимающие его к СЯ и перемещение индуктора начинается с задержкой 0,35 мс. Если высота ПЯ в два раза больше высоты СЯ, то на индуктор в начальный момент времени действуют ЭДУ, отталкивающие его от СЯ, и его перемещение начинается с задержкой 0,1 мс. Если высоты СЯ и ПЯ равны, то до момента времени 0,15 мс на индуктор практически не действуют ЭДУ и перемещение индуктора начинается с задержкой 0,25 мс. Установлены комбинации геометрических параметров якорей, при которых действуют как наибольшие, так и наименьшие импульсы ЭДУ. Наибольшие скорости развивает наиболее низкий ПЯ, причем высота СЯ на них практически не влияет. С увеличением массы исполнительного элемента происходит увеличение токов в активных элементах преобразователя и уменьшение скоростей индуктора и ПЯ. При этом максимальные значения ЭДУ, действующих на индуктор, уменьшаются, а на якоря – увеличиваются.*** Библ. 12, рис. 7.

*Ключевые слова:* **линейный импульсно-индукционный электромеханический преобразователь, математическая модель, подвижный индуктор, стационарный якорь, подвижный якоря, электромеханические процессы.**

**Introduction**. Linear pulsed electromechanical converters are designed to provide high speed of the actuating element (AE) on a short active section, and/or to create shock force pulses [1-4]. Such converters are used in many branches of science and technology as electromechanical accelerators and shock-power devices [5-7]. The most widely used are linear pulse-induction electromechanical converters (LPIEC) of a coaxial configuration in which the accelerated electrically conductive armature interacts non-contact with a stationary inductor [1, 2, 8]. At excitation of a multi-turn inductor from capacitive energy storage (CES) in an electrically conductive armature made in the form of a copper disk, eddy currents are induced. As a result, the electrodynamic forces (EDF) of the repulsion act on the armature, causing its axial movement together with the AE relative to the inductor.

However, when operating in a dynamic mode with a rapid change in the electromagnetic, mechanical, and thermal parameters, the force and speed indicators of the LPIEC of traditional design are not high enough [9]. One of the ways to increase these indicators is the development of new design schemes of the LPIEC [10, 11]. Since in the traditional LPIEC design with an armature only one side of the inductor interacts inductively, a significant part of the magnetic field from the opposite side of the inductor is scattered into the surrounding space, negatively affecting closely located electronic and biological objects and is not used to create additional EDF.

Let us consider a constructive scheme of a LPIEC of a coaxial configuration, containing a movable inductor, enveloped on opposite sides by two electrically

conductive armatures (Fig. 1). One of the armatures interacts with the fixed stop, and the second one interacts with an actuating element, for example, of a shock-power device.

When the inductor is excited through flexible or sliding contacts from the CES *C*, the EDF of repulsion occur between the inductor and the armature, which leads to the movement of the movable armature (MA) relative to the inductor, which in turn repels with respect to the stationary armature (SA). This raises the question of the effect of geometric parameters of armatures on electromechanical processes in LPIEC. Since the radial dimensions of the armatures, as a rule, correspond to the radial dimensions of the inductor, the question arises as to the effect of the axial dimensions of the electrically conductive armatures on the force and speed indicators of the LPIEC.

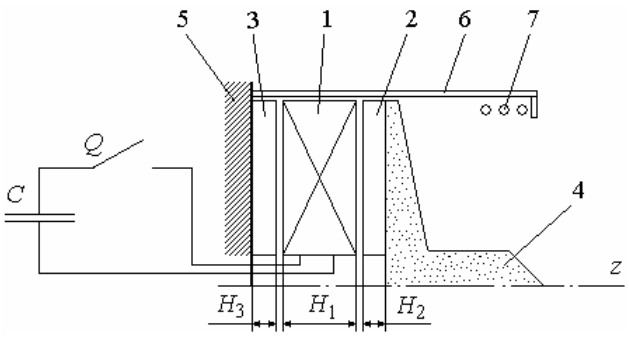


Fig. 1. Constructive scheme of the LPIEC: 1 – inductor; 2 – stationary armature; 3 – movable armature; 4 – actuating element; 5 – stop; 6 – case; 7 – damper spring

**The goal of the paper** is determination of the influence of the height of the mobile and stationary disk armatures covering the movable inductor on electromechanical processes in the LPIEC.

**Mathematical model.** Consider a mathematical model that describes electromechanical processes in LPIEC using lumped parameters of active elements – inductor, stationary and mobile armatures:

$$i_1R_1(T_1)+L_1\frac{di_1}{dt}+\frac{1}{C}\int i_1dt+M_{12}(z)\frac{di_2}{dt}+M_{13}(z)\frac{di_3}{dt}+$$

$$+v_{12}(t)i_2\frac{dM_{12}}{dz}+v_{13}(t)i_3\frac{dM_{13}}{dz}=0;\ \frac{1}{C}\int_0^t i_1dt=U_0;\ (1)$$

$$i_2R_2(T_2)+L_2\frac{di_2}{dt}+M_{12}(z)\frac{di_1}{dt}+M_{23}(z)\frac{di_3}{dt}+i_1\xi_1+i_3\xi_3=0;(2)$$

$$i_3R_3(T_3)+L_3\frac{di_3}{dt}+M_{13}(z)\frac{di_1}{dt}+M_{23}(z)\frac{di_2}{dt}+i_1\xi_2+i_2\xi_3=0;(3)$$

$$i_1i_3\frac{dM_{13}}{dz}=i_1i_2\frac{dM_{12}}{dz}+(m_1+m_2+m_e)\frac{dv_{13}}{dt}+K_Tv_{13}(t);(4)$$

$$i_1i_2\frac{dM_{12}}{dz}=i_2i_3\frac{dM_{23}}{dz}+(m_2+m_e)\frac{dv_{12}}{dt}+K_T\cdot(v_{13}(t)+v_{12}(t))+$$

$$+0.125\pi\gamma_a\beta_aD_{2m}^2[v_{12}(t)+v_{13}(t)]^2+K_P[\Delta z_{12}(t)+\Delta z_{13}(t)],(5)$$

where $\xi_1=v_{12}(t)\frac{dM_{12}}{dz}$; $\xi_2=v_{13}(t)\frac{dM_{13}}{dz}$; $p$=1, 2, 3 are the indexes of the inductor, MA and SA; $\xi_3=(v_{12}(t)+v_{13}(t))\frac{dM_{23}}{dz}$; $R_p(T_p)$, $L_p$, $i_p$ are the resistance, inductance and current of the $p$-th active element, respectively; $M_{12}(z)$, $M_{13}(z)$, $M_{23}(z)$ are the mutual inductances between corresponding $p$-th active elements; $v_{13}(t)$, $v_{12}(t)$ are the speeds of the inductor relative SA and MA along the $z$-axis, respectively; $\Delta z_{13}(t)$, $\Delta z_{12}(t)$ are the displacements of the inductor relative SA and of the MA relative inductor, respectively; $m_1$, $m_2$, $m_e$ are the masses of the inductor, MA and actuating element, respectively.

The coupled solution of equations (1) – (3) allows us to reduce them to one differential equation:

$$a_4\frac{d^4i_1}{dt^4}+a_3\frac{d^3i_1}{dt^3}+a_2\frac{d^2i_1}{dt^2}+a_1\frac{di_1}{dt}+a_0=0,\quad (6)$$

where $a_4=L_1b_1+M_{13}d_2+M_{12}d_3$;

$$a_3=R_1b_1+R_2b_2+R_3b_3+2(e_1d_1+e_2d_2+e_3d_3);$$

$$a_2=b_1/C+L_1(R_2R_3-e_1^2)+L_2(R_1R_3-e_2^2)+L_3(R_1R_2-e_3^2)+$$

$$+2[M_{12}(e_1e_2-R_3e_3)+M_{13}(e_1e_3-R_2e_2)+M_{23}(e_2e_3-R_1e_1)];$$

$$a_1=R_1(R_2R_3-e_1^2)+e_2(e_1e_3-R_2e_2)+e_3(e_1e_2-R_3e_3)+$$

$$+(R_2L_3+R_3L_2-2M_{23}e_1)/C;$$

$$a_0=(R_2R_3-e_1^2)/C;\ b_1=L_2L_3-M_{23}^2;\ b_2=L_1L_3-M_{13}^2;$$

$$b_3=L_1L_2-M_{12}^2;\ d_1=M_{12}M_{13}-L_1M_{23};$$

$$d_2=M_{12}M_{23}-L_2M_{13};\ d_3=M_{13}M_{23}-L_3M_{12};$$

$$e_1=(v_{13}+v_{12})\frac{dM_{23}}{dz};\ e_2=v_{13}\frac{dM_{13}}{dz};\ e_3=v_{12}\frac{dM_{12}}{dz}.$$

The characteristic equation of the differential equation (6)

$$a_4x^4+a_3x^3+a_2x^2+a_1x+a_0=0 \quad (7)$$

by means of a substitution $\varpi=x+0.25a_3/a_4$ is transformed into the reduced form with a cubic resolvent:

$$\varpi^3+q_1\cdot\varpi^2+q_2\cdot\varpi-q_3^2=0,\quad (8)$$

where $q_1=2\frac{a_2}{a_4}-0.75\left(\frac{a_3}{a_4}\right)^2$;

$$q_2=3\left(\frac{a_3}{2\cdot a_4}\right)^4-\frac{a_3^2\cdot a_2}{a_4^3}+\frac{a_1\cdot a_3+a_2^2}{a_4^2}-4\frac{a_0}{a_4};$$

$$q_3=\left(\frac{a_3}{2\cdot a_4}\right)^3-0.5\frac{a_2\cdot a_3}{a_4^2}+\frac{a_1}{a_4}.$$

If the discriminant of the resolvent

$$D=(u/3)^3-(v/2)^2,\quad (9)$$

where $u=q_2-q_1^2/3$; $v=2\cdot q_1^3/27-q_1\cdot q_2/3-q_3^2$, is less than zero, then, using the trigonometric solution of equation (8), we obtain:

$$\varpi_p=2\cdot\sqrt{\left(-\frac{u^3}{27}\right)^{0.5}}\cos\left(\frac{2\pi(p-1)}{3}+\frac{\arccos\left(-0.5v\sqrt{-27/a_3^3}\right)}{3}\right).(10)$$

In this case, the roots of equation (7):

$$x_l=0.5\cdot\left(\pm\sqrt{\varpi_1}\pm\sqrt{\varpi_2}\pm\sqrt{\varpi_3}\right)-0.25\cdot a_3/a_4,\quad (11)$$

where $l$ = 1, 2, 3, 4.

If all the roots of (11) are real, then for the currents in the $p$-th active elements of the LPIEC we can write:

$$i_p=\frac{U_0\iota}{a_4\vartheta},\quad (12)$$

where

$$\iota = A_{p1}\exp(x_1 t) + A_{p2}\exp(x_2 t) + A_{p3}\exp(x_3 t) + A_{p4}\exp(x_4 t)$$

$$\vartheta = \gamma_{21}\gamma_{43}(\delta_{21}+\delta_{43}) + \gamma_{24}\gamma_{31}(\delta_{24}+\delta_{31}) + \gamma_{32}\gamma_{41}(\delta_{32}+\delta_{41}),$$

$$A_{p1} = \gamma_{32}(\alpha_4 - \Theta_p\delta_{32}) + \gamma_{24}(\alpha_3 - \Theta_p\delta_{24}) + \gamma_{43}(\alpha_2 - \Theta_p\delta_{43});$$

$$A_{p2} = \gamma_{13}(\alpha_2 - \Theta_p\delta_{13}) + \gamma_{41}(\alpha_3 - \Theta_p\delta_{41}) + \gamma_{34}(\alpha_1 - \Theta_p\delta_{34});$$

$$A_{p3} = \gamma_{21}(\alpha_4 - \Theta_p\delta_{21}) + \gamma_{42}(\alpha_1 - \Theta_p\delta_{42}) + \gamma_{14}(\alpha_2 - \Theta_p\delta_{14});$$

$$A_{p4} = \gamma_{12}(\alpha_3 - \Theta_p\delta_{12}) + \gamma_{31}(\alpha_2 - \Theta_p\delta_{31}) + \gamma_{23}(\alpha_1 - \Theta_p\delta_{23});$$

$n = 2, 3;\ m = 5 - n$;

$$\gamma_{kl} = x_k - x_l;\ \alpha_k = (\Lambda_p x_k - \Xi_p)x_k^2;\ \delta_{kl} = x_k^2 x_l^2;$$

$$\Theta_1 = -b_1;\ \Theta_n = -d_m;\ \Lambda_1 = \zeta_1/a_4;\ \Lambda_n = \zeta_n/a_4;$$

$$\Xi_1 = \left[a_4 b_1^2/C - \zeta_1(R_1 b_1 + e_2 d_2 + e_3 d_3) - \zeta_2(R_2 d_3 + e_3 b_1 + e_1 d_2) - \right.$$
$$\left. - \zeta_3(R_3 d_2 + e_2 b_1 + e_1 d_3)\right] / a_4^2;$$

$$\Xi_n = \left[a_4 b_1 d_m/C - \zeta_1(R_1 d_m + e_m b_n + e_n d_1) - \zeta_n(R_n b_n + e_m d_m + e_1 d_1) - \right.$$
$$\left. - \zeta_m(R_m d_1 + e_n d_m + e_1 b_n)\right] / a_4^2;$$

$$\zeta_1 = R_1 b_1^2 + R_2 d_3^2 + R_3 d_2^2 + 2\left[b_1(e_2 d_2 + e_3 d_3) + e_1 d_2 d_3\right];$$

$$\zeta_n = d_m(R_1 b_1 + R_n b_n) + R_m d_1 d_n + e_m(b_1 b_n + d_m^2) - (e_n b_1 + e_1 d_m) \times$$
$$\times L_1 M_{nm} - L_n M_{1m}(e_n d_m + e_1 b_n) - L_m M_{1n}(e_1 d_1 + e_n d_n).$$

If the discriminant of the resolvent (9) is greater than zero, then, using Cardano solution for equation (8), we obtain one real and two complex conjugate roots:

$$\varpi_1 = \phi + \zeta - q_1/3;\quad \varpi_{2,3} = \varepsilon \pm j\chi, \qquad (13)$$

where $\phi = \sqrt[3]{-0.5\cdot v + \sqrt{D}}$; $\zeta = \sqrt[3]{-0.5\cdot v - \sqrt{D}}$;

$\varepsilon = -0.5\cdot(\phi + \zeta) - q_1/3$; $\chi = 0.5\cdot\sqrt{3}(\phi - \zeta)$.

In this case, the roots of equation (7) have the form:

$$x_{1,2} = 0.5\cdot\sqrt{\varpi_1} - 0.25\cdot a_3/a_4 \pm \sqrt{0.5\cdot\left(\varepsilon + \sqrt{\varepsilon^2 + \chi^2}\right)};$$

$$x_{3,4} = \sigma \pm j\xi, \qquad (14)$$

where $\sigma = 0.5\cdot\sqrt{\varpi_1} - 0{,}25\cdot a_3/a_4$;

$$\xi = \sqrt{0.5\cdot\left(-\varepsilon + \sqrt{\varepsilon^2 + \chi^2}\right)}.$$

If $x_1$ and $x_2$ are real and different, the currents in the $p$-th active elements can be represented as:

$$i_p = \frac{U_0\lambda}{a_4\aleph}, \qquad (15)$$

where

$$\aleph = x_1 x_2\left(3\sigma^2 - 2\sigma\chi_1 - \xi^2 + x_1 x_2\right) + \chi_2(\chi_2 + \chi_3 - 2\sigma\chi_1);$$

$$\lambda = B_{p1}\exp(x_1 t) + B_{p2}\exp(x_2 t) + \exp(\sigma\cdot t)\left[B_{p3}\cos(\xi t) + B_{p4}\sin(\xi t)\right];$$

$$B_{p1} = \left\{\Theta_p\left[x_2^2\left(3\sigma^2 - \xi^2 - 2x_2\sigma\right) - \chi_2^2\right] + \Lambda_p\left[2\sigma\chi_2 - x_2\left(3\sigma^2 - \xi^2 - x_2^2\right)\right] - \right.$$
$$\left. - \Xi_p\left[(\sigma - x_2)^2 + \xi^2\right]\right\}/(x_2 - \xi);$$

$$B_{p2} = \left\{\Theta_p\left[\chi_2^2 + \sigma^2\left(\xi^2 - 3\sigma^2 + 2x_1\sigma\right)\right] + \Lambda_p\left[x_1\left(3\sigma^2 - \xi^2\right) - 2\sigma\chi_2\right] + \right.$$
$$\left. + \Xi_p(\chi_2 - 2x_1\sigma)\right\}/(x_2 - \xi);$$

$$B_{p3} = \Theta_p\left[\left(\xi^2 - 3\sigma^2\right)\chi_1 + 2\sigma\chi_3\right] + \Lambda_p\left[\left(3\sigma^2 - \xi^2\right) - \chi_3\right] + $$
$$+ \Xi_p(\chi_1 - 2\sigma);$$

$$B_{p4} = \left\{\Theta_p\left[\chi_3\left(\xi^2 - \sigma^2\right) + \chi_1\sigma\left(\sigma^2 - 3\xi^2\right) + x_1^2 x_2^2\right] + \Lambda_p(\chi_3\sigma - \right.$$
$$\left. - x_1 x_2\chi_1 + 3\sigma\xi^2 - \sigma^3\right) + \Xi_p\left(\sigma^2 - \xi^2 + x_1 x_2 - \sigma\xi_1\right)\right\}/\xi;$$

$\chi_1 = x_1 + x_2$; $\chi_2 = \sigma^2 + \xi^2$; $\chi_3 = x_1^2 + x_1 x_2 + x_2^2$.

The displacements of the inductor relative to the SA, as well as the MA relative to the inductor on the basis of equations (4) and (5) can be represented in the form of recurrence relations:

$$\Delta z_{13}(t_{k+1}) = \left[i_1(t_k)\left(i_3(t_k)\frac{dM_{13}}{dz} - i_2(t_k)\frac{dM_{12}}{dz}\right) - K_T v_{13}(t_k)\right]\times$$
$$\times 0.5\frac{\Delta t^2}{m_1 + m_2 + m_e} + \Delta z_{13}(t_k) + v_{13}(t_k)\Delta t, \qquad (16)$$

$$\Delta z_{12}(t_{k+1}) = \Delta z_{12}(t_k) + v_{12}(t_k)\Delta t + \frac{\Delta t^2}{2(m_2 + P)}\times$$
$$\times\left[\left(i_1(t_k)\frac{dM_{12}}{dz} - i_3(t_k)\frac{dM_{23}}{dz}\right)i_2(t_k) - K_T\left(v_{12}(t_k) + v_{13}(t_k)\right) - \right.$$
$$- 0{,}125\cdot\pi\cdot\beta_a\gamma_a D_{2m}^2\left[v_{12}(t_k) + v_{13}(t_k)\right]^2 -$$
$$\left. - K_P\left(\Delta z_{12}(t_k) + \Delta z_{13}(t_k)\right)\right]. \qquad (17)$$

The temperature of the $p$-th active element at moving the armature and inductor, when there is no thermal contact between them, can be described by the recurrence relation [10]:

$$T_p(t_{k+1}) = T_p(t_k)\chi + (1-\chi)\left[T_0 + 4\pi^{-2} i_p(t_k) R_p(T_n)\alpha_{Tp}^{-1}\times\right.$$
$$\left.\times D_{ep}^{-1} H_p^{-1}\left(D_{ep}^2 - D_{ip}^2\right)^{-1}\right], \qquad (18)$$

where $\chi = \exp\left\{-0.25\Delta t D_{ep}\alpha_{Tp} c_p^{-1}(T_p)\gamma_p^{-1}\right\}$; $D_{ep}$, $D_{ip}$ are the outer and inner diameters of the $p$-th active element, respectively; $\alpha_{Tp}$ is the heat transfer coefficient of the $p$-th active element; $c_p$ is the heat capacity of the $p$-th active element.

The initial conditions of the system of equations (1) – (18): $T_p(0)=T_0$ is the temperature of the $p$-th active element; $i_p(0)=0$ is the current of the $p$-th active element; $\Delta z(0)$= 1 mm is the initial axial distance between the armatures and the inductor; $u_c(0)=U_0$ is the voltage of the CES; $v_z(0)=0$ is the armature speed along the $z$-axis.

In order to take into account the complex of interconnected electric, magnetic, thermal and mechanical processes and various nonlinear dependencies, the transient process is divided into a large number of time intervals $\Delta t = t_{k+1} - t_k$ within which all quantities are assumed to be unchanged. With such a numerical-analytical approach within a small interval $\Delta t$ the previously defined analytical expressions are used to calculate the basic quantities, and the transient process is calculated using iterative relationships using computer.

**LPIEC main parameters.** Let us consider LPIEC of a coaxial configuration, in which both armatures are made in the form of a flat disc of technical copper, one of whose sides faces the inductor.

*Inductor*: outer diameter $D_{ex1}$=100 mm, inner diameter $D_{in1}$=10 mm, height $H_1$ = 10 mm, copper bus section $a\times b$=1.8×4.8 mm$^2$, bus number of turns $N_1$= 46. The inductor is made in the form of a double-layer winding with external electrical terminals.

*Armatures:* outer diameter $D_{ex2,3}$ = 100 mm, inner diameter $D_{in2,3}$ = 10 mm, height $H_2 = H_3$ = 3 – 7 mm.

*CES:* capacitance $C$ = 500 μF, voltage $U_0$=1.5 kV. Actuating element has mass $m_e$ = 1 kg.

**LPIEC electromechanical characteristics.** We consider the influence of the height of armatures on electromechanical processes of the LPIEC. The height of the MA will be estimated by a dimensionless geometric parameter $h_2^* = H_2 H_1^{-1}$, and the height of the SA by a parameter $h_3^* = H_3 H_1^{-1}$.

Let us consider the electromechanical characteristics of the LPIEC having various combinations of the heights of the SA and the MA.

Fig. 2 shows the electromechanical characteristics of the LPIEC, in which the height of the SA is twice the height of the MA (armatures parameters $h_2^*$=0.3, $h_3^*$=0.6).

The current in the inductor with density $j_1$ has a vibrationally damped character. The maximum inductor current density is A/mm$^2$. At the initial moment of the operation process the current densities in the MA $j_2$ and in the SA $j_3$ have a polarity opposite to the inductor. The maximum current density in the MA is 554.6 A/mm$^2$, and in the SA 303 A/mm$^2$. Due to the interaction of currents, on the MA, electrodynamic forces of repulsion $f_{z2}$ act with maximum value of 13.6 kN.

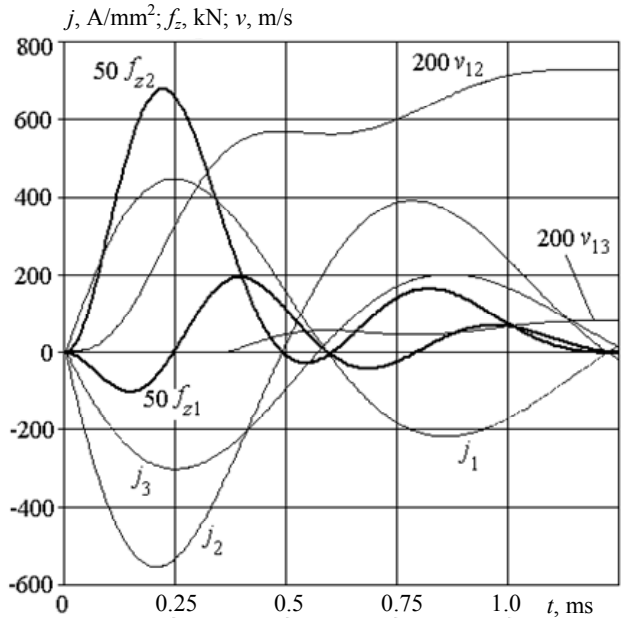


Fig. 2. Electromechanical characteristics of the LPIEC with armatures geometrical parameters $h_2^*$=0.3, $h_3^*$=0.6

In the interval 0.5-0.65 ms EDF change direction, after which a repetition of repulsive forces, but much less than in the original one, takes place. As a result, the MA moves relative to the inductor at a speed $v_{12}$ the maximum value of which is 3.65 m/s.

On the inductor at the initial instant of time, negative EDFs $f_{z1}$ act, pressing it to the SA. However, after 0.25 ms, these EDFs, changing the direction, repel the inductor from the SA with a maximum value of 3.9 kN. As a result, the inductor moves relative to the SA with a speed $v_{13}$ the maximum value of which is 0.4 m/s. And the displacement of the inductor begins with a delay of 0.35 ms. The value of the maximum speed of the MA relative to the SA is 4.05 m/s.

Fig. 3 shows the electromechanical characteristics of the LPIEC, in which the height of the MA is twice the height of the SA (armatures parameters $h_2^*$=0.6, $h_3^*$=0.3).

In this LPIEC, as in the considered above, the character of the current flow is preserved. The maximum current density in the inductor $j_1$ slightly increases to 450.1 A/mm$^2$. The maximum current density $j_2$ in the MA decreases to 294.3 A/mm$^2$, and in SA $j_3$ the current density rises to 573 A/mm$^2$. As a result, the maximum EDF of repulsion acting on $f_{z2}$ decreases to 12.7 kN. As a result, the maximum speed of moving the MA relative to the inductor $v_{12}$ decreases to 2.95 m/s.

However, in this LPIEC, positive EDF $f_{z1}$ act on the inductor at the initial instant of time, repelling it from the SA and its movement begins in about 0.1 ms. The maximum value of these forces is observed in the second peak of repulsion, reaching 2.18 kN. As a result, the inductor moves relative to the SA with a velocity $v_{13}$, the maximum value of which reaches 0.63 m/s. The maximum speed of the MA relative to the SA $v_{23}$ is 3.58 m/s. The decrease in the speed of the MA can be explained by its increased mass.

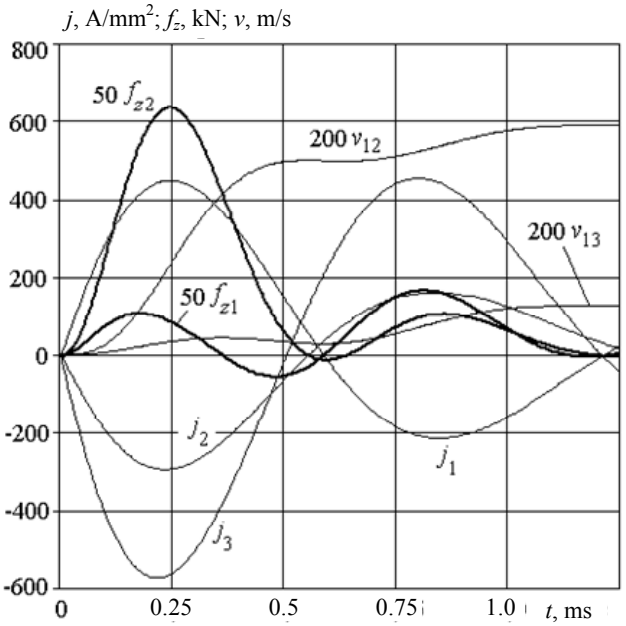


Fig. 3. Electromechanical characteristics of the LPIEC with armatures geometrical parameters $h_2^*$=0.6, $h_3^*$=0.3

Let us consider the LPIEC variant, in which the heights of the SA and the MA are equal. Fig. 4 presents the electromechanical characteristics of the LPIEC with parameters $h_2^*$=0.4, $h_3^*$=0.4.

In this LPIEC the maximum current density in the inductor $j_1$ is 442.8 A/mm$^2$. The currents in the armatures, especially in the initial part of the process, where there is no movement of the active elements, are practically the same. The maximum current density $j_2$ in the MA is 420.3 A/mm$^2$, and in the SA $j_3$ it is 434.8 A/mm$^2$. The maximum EDF of repulsion acting on $f_{z2}$ is 12.8 kN, which results in the displacement of the MA relative to the inductor at a speed of $v_{12}$, the maximum value of which is 3.28 m/s.

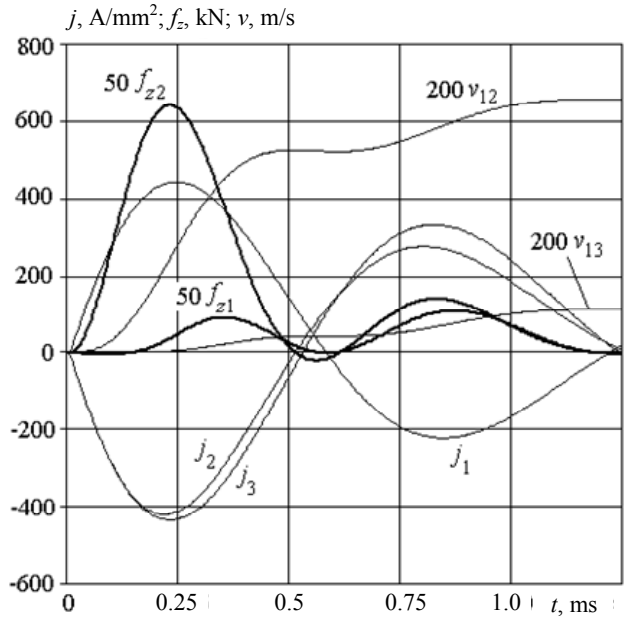


Fig. 4. Electromechanical characteristics of the LPIEC with armatures geometrical parameters $h_2^*$=0.4, $h_3^*$=0.4

In this LPIEC, the EDF $f_{z1}$ is practically not effective on the inductor until the time 0.15 ms. As a result, the displacement of the inductor relative to the SA begins almost in 0.25 ms. The maximum value of these forces is observed in the second peak of repulsion and is only 1.85 kN. As a result, the inductor moves relative to the SA with a speed $v_{13}$, the maximum value of which is 0.56 m/s. The maximum speed of the MA relative to the SA $v_{23}$ is 3.84 m/s.

**LPIEC force and speed indicators.** Let us consider influence of the geometrical parameters of the SA $h_2^* \in [0.3; 0.7]$ and the MA $h_3^* \in [0.3; 0.7]$ on the value of the EDF impulse $F_{zp} = \int f_{zp} dt$, where $p$ = 1, 2, 3 are the indexes of the inductor, MA and SA.

The values of the EDF impulses acting on the inductor $F_{z1}$ are much smaller than the values of the impulses acting on the MA $F_{z2}$ and SA $F_{z3}$. The maximum values of the EDF impulse $F_{z1}$, acting on the inductor, arise at geometrical parameters of armatures $h_3^*$=0.4 and $h_2^*$=0.7 (Fig. 5). The minimum values of $F_{z1}$ arise when $h_3^*$=0.7 and $h_2^*$=0.4. The largest value of the EDF impulse $F_{z1}$ at any height of the MA is realized for a SA with a parameter $h_3^*$=0.4.

The smallest values of the EDF impulse $F_{z2}$ acting on the MA, on the contrary, arise for $h_3^*$=0.4 (the minimum value takes place for a high MA $h_2^*$=0.7.). The greatest values of the EDF impulse $F_{z2}$ occur at $h_2^*$=0.42-0.45 (the maximum value takes place at a high SA $h_3^*$=0.7).

The largest values of the EDF impulse $F_{z3}$, acting on the SA, arise for $h_3^*$=0.4 (the maximum value occurs for $h_2^*$=0.7). And the largest values of the EDF impulse $F_{z3}$ take place when $h_2^*$=0.4 (the minimum value occurs for $h_3^*$=0.7).

Let us consider the influence of the geometric parameters of the SA $h_2^* \in [0.3; 0.7]$ and MA $h_3^* \in [0.3; 0.7]$ on the speed of the inductor and the MA, realized at the end of the operating process (Fig. 6).

The maximum value of the speed of the MA relative to the inductor $V_{12}$ is realized with its minimum height $h_2^*$=0.3 and the maximum height of the SA $h_3^*$=0.7, and the minimum value of the speed of the MA relative to the inductor $V_{12}$ is realized at its maximum height $h_2^*$=0.7 and the minimum height of the SA $h_3^*$=0.3.

In turn, the highest values of the speeds of the displacement of the inductor relative to the SA $V_{13}$ occur at a relatively low SA $h_3^*$=0.4 (the maximum speed occurs at a high MA $h_2^*$=0.7). The lowest values of the speeds $V_{13}$ are realized at $h_2^*$=0.45 (the minimum speed $V_{13}$ occurs for high SA $h_3^*$=0.7).

Of greatest interest is the speed of the displacement of the MA relative to the SA $V_{23}$. As the calculations show, the highest speeds $V_{23}$ the lowest MA $h_2^*$=0.3 develops, and the height of the SA does not affect it practically. However, with the increase in the height of the MA, the influence of the SA begins to affect. In this case, it is expedient to select the height of the SA with geometric parameters $h_3^*$= 0.4-0.42.

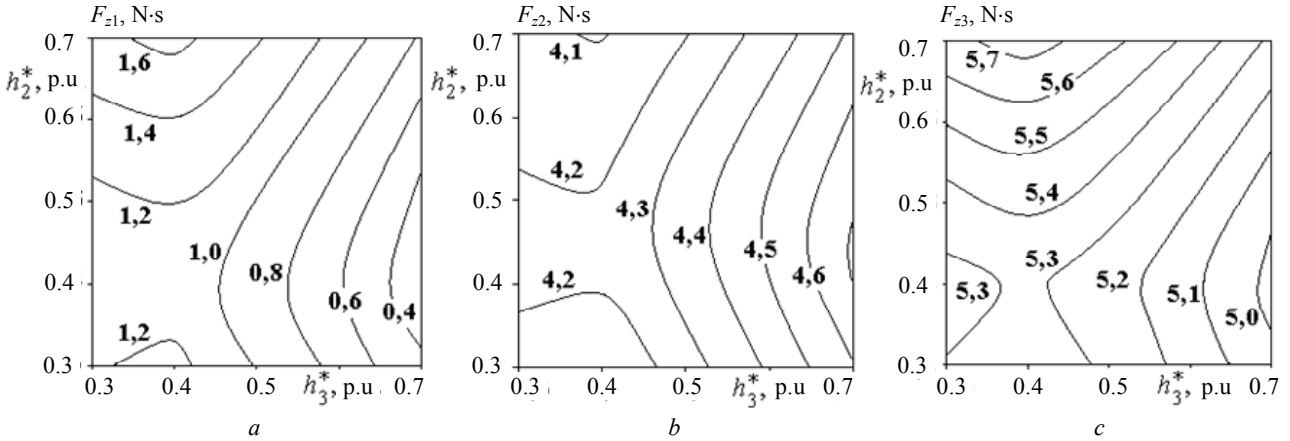


Fig. 5. Dependence of the EDF impulses acting on the inductor (*a*), MA (*b*) and SA (*c*) on the geometrical parameters $h_2^*$ and $h_3^*$

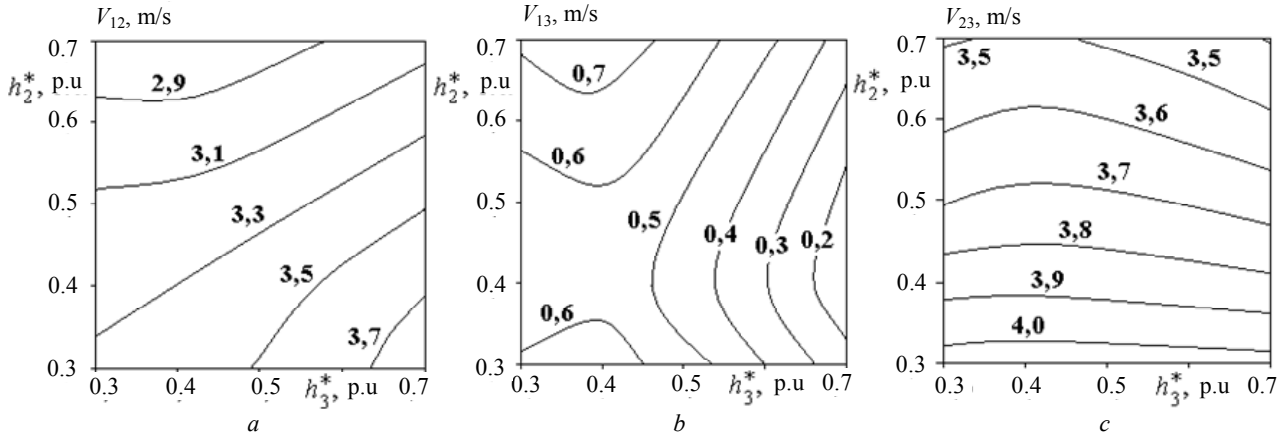


Fig. 6. Dependence of the speeds of the MA relative to the inductor (*a*), of the inductor relative to the SA (*b*) and the MA relative to the SA (*c*) on the geometrical parameters $h_2^*$ and $h_3^*$

**Effect of the mass of the actuating element on the LPIEC indicators.** In order to more fully understand the electromechanical processes in the LPIEC, let us consider the effect of the mass of the actuating element $m_e$ on its electromechanical indicators. Fig. 7 shows the dependencies of the indicators of the LPIEC having geometrical parameters of armatures $h_2^*$=0.5, $h_3^*$=0.5, on the mass of the actuating element. With an increase in the mass $m_e$, there is a significant decrease in the speed of displacement of the inductor relative to the SA $V_{13}$, which practically decreases to zero even at a mass $m_e$=3 kg. The speed of the MA relative to the inductor $V_{12}$ with an increase in the mass of the actuating element from 0 to 5 kg decreases from 9.83 m/s to 0.9 m/s.

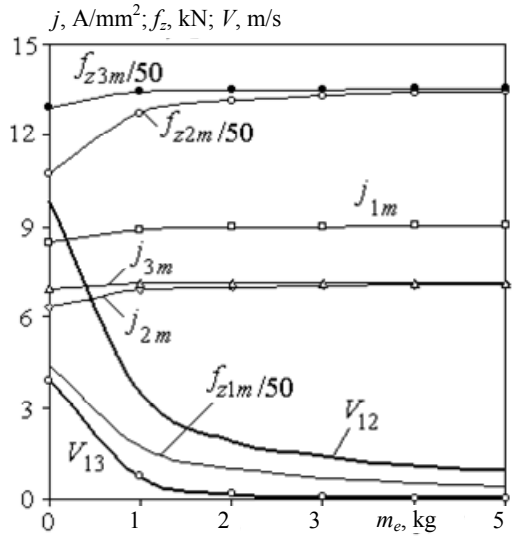


Fig. 7. Dependencies of the indicators of the LPIEC with parameters $h_2^*$=0.5, $h_3^*$=0.5 on the mass of the actuating element

Dependencies of the maximum EDF values acting on the active elements of the LPIEC, on the mass of the actuating element, have the following features. With increasing mass $m_e$, the maximum EDF values acting on the inductor $f_{z1m}$ decrease and on the armatures increase. Moreover, the maximum EDFs acting on the MA $f_{z2m}$ are smaller than the analogous forces acting on the SA $f_{z3m}$. However, as the mass of the actuating element increases, these forces tend to equalize. Obviously, with a fully retarded MA, these EDFs will be equal.

With an increase in mass $m_e$, there is an increase in currents both in the inductor and in the armatures, especially strongly in the interval 0 ... 1 kg. This can be explained by a stronger induction interaction of the inductor with armatures, which are in a strong magnetic coupling.

**Conclusions**.

1. A mathematical model is developed that describes the electromechanical processes of LPIEC with a movable inductor interacting with stationary and mobile electrically conductive armatures.

2. The effect of armatures heights on electromechanical processes of LPIEC was established. It is shown that at the initial moment of the operating process, the currents in the armatures have a polarity opposite to the inductor current.

3. It is shown that if the height of the SA is two times more than the height of the MA, then the EDF acts on the inductor at the initial instant of time, pressing it to the SA, and the displacement of the inductor begins with a delay of 0.35 ms. If the height of the MA is twice the height of the SA, then the EDFs act on the inductor at the initial instant of time, repelling it from the SA, and its movement begins with a delay of 0.1 ms. If the heights of the SA and the MA are equal, then until the time 0.15 ms the EDFs practically does not act on the inductor and the inductor moving relative to the SA begins with a delay of 0.25 ms.

4. The influence of the heights of the disk armatures on the values of the EDF impulses acting on the inductor and the armatures is established. The values of the EDF impulses acting on the inductor are much smaller than the EDF impulses acting on the armatures. Combinations of armatures heights are established, in which both the largest and the smallest impulses of the EDF act on them and on the inductor.

5. The effect of the geometric parameters of the SA and the MA on the speeds of the inductor and the MA is established. The highest speeds are developed by the lowest MA, and the height of the SA practically has no effect on them. However, with the increase in the height of the MA, the influence of the SA begins to affect. In this case, it is expedient to choose the height of the SA with a geometric parameter $h_3^*$=0.4-0.42.

6. It is shown that with an increase in the mass of the actuating element, the currents in the active elements of

the LPIEC increase and the speeds of the inductor and the MA decrease. In this case, the maximum values of the EDFs acting on the inductor reduce, and on the armatures increase. The maximum EDFs acting on the MA are less than similar forces acting on the SA.

REFERENCES


*1.* Balikci A., Zabar Z., Birenbaum L., Czarkowski D. Improved performance of linear induction launchers. *IEEE Transactions on Magnetics*, 2005, vol.41, no.1, pp. 171-175. **doi: 10.1109/tmag.2004.839283.**

*2.* D.-K. Lim, D.-K. Woo, I.-W. Kim, D.-K. Shin, J.-S. Ro, T.-K. Chung, H.-K. Jung. Characteristic Analysis and Design of a Thomson Coil Actuator Using an Analytic Method and a Numerical Method. *IEEE Transactions on Magnetics*, 2013, vol.49, no.12, pp. 5749-5755. **doi: 10.1109/tmag.2013.2272561**.

*3.* Tomashevsky D.N., Koshkin A.N. Modeling of linear impulse electric motors. *Russian Electrical Engineering*, 2006, no.1, pp. 24-27. (Rus).

*4.* Bolyukh V.F., Oleksenko S.V., Shchukin I.S. Comparative analysis of linear pulse electromechanical converters electromagnetic and induction types. *Technical Electrodynamics*, 2016, no.5, pp. 46-48. (Rus).

*5.* Young-woo Jeong, Seok-won Lee, Young-geun Kim, Hyun-wook Lee. High-speed AC circuit breaker and high-speed OCD. *22nd International Conference and Exhibition on Electricity Distribution (CIRED 2013)*, 2013, 10-13 June, Stockholm, Paper 608. **doi: 10.1049/cp.2013.0834.**

*6.* Ivanov V.V., Paranin S.N., Nozdrin A.A. Semiautomatic installation of magnetic pulse compaction of powders. *Materialovedenie*, 2011, no.7, pp. 42-45. (Rus).

*7.* Ivashin V.V., Penchev V.P. Features of the dynamics of work and energy diagrams of pulsed electromagnetic drive with parallel and series connection of excitation windings. *Electrical engineering*, 2013, no.6, pp. 42-46. (Rus).

*8.* Bolyukh V.F., Luchuk V.F., Rassokha M.A., Shchukin I.S. High-efficiency impact electromechanical converter. *Russian electrical engineering*, 2011, vol.82, no.2, pp. 104-110. **doi: 10.3103/s1068371211020027**.

*9.* Bolyukh V.F., Shchukin I.S. *Lineinye induktsionno-dinamicheskie preobrazovateli* [Linear induction-dynamic converters]. Saarbrucken, Germany, LAP Lambert Academic Publ., 2014. 496 p. (Rus).

*10.* Bissal A., Magnusson J., Engdahl G. Comparison of two ultra-fast actuator concept. *IEEE Transactions on Magnetics*, 2012, vol.48, no.11, pp. 3315-3318. **doi: 10.1109/tmag.2012.2198447.**

*11.* Schneider Electric Industries SAS. *Electric switching device with ultra-fast actuating mechanism and hybrid switch comprising one such device*. Patent USA, no.8686814, 2014.

*12.* Bolyukh V.F., Shchukin I.S. The thermal state of an electromechanical induction converter with impact action in the cyclic operation mode. *Russian electrical engineering*, 2012, vol.83, no.10, pp. 571-576. **doi: 10.3103/s1068371212100045**.



*Received 05.01.2018*



*V.F. Bolyukh*[1], *Doctor of Technical Science, Professor,*
*A.I. Kocherga*[1], *Postgraduate Student,*
*I.S. Schukin*[2], *Candidate of Technical Science, Associate Professor,*
[1] National Technical University «Kharkiv Polytechnic Institute»,
2, Kyrpychova Str., Kharkiv, 61002, Ukraine,
phone +380 57 7076427,
e-mail: vfbolyukh@gmail.com
[2] Firm Tetra, LTD,
2, Kyrpychova Str., Kharkiv, 61002, Ukraine,
phone +380 57 7076427,
e-mail: tech@tetra.kharkiv.com.ua



*How to cite this article:*
Bolyukh V.F., Kocherga A.I., Schukin I.S. Investigation of a linear pulse-induction electromechanical converter with different inductor power supply circuits. *Electrical engineering & electromechanics*, 2018, no.2, pp. 11-17. **doi: 10.20998/2074-272X.2018.2.02.**

UDC 621.313.323 **doi: 10.20998/2074-272X.2018.2.03**

V.S. Malyar, A.V. Malyar

# STUDYING THE EFFECT OF AN ADDITIONAL ACTIVE RESISTANCE IN THE FIELD WINDING CIRCUIT ON STARTING CHARACTERISTICS OF SALIENT-POLE SYNCHRONOUS MOTORS

***On the basis of the developed method for calculating steady-state asynchronous operation modes of salient-pole synchronous motors, a procedure of mathematical modelling of the starting characteristics is proposed. The problem of calculating the steady-state asynchronous mode is solved as a boundary value one for differential equations of motor circuit electrical equilibrium. Algebraization of the system of differential equations is carried out by approximating the equations of state using cubic spline functions on a grid of period nodes, taking into account the periodic law of variation of the coordinates. This results in the changeover from continual values to nodal ones. The starting static characteristics are calculated using the parameter continuation method. The study of the effect of the starting resistance value on the asynchronous characteristics of the motor relied on a mathematical model of the motor taking into consideration real field circuits, saturation and asymmetry of the magnetic path.*** References 10, figures 5.

*Key words*: **salient-pole synchronous motor, asynchronous operation mode, starting resistance, static characteristics, boundary value problem, spline approximation**.

***На основе разработанного метода расчета установившихся асинхронных режимов явнополюсных синхронных двигателей предложена методика математического моделирования пусковых характеристик. Задача расчета стационарного асинхронного режима решается как краевая для дифференциальных уравнений электрического равновесия контуров двигателя. Алгебраизация системы дифференциальных уравнений осуществляется путем аппроксимации уравнений состояния кубическими сплайн-функциями на сетке узловых точек периода с учетом периодического закона изменений координат. В результате осуществляется переход от их континуальных значений к узловым. Расчет пусковых статических характеристик осуществляется методом продолжения по параметру. Для исследования влияния величины пускового сопротивления на асинхронные характеристики двигателя использовано математическую модель двигателя, в которой учитываются реальные контуры пусковой обмотки, насыщение и несимметрия магнитопровода.*** Библ. 10, рис. 5.

*Ключевые слова:* **явнополюсный синхронный двигатель, асинхронный пуск, пусковое сопротивление, статические характеристики, краевая задача, аппроксимация сплайнами**.

**Introduction.** The use of synchronous motors (SMs) for high-power electric drives provides high technical and economic indicators, but there is a problem of their start-up [1-3]. SMs are manufactured mostly with salient poles, on which an excitation winding is located. To access the synchronous mode, it is necessary to accelerate the rotor of the motor to close to the synchronous speed of rotation, after which to supply direct current to the winding excitation, causing the rotor to enter the synchronization with the magnetic field of the stator winding.

The problem of starting synchronous motors, which operate in powerful electric drives, is one of the main [4-6]. This problem is especially relevant for those synchronous electric drives, in which the start is carried out under load. Its essence is to provide the necessary starting torque, which is conditioned by the operating conditions of the drive. In practice, there are various methods of start-up and circuits that implement them, which are characterized by disadvantages and advantages. The choice of a particular method for solving the problem of start-up requires effective in relation to the adequacy methods for obtaining functional dependencies that would enable to analyze both qualitative and quantitative aspects of the dynamics of the starting process. They are the basis for the development of starting systems [4], which ensure the technological reliability of electrical equipment and its cost-effectiveness for electricity consumption, which is important for electric drives, which operate under frequent start-ups.

As is known, the main method of starting a SM is asynchronous start, which is carried out by its direct switching on the nominal voltage, and the electromagnetic torque develops due to the position of the starter winding located at the poles of a salient rotor [2]. Generally, the excitation winding is closed at the start time on a discharge active resistance with a value that is (5-10) times more than its own resistance $r_f$, less frequently short-circuit. The purpose of this resistance is to avoid overvoltage in the excitation winding at the beginning of the asynchronous start-up. The problem of the effect of an additional starting resistance in the excitation winding on the value of electromagnetic torque was generally not considered or investigated using so simplified mathematical models that reliable results are unlikely.

The electromagnetic torque, created in the asynchronous mode by the starting winding of the SM rotor, lacking for its start-up under the load, therefore different techniques for its increase are used [5, 6]. For example, one of ways to solve the problem of increase the SM starting characteristics is serial connection of capacitors to the excitation windings which compensate its inductive resistance, but of the wrong choice of their capacities can call result in the phenomena of the voltage resonance or to decrease the starting electromagnet torque instead of its increase [7]. These disadvantages are enhanced by the way to improve the startup characteristics by using active resistance in the excitation winding [1]. However, the problem of completing an

asynchronous start-up of SM, its excitation winding is shorted to an active resistance, despite of its importance for practice, is still not solved till now.

The problem of the reasonable choice of the value of the additional resistance in the field winding can be solved by the way of mathematical modeling, but it requires utilization of the improved SM mathematical models and the development of effective numerical analysis techniques.

**The goal of the paper** is development of a mathematical model and technique of calculation of asynchronous modes of SM in order to study the influence of active resistance in the circuit of excitation winding on the starting characteristics of SM.

**A mathematical model.** We consider the SM, whose stator winding is powered by a three-phase network, and on the rotor is a starter winding with $n$ rods at each pole and an excitation winding.

As is known [2], the stable synchronous modes of SM can be analyzed on the basis of the use of equivalent circuits, but under the conditions of non-synchronous rotation of the rotor, even in steady state, the electromagnetic processes occurring in the electric circuits of the motor are dynamic. And since equivalent circuits do not allow to take into account the main factors influencing the dynamics of processes in the SM, they are not suitable for analysis of asynchronous modes of the SM.

Due to the salient pole construction of the rotor and the asymmetry of the starting winding, the distribution of the magnetic flux density in the air gap differs from the sinusoidal, and the electromagnetic torque in the asynchronous mode has a constant component and a variable one that fluctuates with a double frequency. In addition, as a result of saturation of the SM magnetic circuit, the flux linkages of the circuits, and hence electromagnetic parameters, are nonlinearly dependent on all its currents.

The practice of calculating processes in SM shows that the initial determining influence on the behavior of the motor in asynchronous mode is due to a starting winding, and therefore the accuracy of the results of the calculation depends on the adequacy of its description in the mathematical model. Other factors are the non-sinusoidal distribution of the magnetizing forces of the electrical circuits of the SM and the saturation of the magnetic system. Only taking into account these factors in their interconnection can serve as the basis for the development of appropriate calculation methods based on the use of modern numerical methods.

Asynchronous modes of the SM are described by the nonlinear system of differential equations (DE) of the electromechanical equilibrium, which can be written in real phase or in transformed coordinate systems. The choice of the coordinate system is determinative because a possibility to take into account factors influencing the dynamics of processes depends on it. In addition, for a salient-pole SM the technique of the starting winding modeling is important: as two equivalent or real physical circuits.

Most of the analysis tasks do not require the use of mathematical modeling of processes in each rod of the starting winding, so it can be equivalented with two orthogonal circuits oriented on the longitudinal ($d$) and transverse ($q$) axes [2]. Since in creating an electromagnetic torque in asynchronous mode the starting winding is decisive, in order to obtain adequate results, we consider the real circuits formed by its rods [10], between which there are nonlinear mutual inductive connections due to the saturation of the magnetic core. However, the winding of a stator, since it is symmetric and is fed by a symmetric three-phase voltage system, can be considered in the known $d$, $q$ coordinate axes. Under these conditions, the process of asynchronous start-up of the SM in the case of closing the excitation winding to the active resistance $r_a = k \cdot r_f$, where $k$ is the multiplicity of the additional resistance, is described by the nonlinear system of DE of electromagnetic equilibrium of the circuits

$$\begin{aligned}
\frac{d\psi_d}{dt} &= \omega\psi_q - ri_d + U_m \sin\theta ;\\
\frac{d\psi_q}{dt} &= -\omega\psi_d - ri_q + U_m \cos\theta ;\\
\frac{d\psi_1}{dt} &= -r_{1,1}i_1 + r_{1,2}i_2 - r_{1,n}i_n ;\\
&\dots \qquad (1)\\
\frac{d\psi_n}{dt} &= -r_{n,1}i_1 + r_{n,n-1}i_{n-1} - r_{n,n}i_n ;\\
\frac{d\psi_f}{dt} &= -\left(r_f + r_a\right) i_f ,
\end{aligned}$$

where $\psi_k$, $i_k$ ($k = d, q, 1, \dots, n, f$) are the flux linkages and currents of the corresponding circuits; $r$, $r_f$, $r_{jk}$ are the active resistances of windings: of the stator, field and damping circuits ($r_{jk}$), intrinsic – at $j=k$ and mutual – at $j \neq k$; $\theta$ is the angle of rotor runoff.

The DEsystem (1), supplemented by the equation of rotor motion, allows us to investigate the transients in asynchronous modes of operation of the SM. Obviously, the transient asynchronous startup requires a numerical integration of the DE in a time interval sufficient for the motor to output to the asynchronous mode. However, for the design of the SM and, in particular, the corresponding starting systems for electric drives [4], and the study of their starting properties, it is necessary to have an effective algorithm for calculating static characteristics, which would enable to investigate the influence of the starting winding and excitation winding parameters on the processes in the SM in the starting mode.

As is well known [2], in the asynchronous mode of the salient-pole SM, the angle $\theta$ the rotor runoff is continuously increasing by law

$$\theta = -\omega_0 \int s dt + \theta_0 ,$$

where $\theta_0$ is its initial value, $s = 1, 0 - \omega/\omega_0$, $\omega_0$, $\omega$ are the angular speed of the voltage power and angular rotor speed of the motor, expressed in electric radians.

Since with unbounded growth of the angle $\theta$ the functions $\sin\theta$ and $\cos\theta$, which determine the value of the applied voltage, are changed according to the periodic law, then the flux linkage, the circuit currents and, as a consequence, the electromagnetic torque, are periodic

functions. The sliding $s$ of the rotor within the period fluctuates relative to the mean value

$$s_0 = \frac{1}{T}\int_0^{T_a} s dt ,$$

however, for solving most tasks it can be accepted unchanged and equal to the average value.

**A technique of problem solution.** Investigation of the influence of the active resistance in the circuit of the excitation winding on the electromagnetic torque can be made on the basis of the calculation of the static characteristic, which is obtained [2] by calculating the sequence of stable asynchronous modes, which are calculated for different values of sliding. The lawfulness of such an approach is due to the fact that the mechanical time constant is far greater than electromagnetic. Since in the stable asynchronous mode with sliding $s$ processes in the SM are changed with the period

$$T_a = 2\pi/(s\omega_0),$$

then the task of its calculation is to determine the periodic dependencies of the coordinates. Their calculation by solving an evolutionary problem requires the integration of the DE system in a significant time interval, and therefore not suitable for the calculation of static characteristics. Calculate these dependencies with the minimum computations can be by solving the boundary value problem for the DE system (1) with periodic boundary conditions [9].

In order to reduce the description of the calculation algorithm for the periodic dependencies of the coordinates of the mode on the $T_a$ period, we write the DE system (1) by one vector equation

$$\frac{d\vec{\psi}}{dt} = \vec{z}\left(\vec{\psi},\vec{i},\vec{u},t\right), \qquad (2)$$

where

$$\vec{z} = \begin{array}{|c|}\hline U_m \sin\theta + \omega_0(1-s)\psi_q - ri_d \\ \hline U_m \cos\theta - \omega_0(1-s)\psi_d - ri_q \\ \hline -r_{11}i_1 + r_{12}i_2 - r_{1n}i_n \\ \hline \vdots \\ \hline -r_{n1}i_1 + r_{n,n-1}i_{n-1} - r_{nn}i_n \\ \hline -\left(r_f + r_a\right) i_f \\ \hline \end{array} .$$

The equation (2) includes the time coordinate $t$, and therefore, calculating with its use of static characteristics is a problem. However, in the condition of constant sliding, it describes the stationary asynchronous mode of the SM, which is characterized by a periodic non-harmonic change in coordinates. Due to the nonlinear electromagnetic connections between the motor circuits, the DE system (2) describing electromagnetic processes can not be reduced to algebraic ones by the transition to a complex variable, and the calculation of the steady state is to determine the functional dependencies of instantaneous coordinate values during the $T_a$ period.

Determining these dependencies is a boundary value problem for the DE system (2). In mathematics, as a rule, boundary-value problems are considered for second-order DEs, but due to the fact that boundary conditions are given by periodic dependencies, their definition is possible for first order DEs. To solve the boundary-value problem, the DE system (2) needs to be algebratized on a period, that is, to make a transition from differential equations to algebraic ones.

Different methods of algebrization are known in the literature, among which are the difference methods of various orders, collocation, including trigonometric, and others. However, projective methods [8] proved most effective, the essence of which is that the solution of the operator equation in a given subspace is determined by projecting a differential equation on some other subspace. Projection methods are the basis for constructing various computational schemes for solving boundary value problems [8]. The difference between them is to choose basic functions for approximation of the corresponding curves. In the paper the method of analysis of asynchronous modes of SM operation is proposed by the projection method developed on the basis of the use of cubic splines [9]. The essence of the method is the transition from the DE system (2) of a continuous variable to discrete algebraic equations. For this we divide the period $T$ into $m$ intervals $h_j = t_j - t_{j-1}$ $\left(j = \overline{1,m}\right)$ and on each of them the components of the vector $\vec{\psi}$ are approximated by splines of the third order of the form

$$\psi(t) = a_j + b_j\left(t_j - t\right) + c_j\left(t_j - t\right)^2 + d_j\left(t_j - t\right)^3, \qquad (3)$$

where $a_j$, $b_j$, $c_j$, $d_j$ are the spline coefficients, the relations between which are determined by the properties of the spline functions, which in the nodes of the mesh are linked together by the value of functions and are twice differentiated throughout the period. The relationships between the spline coefficients follow from its properties and are determined for each coordinate of the vector $\vec{\psi}$ only by the mesh of nodes in the period

$$\frac{3}{h_j}a_{j-1} - \left(\frac{3}{h_j} + \frac{3}{h_{j+1}}\right)a_j + \frac{3}{h_{j+1}}a_{j+1} = \qquad (4)$$
$$= h_j c_{j-1} + 2\left(h_j + h_{j+1}\right) c_j + h_{j+1}c_{j+1}.$$

$$b_j = \frac{a_{j-1} - a_j}{h_j} - \frac{h_j}{3}\left(c_{j-1} - 2c_j\right). \qquad (5)$$

In the matrix form equation (4), taking into account the conditions of the periodicity of the spline $a_{n+j} = a_j$, $c_{n+j} = c_j$, has a form

$$W_{21}\vec{A} + W_{22}\vec{C} = 0 , \qquad (6)$$

where $\vec{A} = \left(a_1,...,a_N\right)^*$; $\vec{C} = \left(c_1,...,c_N\right)^*$, and the upper index (*) means the transposition of the vector.

Equation (2) for the $j$-th node of the mesh has a form

$$\left.\frac{d\vec{\psi}}{dt}\right|_j = \vec{z}_j\left(\vec{\psi}_j,\vec{i}_j,\vec{u}_j\right), \qquad (7)$$

in which $\vec{u}_j = \left(U_m \sin\theta_j, U_m \cos\theta_j, 0,...,0\right)^*$.

Because, as it follows from (3), in the $j$-th node

$$a_j = y_j ; \qquad b_j = -\left.dy/dt\right|_j = -\vec{z}_j ,$$

equation (5) has a form

$$\frac{a_{j-1} - a_j}{h_j} - \frac{h_j}{3}\left(c_{j-1} - 2c_j\right) = -z_j$$

or in the matrix form

$$W_{11}\vec{A}+W_{12}\vec{C}=-\vec{Z}\,, \qquad (8)$$

where $\vec{Z}=(z_1,...,z_m)^*$. Consequently, the problem of determining the spline (3) is reduced to the determination of the coefficients $a_j$ and $c_j$.

Defining a vector $\vec{C}$ from equation (6), we obtain the equation for determining the nodal values of the coordinates (vector $\vec{A}$)

$$\left(W_{11}+W_{12}W_{22}^{-1}W_{21}\right)\vec{A}=-\vec{Z}\,, \qquad (9)$$

where $W_{11}$, $W_{12}$, $W_{21}$, $W_{22}$ are the block-matrices of size $m\times m$, the elements of which are determined exclusively by the coefficients of the equations (4), (5).

The obtained system (9) of the algebraic equations of the $km$ order, where $k = 2+m+1$ is the number of equations of the DE system DR, is a discrete reflection, which approximates it on the mesh of nodes of the period $T_a$ of the repetition of the process. It includes coordinate values that correspond to fixed values of the time coordinate $t_j$ in the nodes of the period, the relationships between which at each time point are nonlinear. Because $\vec{A}=\vec{\psi}$, a $\vec{Z}=\vec{Z}(\vec{\psi},\vec{u})$, and, moreover, $\vec{\psi}=\vec{\psi}(\vec{i})$. it can be presented as a nonlinear equation of the form

$$\vec{Q}(\vec{\Psi},\vec{I},\vec{U})=0\,. \qquad (10)$$

Its solution is the values of the vector

$$\vec{I}=(\vec{i}_1,...,\vec{i}_j,...,\vec{i}_m)^*, \quad \vec{i}_j=(i_{dj},i_{qj},i_{1j},...,i_{nj},i_{fj})^*,$$

which are determined by the vector of applied voltages and electromagnetic parameters of SM.

For the solution of the nonlinear algebraic system (10), the method of continuation by the parameter [8, 9] in combination with the iterative method of Newton is applied, according to which on each $l$-th step iteration the vector $\vec{I}$ is corrected by the formulas

$$\vec{I}^{(l+1)}=\vec{I}^{(l)}-\Delta\vec{I}^{(l)}; \quad W\Delta\vec{I}^{(l)}=\vec{Q}^{(l)},$$

where $\vec{Q}^{(l)}$ is the vector of the discrepancy of the system (10) at $\vec{I}=\vec{I}^{(l)}$.

The inducing force in equation (10) is the vector $\vec{U}=(\vec{u}_1,...,\vec{u}_m)^*$, increasing which from zero to nominal value, we obtain the values of vectors $\vec{\Psi}$ and $\vec{I}$ that correspond to the specified value of sliding $s = s_0$. The obtained coordinate values are the initial conditions for the calculation of static characteristics.

Elements of the blocks of the Jacobi matrix are differential inductive resistances of the motor circuits which are determined by calculating the equivalent circuit of the magnetic circuit of the SM in accordance with the accepted model [10]. The result of the calculation of the magnetic circuit is the determination of the magnetic flux density curve in the air gap of the motor by the theory of circuits, which enables to determine the flux linkages of the circuits that belong to the vector of discrepancies and depend on the set of currents of all motor circuits.

To study the effect of the value of the additional active resistance in the winding of excitation on the starting characteristics it is necessary, by setting the value of sliding, according to the above algorithm, to determine the value of coordinates of the mode with the value of the starting resistance in the excitation winding $r_a$ = 0, and then to increase its value within the required limits, correcting the discrepancy by the Newton method. The set of coordinates defined at each step of integration, allows us to determine the multidimensional characteristic as their dependence on the starting resistance in the excitation winding.

Similarly, the calculation of static starting characteristics as coordinate dependencies on sliding is performed. In this case, the additional resistance in the excitation winding is assumed unchanged, and sliding varies within the specified range.

To study the transient process of starting a SM, it is necessary together with the DE system (1) to integrate by a numerical method the equation of the mechanical equilibrium of the rotor

$$\frac{d\theta}{dt}=\frac{\omega}{\omega_0}-1\,;$$

$$\frac{d\omega}{dt}=\frac{p_0}{J}\left(\frac{3}{2}p_0\left(\psi_d i_q-\psi_q i_d\right)-M_c\right), \qquad (11)$$

where $p_0$ is the number of pairs of poles; $J$ is the moment of inertia of the electric drive system; $M_c$ is the moment of loading on the motor shaft.

At each step of integration to determine the electromagnetic parameters, which are the elements of the matrix $\partial\vec{\psi}/\partial\vec{i}$ of differential inductances of the motor circuits, it is necessary to solve a system of equations that describes the branched magnetic circuit of the SM.

Note that when calculating the periodic change of coordinates by the method of solving a boundary value problem, the magnetic state is calculated only for node points of the period, which is much smaller than their calculation by the method of setting.

**Results of investigations.** Below are examples of calculation results based on the developed method of stable modes and static characteristics of salient-pole synchronous motors СДС3-17-41-16 ($P$ = 1600 W, $U$ = 6000 V, $2p$ = 16; $n$ = 8) and СДН3-2-19-49-24 ($P$ = 1600 kW, $U$ = 6000 V, $2p$ = 24; $n$ = 5), which differ in the number of pairs of poles and rods at the pole.

An example of the periodic dependencies of the excitation current and the electromagnetic torque of the СДС3 motor at sliding $s$ = 1.0 is shown in Fig. 1.

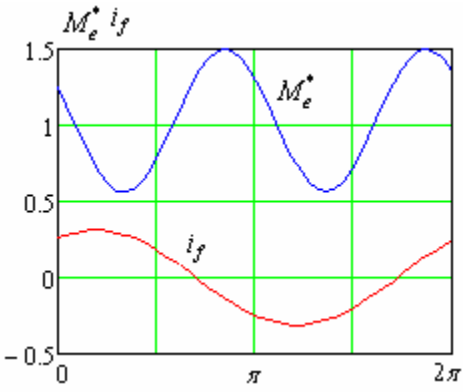


Fig. 1. Periodic current dependencies in the excitation winding of the СДС3 motor and the electromagnetic torque with a short excitation winding

As can be seen from Fig. 2, the dependence of the starting ($s$ = 1) electromagnetic torque on the additional resistance in the excitation winding for the SM of the same power, but with different number of pairs of poles and rods on each of them significantly differ. The calculation of the dependence of the propulsion electromagnetic torque on the starting resistance allows one to determine its value, at which the maximum torque will be.

Analysis of the calculation results (Fig. 2) shows that the 5-10-time value of the starting resistance, which is usually used, is not optimal in terms of providing the maximum value of the starting torque. However, a significant overstatement of the starting resistance can give a reverse effect.

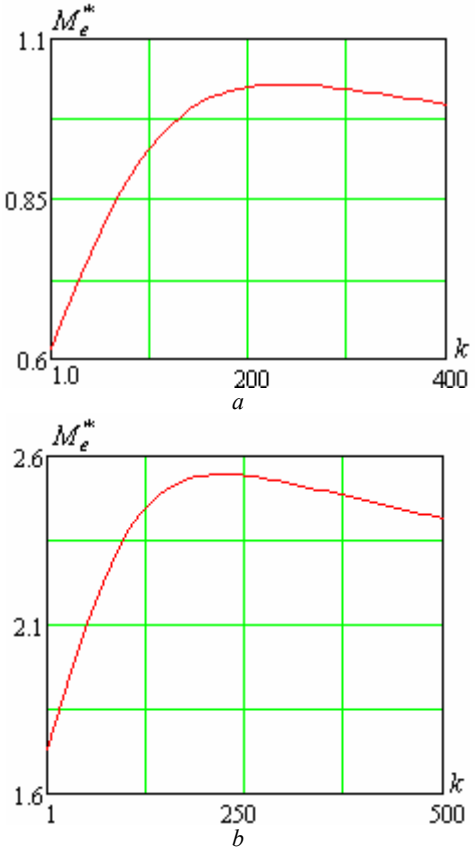


Fig. 2. Dependencies of the starting ($s$ = 1) electromagnetic torque on the multiplicity of the additional resistance in the excitation winding for the motors СДСЗ (*a*) and СДНЗ (*b*)

The developed mathematical model and calculation technique allows to investigate the effect on the asynchronous characteristics of the starting winding and excitation winding separately, which is important both for the design of the starting winding, and the development of optimal systems for automated control of the starting of the SM. To do this, in the program of calculating, the resistance of the winding, which must be excluded from consideration, is multiplied by a large ($10^3$–$10^6$) number. An example of the results of such studies is shown in Fig. 3, of which it is evident how different the created by the field winding asynchronous moments for different motors. In particular, at the first moment of the asynchronous start-up the asynchronous torque generated by the excitation winding, has little effect on the electromagnetic torque as a whole. Its maximum value is manifested in small sliding, but it is, as can be seen from Fig. 3, is significantly different for different motors.

In the absence of a starting winding in the vicinity of the sliding value $s$ = 0.5 in the curve of the asynchronous moment, the uniaxial effect is manifested (curve in Fig. 4,*b*). However, due to the salient polarity of the SM rotor, the failure in the curve of the electromagnetic torque is practically leveled by the starting winding, although for a sufficiently large value of the starting resistance in the excitation winding it manifests itself (Fig. 5). The corresponding choice of the value of the starting resistance can achieve not only increasing the starting torque but also maximizing it (Fig. 5). In addition, at the same time, the starting current in the stator winding decreases somewhat.

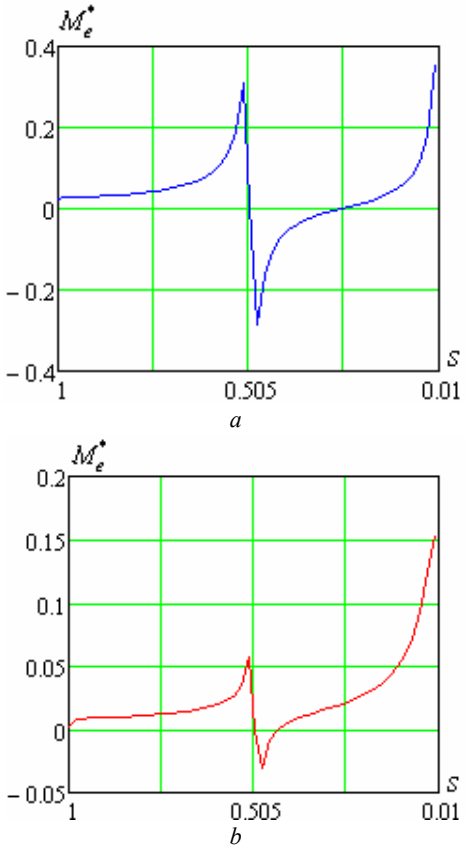


Fig. 3. Starting characteristics of the electromagnetic torque that is created by an excitation winding in the absence of a starting winding for motors СДСЗ (*a*) and СДНЗ (*b*)

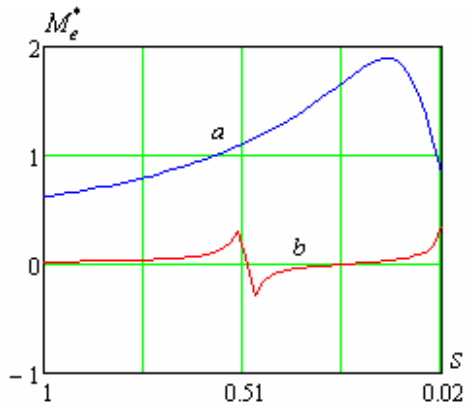


Fig. 4. Mechanical characteristics of the motor СДСЗ: *a* – with a shorted excitation winding and a starting winding; *b* – in the absence of a starting winding

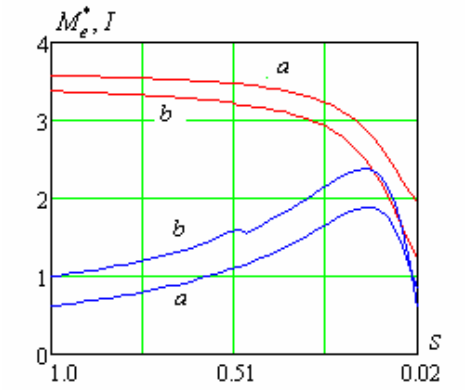


Fig. 5. Dependencies of the electromagnetic torque and the current of the motor СДСЗ on the sliding with shorted ($r_a = 0$) excitation winding – (*a*) and closed on the additional resistance $r_a = 250\ r_f$ – (*b*).

**Conclusions.**

1. A mathematical model and technique of calculation of asynchronous modes and static characteristics of salient-pole synchronous motors are developed, which makes it possible to investigate the influence of the value of the starting active resistance in the excitation winding on the value of the electromagnetic torque.

2. It is shown that by connection of the resistors in the excitation winding, it is possible not only to increase the driving electromagnetic torque of the motor, but also to influence its starting characteristics in general.

3. The developed mathematical model and calculation technique can be used in the process of designing salient-pole synchronous motors for optimization of their starting resistance and starting winding in order to form the starting characteristics required for a specific electric drive.

REFERENCES

***1.*** Abramovich B.N. About starting resistance ratio of synchronous motors. *Electrical engineering industry. Electric machines*, 1974, no.4(38), pp. 14-15. (Rus).

***2.*** Voldek A.I., Popov V.V. *Elektricheskiye mashiny. Mashiny peremennogo toka* [Electric machines. AC machines]. Saint Petersburg, Piter Publ., 2010. 350 p. (Rus).

***3.*** Baskov S.N., Radionov A.A., Usatyi D.Yu. Start of asynchronous motors in electric drives with increased starting torque. *Russian Electromechanics*, 2004, no.2, pp. 47-49. (Rus.)

***4.*** Chornyy A.P., Gladyr A.I., Osadchuk Yu.G., Kurbanov I.R., Voshun A.N. *Puskovyje sistemy nereguliruemykh elektroprivodov* [Start-up systems of unregulated electric drives]. Kremenchug, Scherbatykh A.V. Publ., 2006. 280 p. (Rus).

***5.*** Pivnyak G.G, Kirichenko V.I, Boroday V.A. About new direction in improvement large synchronous electric motors. *Technical electrodynamics. Thematic issue «Problems of modern electrical engineering»*, 2002, chapter 2, pp. 62-65. (Rus).

***6.*** Kirichenko V.I., Boroday V.A., Yalanskiy A.A. Improved properties of starting modes of large synchronous machines. *Visnik Of The Volodymyr Dahl East Ukrainian National University*, 2003, no.6(64), pp. 38-40. (Rus).

***7.*** Malyar V.S., Malyar A.V., Dobushovska I.A. Simulation of asynchronous modes of synchronous motors with capacitors in the excitation circuit. *Electrical engineering & electromechanics*, 2012, no.5, pp. 31-33. (Ukr). **doi: 10/20998/2074-272X.2012.5.06**.

***8.*** Ortega J., Poole W. *An introduction to numerical methods for differential equations*. Boston, Jr. Pitman Publ. Inc., 1981. 344 p.

***9.*** Malyar V.S, Malyar A.V. Mathematical simulation of periodic modes of electrotechnical appliances. *Electronic modeling*, 2005, vol.27, no.3, pp. 39-53. (Rus).

***10.*** Filts R.V, Lyabuk N.N. *Matematicheskoye modelirovaniye yavnopolyusnykh sinkhronnykh mashin* [Mathematical simulation of salient-pole synchronous motor]. Lviv, Svit Publ., 1991. 176 p. (Rus).

*Received 06.01.2018*

*V.S. Malyar*[1], *Doctor of Technical Science, Professor,*
*A.V. Malyar*[1], *Doctor of Technical Science, Professor,*
[1] Lviv Polytechnic National University,
12, S. Bandera Str., Lviv, 79013, Ukraine,
phone +380 32 2582119,
e-mail: mvs@polynet.lviv.ua; svmalyar@polynet.lviv.ua

*How to cite this article:*
Malyar V.S., Malyar A.V. Studying the effect of an additional active resistance in the field winding circuit on starting characteristics of salient-pole synchronous motors. *Electrical engineering & electromechanics*, 2018, no.2, pp. 18-23. **doi: 10.20998/2074-272X.2018.2.03.**

UDC 621.316:629.4.048.7 **doi: 10.20998/2074-272X.2018.2.04**

A.M. Andryushchenko, V.R. Nikulshin, A.E. Denysova

# ADVANTAGES OF ELECTRICAL HEATING SYSTEMS WITH NIGHT HEAT ACCUMULATION IN UKRAINIAN CONDITIONS

***Purpose. To develop electrical heating systems with night heat accumulation and to prove its advantages comparable with others possible variants of heating. Methodology. We have purposed a methodology which is based on the current Standards of Ukraine and included few main assumptions: the efficiency of the electric boiler is assumed equal 100 %; the dependence of the building heating load on the outside temperature is linear; all the variants of different energy resources calculating for the system operating correspond to the adequate (depending on weather) regulation. Methodology allows to determine the main technical characteristics of the system taking into account the possibility of switching on the electric boiler in the daytime using the half-loading. On the base of suggested methodology was developed the calculation program for determine the monthly consumption of heat by the building and estimate the cost of heating using different energy sources. This program also allows to compare the payment for centralized heat supply services at the tariff for the consumed heat with a payment for the heated area tariff. Results. We have obtained a method for electrical heating systems with night heat accumulation calculation. Method bases on the current Standards in Ukraine and allows to determine the main technical characteristics of the system taking into account the possibility of switching on the electric boiler in the daytime. On the base of suggested method was developed the calculation program for determine the monthly consumption of heat by the building and estimate the cost of heating using different energy resources. This program also allows to compare the payment for centralized heat supply services at the tariff for the consumed heat with a payment for the heated area tariff. Originality. For the first time we have suggested methodology and developed the calculation program for electrical heating systems with night heat accumulation which is based on the Ukrainian Standards and allows to determine the monthly consumption of heat by the building and estimate the cost of heating using different energy sources. Practical value. We have developed a method and calculation program which allows to design the energy saving electrical heating systems with night heat accumulation. We have demonstrated on the numerical example for the real weather conditions of Kyiv city the economical advance of using electric heating with night heat accumulation comparable with all others options (centralized heat supply, gas heating, pellet heating). For December 2017 tariffs in Ukraine, the cost of electrical heating with night heat accumulation are two times lower than in the case of centralized heat supply with payment for consumed heat. We have proved that the refund period for implementation of electrical heating systems with night heat accumulation instead of centralized heat supply services at the tariff for the consumed heat is less than 3 years, and for centralized heat supply services at the tariff for the heated area tariff is less than 1 year.*** References 10, tables 4, figures 2.

*Key words*: **energy saving, electrical heating, night heat accumulation, cost of heating for different energy resources.**

***Цель. Цель исследования - разработка системы электрического отопления с ночным аккумулированием теплоты и обоснование ее энергосберегающего характера по сравнению с другими возможными вариантами отопления. Методика. Методика основана на современных стандартах Украины и включает следующие основные допущения: коэффициент полезного действия электрического котла принимается равным 100 %; зависимость отопительной нагрузки здания от внешней температуры считается линейной; для всех расчетных вариантов отопления, использующих различные энергетические ресурсы, режим работы системы отопления отслеживает погодные условия в соответствии с температурой наружного воздуха. Методика предусматривает определение основных технических характеристик системы с учетом возможности включения электрического бойлера в дневное время на половину расчетной нагрузки. Результаты. На основе предложенного метода была разработана расчетная программа для определения ежемесячного теплопотребления здания и расчета стоимости отопления при использовании различных энергетических ресурсов. Эта программа также позволяет сопоставлять стоимости централизованного теплоснабжения как по потребленной теплоте, так и при оплате по величине отапливаемой площади. Научная новизна. Впервые приведены метод и программа расчета систем электроотопления с ночным аккумулированием теплоты, учитывающие действующие стандарты Украины и позволяющие определять основные технические характеристики системы, а также рассчитывать стоимости отопления при использовании различных видов энергетических ресурсов. Практическое значение. Использование предлагаемой методики позволяет проектировать энергосберегающие системы электрического отопления с ночным аккумулированием теплоты. Приведен численный пример для реальных погодных условий г. Киева. Показано, что срок окупаемости перехода на электроотопление для варианта замены централизованного теплоснабжения с оплатой за потребленную теплоту составляет менее 3 лет, для варианта замены централизованного теплоснабжения с оплатой за отапливаемую площадь составляет менее 1 года.*** Библ. 10, табл. 4, рис. 2.

*Ключевые слова*: **энергосбережение, электроотопление, ночная аккумуляция теплоты, расходы на разные виды энергетических ресурсов.**

**Introduction.** The sharp and uneven rise in the cost of different types of energy used for heating encourages the search for alternative economic solutions.

Reducing heating costs can be achieved by reducing the heat loss by building envelopes as a result of their thermo-modernization [1], as well as

through the transition to the use of alternative energy resources.

Among alternatives, primarily for large cities, in recent years, electric heating with night-time heat accumulation [2] and electric heating of the heat-carrier at night at centralized heat supply systems are considered.

In both cases, the effect of equalizing the daily schedule of the electric load of the integrated power system of Ukraine will be achieved, which will have a beneficial effect on its operation due to the more complete loading of the Ukrainian NPPs, which produce the electric power at the lowest cost in comparison with other types of generation. Another positive aspect of the application of electric heating, provided it is sufficiently distributed, is the saving of natural gas.

The simplest version of electric heating was considered - the use of thermal electric heaters, not heat pumps.

Heat pumps, as is known, would allow about three times to reduce the cost of electricity for heating, but at the same time they would have to require thousands of USD investments with a payback period from 3 years and more that in the current economic situation for Ukraine is not acceptable.

The problem of finding effective solutions for different heating systems has been relevant over the past decades and will remain so in the near future and in the foreseeable future.

The number of publications on this subject is tens of thousands. Therefore, let us dwell only on some of them.

Much of the publications are devoted to systems of centralized heating (both from combined heat and power plants and from boiler houses).

Of particular interest to this work are publications, including domestic ones, which deal with issues of heating with the accumulation of heat.

In [3], the search for rational combinations of systems of electric heating with renewable energy sources is carried out, economically justified heating tariffs are given in [4], in [5] possibilities of rational arrangement of heat accumulators with systems of electrical are estimated heating, in [6] the possibilities of taking into account the need of hot water supply in systems of electric heating are shown, in [7] the influence of market factors on the efficiency of systems of electric heating is estimated, [8] the possibilities of efficient use of heat accumulators as for electric heating, and hot water supply are shown.

In contrast, in this paper, the emphasis is not on the theoretical description of the calculation of the heating systems itself, but on the practical results of such calculations.

Hence, the following problem arises - the determination of the required heating load of the building (regardless of the specific type of indoor heating system used), comparisons on this basis of various possible options for the supply of heat to the building and the choice of the most economical of them.

**The goal of the investigation** is the substantiation of the energy saving nature of the electric heating system with night-time accumulation of heat in comparison with other possible variants of heating.

To achieve the goal, the following tasks must be solved:

- to develop a method and a calculation program to determine the main technical characteristics (useful volume of the tank-accumulator of hot water and the power of the electric heater) of the electricity system of heating with an accumulator of heat and electricity accounting for a three-zone tariff;
- to compare the cost of district heating with gas heating, with round-the-clock electric heating at electricity accounting for a single-zone tariff, as well as with pellet heating;
- to bring a numerical example of the calculation and a comparative analysis of the cost of heating the office building located in the city of Kyiv (under the actual weather conditions in this city) and show the advantages of a heating system with nightly heat accumulation.

**Brief description of the system of heating with an accumulator of heat.** Charging the heat accumulator [9] (Fig. 1) is performed when the electric boiler and circulation pump of the charging circuit are switched on, mainly at night.

The supply of heat-carrier to the heating devices of the building is provided by the circulating pump of the flow path continuously throughout the heating season.

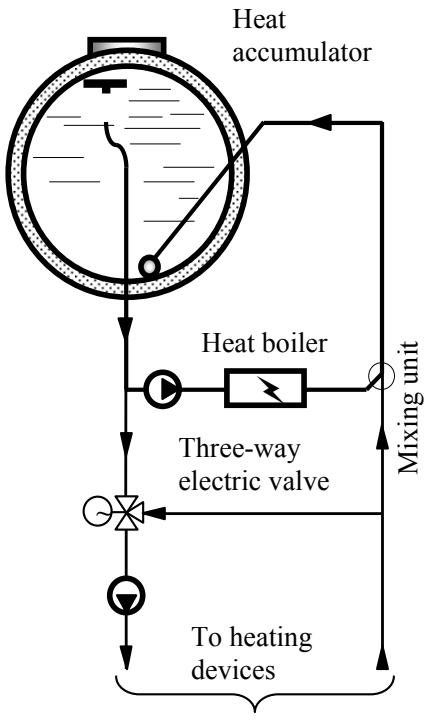


Fig. 1. Principle diagram of the electric heating system with a water thermal accumulator

The scheme provides the weather control of the temperature of the heat-carrier supplied to the heating devices by mixing the part of the rotary heat-carrier with a three-way electric valve.

Thus, it provides energy-saving mode of operation and the required heating load of the system, depending on the temperature of the outside air.

**Method of calculation.** The following assumptions are accepted in the calculation:

- the heat accumulator and the electric boiler are located directly in the heating room, therefore the loss of heat through thermal insulation of the accumulator and through the surface of the electric boiler is not taken into account;
- the efficiency of the electric boiler is taken equal to 100 %;
- the dependence of the heating load of the building on the temperature of the outside air is linear: the external temperature +18 °C corresponds to the zero heating load, the minimum design temperature of the outside air corresponds to 100 % of the heating load of the building in accordance with the statistical climatic data [10]; heating operates only at ambient temperatures below +8 °C;
- it is assumed that in all variants of use of different energy resources the system operates in the mode of adequate weather regulation;
- the useful temperature difference of the heat-carrier in a fully charged thermal accumulator and completely discharged one is 35 K;
- calculation of the current value of the temperature of the heat-carrier in the volume of the heat accumulator during operation of the system is carried out on the model of perfect mixing, without taking into account temperature stratification;
- tariffs and prices for various energy resources are taken in accordance with [10] as of December 2017.

The method of calculation takes into account the possibility of switching on the electric boiler in the daytime, in the semi-peak period of the load of the power system, at ambient temperatures below the set temperature of only night electricity consumption $t^{night}$, while also envisaging the switching on of the electric boiler for incomplete power.

At the linear relationship between the temperature of the outside air and the heating load of the building, the proportion of the total heating load of the building, depending on the temperature of the outside air, will be:

$$q/q^{calc} = \varphi^{q} = (t_{in}^{calc} - t)/(t_{in}^{calc} - t^{calc}), \quad (1)$$

where $q$ is the specific heating load of the building, W/m$^2$, at the current value of the temperature of the outside air $t$, °C; $q^{calc}$ is the specific maximal heating load of the building, W/m$^2$, at the normative minimal value of the temperature of the outside air, °C; $t_{in}^{calc}$ = +18 °C is the calculated air temperature at which the heating load equals to zero; $t^{calc}$ is the normative minimal value of the temperature of the outside air, for Kyiv $t^{calc}$ = –22 °C.

Specific normative losses of heat in a building during the heating season are the sum of monthly losses of heat during the heating season:

$$Q_{year}^{norm} = q_{oct} + q_{nov} + q_{dec} + q_{jan} + q_{feb} + q_{mar} + q_{apr}, \text{ kW·h/m}^2, \quad (2)$$

where $q_{oct}$ ... $q_{apr}$ are the monthly specific losses of heat, kW·h/m$^2$, which taking into account (1) can be represented as:

$$q_{oct} = \varphi^{q}_{oct} \cdot q^{calc} \cdot \tau_{oct} = (18 - t_{oct}) \cdot q^{calc} \cdot \tau_{oct}/(18 - t^{calc}),$$

$$q_{apr} = \varphi^{q}_{apr} \cdot q^{calc} \cdot \tau_{apr} = (18 - t_{apr}) \cdot q^{calc} \cdot \tau_{apr}/(18 - t^{calc}),$$

where $\varphi^{q}_{oct}$ … $\varphi^{q}_{apr}$ are the shares of the total heating load at the average monthly temperatures of the outside air of the respective month of the heating period; $\tau_{oct}$ … $\tau_{apr}$ are the number of hours in the respective month of the heating period, h; $q^{calc}$ is the specific losses of heat of the building, kW/m$^2$, at the normative minimum calculated temperature of the outside air $t^{calc}$, °C; $t_{oct}$ … $t_{apr}$ are the average monthly air temperatures in the corresponding month, °C.

Then:

$$q_{year}^{norm} = q^{calc} \cdot [\tau_{oct} \cdot (18 - t_{oct}) + \tau_{nov} \cdot (18 - t_{nov}) + \tau_{dec} \cdot (18 - t_{dec}) + \tau_{jan} \cdot (18 - t_{jan}) + \tau_{feb} \cdot (18 - t_{feb}) + \tau_{mar} \cdot (18 - t_{mar}) + \tau_{apr} \cdot (18 - t_{apr})]/(18 - t^{calc}), \text{ kW·h/m}^2.$$

Consequently, the maximum calculated specific heat losses of the building, kW/m$^2$, at the normative minimum calculated temperature of the outside air, are:

$$q^{calc} = (18 - t^{calc}) \cdot q_{year}^{norm}/[\tau_{oct} \cdot (18 - t_{oct}) + \tau_{nov} \cdot (18 - t_{nov}) + \tau_{dec} \cdot (18 - t_{dec}) + \tau_{jan} \cdot (18 - t_{jan}) + \tau_{feb} \cdot (18 - t_{feb}) + \tau_{mar} \cdot (18 - t_{mar}) + \tau_{apr} \cdot (18 - t_{apr})], \text{ kW/m}^2.$$

The maximum calculated heating load of the building at the normative minimum calculated temperature of the outside air $t^{calc}$ corresponds to the value $\varphi^{q}$ = 1 and equals:

$$\Phi^{calc} = A \cdot q^{calc}, \text{ kW}, \quad (3)$$

where $A$ is the total heating area of the building, m$^2$.

Daily heat consumption of the building at the normative minimum calculated temperature of the outside air $t^{calc}$:

$$Q^{calc} = 24 \cdot \Phi^{calc}, \text{ kW·h/day}. \quad (4)$$

At the minimum calculated temperature of the only nightly electricity consumption $t^{night}$, °C, heating load $\Phi^{night}$ and daily heat consumption of the building $Q^{night}$ will be:

$$\Phi^{night} = \Phi^{calc} \cdot \varphi^{qnight} = \Phi^{calc} \cdot (t_{in}^{calc} - t^{night})/(t_{in}^{calc} - t^{calc}), \text{ kW}; \quad (5)$$

$$Q^{night} = 24 \cdot \Phi^{night}, \text{ kW·h/day}. \quad (6)$$

During the time of preferential night electricity consumption (within 7 hours) at a temperature $t^{night}$ it is necessary to carry out a full charge of a water thermal accumulator simultaneously with the supply of heat for heating the building.

In this case, the supply of heat accumulated in the heat accumulator should provide heating of the building for a full day period of 17 hours.

Consequently, the total amount of heat in the heat accumulator will be:

$$Q^{acc} = 17 \cdot \Phi^{night}, \text{ kW·h}. \quad (7)$$

Since the heat accumulator must be charged for 7 hours at the same time as the heat supply for heating the building, the electric power of the boiler will be:

$$N = \Phi^{night} + Q^{acc}/7, \text{ kW}. \quad (8)$$

Useful volume of heat accumulator:

$$V^{acc} = Q^{acc} \cdot 3600/(c_p \cdot \rho \cdot \Delta T^{acc}), \text{ m}^3, \quad (9)$$

where $c_p$ = 4.19 kJ/(kg·K) is the specific isobaric heat capacity of water; $\rho$ = 1000 kg/m$^3$ is the density of water; $\Delta T^{acc}$ = 35 K is the useful temperature difference in the heat accumulator.

Calculated duration of operation of an electric boiler during daytime during the day at the normative minimum calculated temperature of the outside air:

$$\tau^{day} = (Q^{calc} - Q^{night})/N, \text{ h}. \quad (10)$$

According to the calculations, $\tau^{day}$ should be less than the duration of the half-peak period to exclude the operation of the electric boiler during the peak day period with the most expensive tariff.

On the basis of expressions (1-10) a program has been prepared in MS Excel for variant comparative calculations of systems of electric heating with thermal accumulator.

Below is an example of the calculation of such a heating system of an office building located in the city of Kyiv.

**Results of comparative calculation of heating systems and their discussion.** Output data and calculation results are given in Table 1 for an office building with an area of 1000 m$^2$ with a maximum specific calculated heating load of $q^{calc}$ = 40 W/m$^2$, which corresponds to a well-insulated building.

Estimated total power of the thermal electric heaters of the electric boiler is (at operation mostly at night) 102.9 kW, with a useful volume of thermal accumulator 12.52 m$^3$, while the calculated power of the electric boiler, at a 24-hour operation without a thermal accumulator, is equal to 40 kW.

The calculation is made for the case when at the temperature of the outside air below –12 °C the electric boiler will be switched on at 50 % of the power for heating the heat-carrier in daylight hours.

At minimum calculated temperature, the duration of day-time switching on the electric boiler will not exceed 5 hours.

Table 2 presents the results of calculations of monthly costs for building heating using different energy resources and forms of payment.

Table 3 and Fig. 2 show the results of calculations of total seasonal costs for building heating using different energy resources.

According to the calculation, the total heat consumption of the building during the heating season is 83.9 MW·h, which corresponds practically to the regulatory level of 83 MW·h, hence, the calculated maximum 40W/m$^2$ of the specific heating load corresponds to the normative thermal losses of the building.

The smallest seasonal heating costs in the amount of 41.2 thousand UAH are provided with the use of electric heating with night-time accumulation of heat and with the use of three-zone accounting of electricity consumed. Relatively small expenses of 50.6 thousand UAH correspond to the heating with pellets, but considering the concomitant factors associated with the need for periodic delivery, storage of pellet and waste disposal, the electrical heating is much better.

When using a gas boiler, seasonal expenses will amount to 83.5 thousand UAH, which is twice much as when electrical heating with night-time heat accumulation.

In the case of district heat supply, payment for its services in the amount of 92.8 thousand UAH during the heating season is not much higher than the cost of gas heating.

The largest seasonal heating costs in the amount of 210 thousand UAH arise in the case of monthly payment for district heating services at the tariff 30 UAH for each square meter of heating space during the heating season, that is, in the absence of a registered heat meter.

If you use electric heating without thermal accumulation, then, subject to adequate weather regulation, seasonal costs will be 164.7 thousand UAH, which is less than with district heating with payment for services for the tariff for the heating area.

Table 1

Initial data and technological calculation results

| | |
|---|---|
| Total heating area of the building, m$^2$ | 1000 |
| Maximum specific heating load of the building, W/m$^2$ | 40 |
| Normative maximum seasonal heat losses of the building by ДБН В2.6-31:2016, kW·h/m$^2$ | 83 |
| The minimum external temperature of only night-time electricity consumption (at lower temperatures there is a day-time switching on of the electric coil), °C | –12 |
| The share of electrical power in the daytime operation of the electric boiler, % | 50 |
| Calculated total power of the thermal electric heaters of the electric boiler, kW | 102.9 |
| Calculated power of the thermal electric heaters of the electric boiler with round-the-clock operation without thermal accumulation, kW | 40 |
| Useful difference of temperature of water in a thermal accumulator, K | 35 |
| Useful calculated volume of the thermal accumulator, m$^3$ | 12.52 |
| Basic electricity tariff excluding VAT, kopeck/(kW·h) | 163.545 |
| Cost of consumed heat at centralized heat supply, UAH/Gcal | 1286.07 |
| Cost of district heating at paying for a unit of heating space, UAH/(m$^2$·month) | 30 |
| Cost of natural gas for an industrial boiler-house, UAH/thousand m$^3$ | 9692.4 |
| Cost of natural gas in the composition of the consumed heat at district heat supply, taking into account the efficiency of the gas boiler, UAH/Gcal | 1156.6 |
| Cost of pellets, UAH/t | 2410 |
| Heating capacity of pellets, MJ/kg | 18 |
| Cost of pellet heat, taking into account the efficiency of the pellet boiler, UAH/Gcal | 700.7 |
| Cost of heat for round-the-clock heating without a thermal accumulator, UAH/Gcal | 2282.4 |

Let us consider also expediency of reconstruction of existing heating systems by replacing the heat source with electric heating with a thermal accumulator at a three-zone tariff. The comparison is made with the most widespread heat supply in large cities of Ukraine – centralized (district) heat supply both with payment for consumed heat, and with payment for the heating area.

Table 2

Seasonal heating costs at using various energy resources

| | |
|---|---|
| The heat consumed for the season, Gcal | 72.2 |
| The heat consumed for the season, MW·h | 83.9 |
| Normative maximum seasonal heat losses for a building by ДБН В2.6-31:2016, not more, MW·h | 83 |
| Cost of electricity consumed during the heating season in the presence of adequate weather regulation, thousand UAH | 41.2 |
| Cost of electricity consumed during the heating season at round-the-clock heating without a thermal accumulator, but in the presence of adequate weather regulation, thousand UAH | 164.7 |
| Cost of district heating during the heating season at the tariff for the released heat in the presence of adequate weather regulation, thousand UAH | 92.8 |
| Cost of district heating during the heating season with the tariff for the heated area, thousand UAH | 210 |
| Total amount of consumed gas during the heating season, in the presence of adequate weather regulation, thousand $m^3$ | 8.6 |
| Cost of consumed natural gas during the season for heating, thousand UAH | 83.5 |
| Cost of pellet heating in the presence of adequate weather regulation, thousand UAH | 50.6 |

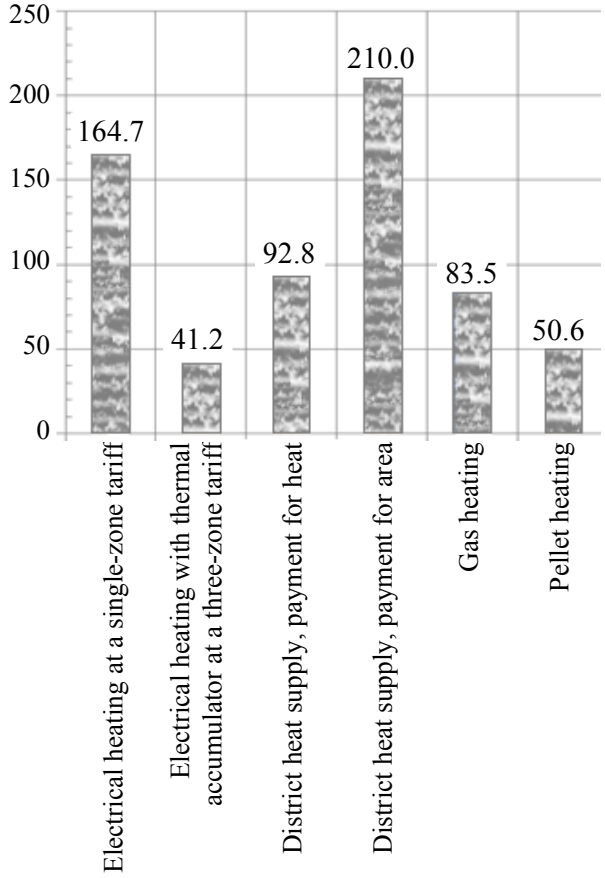


Fig. 2. Seasonal heating costs at using various energy resources, thousand UAH

Table 3

Monthly heating costs when using different energy resources

| Month | Oct. | Nov. | Dec. | Jan. | Feb. | March | April |
|---|---|---|---|---|---|---|---|
| Average temperature, °C | 7.5 | 1.2 | –3.5 | –5.9 | –5.2 | –0.4 | 7.5 |
| Consumed heat, Gcal/month | 3.84 | 10.40 | 13.75 | 15.29 | 13.41 | 11.77 | 3.71 |
| Consumed heat, kW·h/month | 4464 | 12096 | 15996 | 17782 | 15590 | 13690 | 4320 |
| Cost of consumed electricity, thousand UAH/month | 2.19 | 5.93 | 7.85 | 8.72 | 7.65 | 6.72 | 2.12 |
| Cost of consumed electricity at round-the-clock electrical heating without thermal accumulator, thousand UAH/month | 8.76 | 23.74 | 31.39 | 34.90 | 30.60 | 26.87 | 8.48 |
| Cost of district heating when paying for released heat, thousand UAH/month | 4.94 | 13.38 | 17.69 | 19.66 | 17.24 | 15.14 | 4.78 |
| Cost of district heating when paying for heating area, thousand UAH/month | 30 | 30 | 30 | 30 | 30 | 30 | 30 |
| Cost of the equivalent gas consumed for heating, thousand UAH/month | 4.44 | 12.03 | 15.91 | 17.68 | 15.50 | 13.61 | 4.3 |
| Cost of pellet heating, thousand UAH/month | 2.69 | 7.29 | 9.64 | 10.71 | 9.39 | 8.25 | 2.6 |

Calculations of the electrical heating system are presented in the summarized Table 4. Comparison of the total cost of the proposed system of heating (Table 4) with annual costs for district heating (Fig. 2) shows that the payback period for switching to electrical heating from district heating with payment for consumed heat is 2.7 years, and with payment for heating space – 0.83 years.

Thus, the use of electrical heating systems with night-time heat accumulation is not only appropriate for new heating systems, but also for existing ones.

Table 4

Characteristics of the system of electric heating with thermal accumulator

| **Initial data for calculation** | | |
|---|---|---|
| Calculated total power of thermal electric heaters | 102.9 kW | |
| Useful calculated capacity of the heat accumulator | 12.52 $m^3$ | |
| Calculated temperature difference in the charging circulation circuit | 5 K | |
| Estimated temperature difference in the consumption circulation circuit | 10 K | |
| Water speed in the charging circulation circuit | 1.5 m/s | |
| Water speed in the consumption circulation circuit | 1.5 m/s | |
| Water speed in the mixed circulation circuit | 1 m/s | |
| **Results of calculation of main technological characteristics of the heating system** | | |
| Calculated water consumption in the charging circulation circuit | 4.913 kg/s | 17.69 t/h |
| Calculated water consumption in the consumption circulation circuit | 0.955 kg/s | 3.44 t/h |
| Tube diameter of the charging circulation circuit | 0.0646 m | 64.6 mm |
| Tube diameter of the consumption circulation circuit | 0.0285 m | 28.5 mm |
| Diameter of branch pipes of heat accumulator | 0.0864 m | 86.4 mm |
| **Cost indicators of the heating system** | | |
| | cost, UAH | |
| Electrical boiler | 15000 | |
| Circulation pump of the charging circuit | 8300 | |
| Circulation pump of the consumption circuit | 2900 | |
| Heat tank-accumulator | 18000 | |
| Heat insulation | 10000 | |
| Three-way regulating valve Ду32 | 1700 | |
| Servo drive for three-way regulating valve Ду32 | 2500 | |
| Automatic control unit | 16000 | |
| Locking valves, pipes, tees, fittings, heat insulation of communications | 20000 | |
| Construction works | 45000 | |
| Total cost | 139400 | |

**Conclusions.**

1. A method and program of calculation of systems of electric heating with night accumulation of heat is given.

The method takes into account the current Standards of Ukraine and allows to determine the basic technical characteristics of the system, taking into account the possibility of switching the electric boiler into half of the calculated power in daylight hours.

2. The proposed method and developed program allow determining the monthly heat consumption of buildings and calculating the cost of heating using different types of energy resources, as well as comparing the costs of district heating with payment for consumed amount of heat and when paying for the heating area.

3. A numerical example for real weather conditions in Kyiv city has shown the economic benefits of using electric heating with night-time heat accumulation.

According to the Ukrainian tariffs for December 2017, the cost of heating with a nightly accumulation of heat is two times lower than for district heat supply with payment for consumed heat.

4. It is proved that the payback period for switching to electrical heating for the option of replacing district heating with payment for the consumed heat is less than 3 years, and for a variant of the replacement of district heating with payment for the heating area is less than 1 year.

REFERENCES


***1.*** Veeraboina P., Yesuratnam G. Significance of design for energy conservation in buildings: building envelope components. *International Journal of Energy Technology and Policy*, 2013, vol.9, no.1, pp. 34-52. **doi: 10.1504/IJETP.2013.055814**.

***2.*** Arteconi A., Patteeuw D., Bruninx K., Delarue E., D'haeseleer W., Helsen L. Active demand response with electric heating systems: Impact of market penetration. *Applied Energy*, 2016, vol.177, pp. 636-648. **doi: 10.1016/j.apenergy.2016.05.146**.

***3.*** Li J., Fang J., Zeng Q., Z Chen. Optimal operation of the integrated electrical and heating systems to accommodate the intermittent renewable sources. *Applied Energy*, 2016, vol.167, pp. 244-254. **doi: 10.1016/j.apenergy.2015.10.054.**

***4.*** Ziemele J., Gravelsins A., Blumberga A., Blumberga D. Sustainability of heat energy tariff in district heating system: Statistic and dynamic methodologies. *Energy*, 2017, vol.137, pp. 834-845. **doi: 10.1016/j.energy.2017.04.130.**

***5.*** Patteeuw D., K Bruninx., Arteconi A., Delarue E., D'haeseleer W., Helsen L. Integrated modeling of active demand response with electric heating systems coupled to thermal energy storage systems. *Applied Energy*, 2015, vol.151, pp. 306-319. **doi: 10.1016/j.apenergy.2015.04.014**.

***6.*** Parasochka S.O., Hrjashhevs'kyj V.M. Regarding electrical heating with accumulation and heat water supply. *Housing and communal services of Ukraine*, 2009, no.8(21), pp. 34-37. (Ukr).

***7.*** Paraska G.B., Mykoljuk O.A. Efficiency of electrical heating systems usage. *Power Engineering: economics, technique, ecology*, 2015, no.4, pp. 73-79. (Ukr).

***8.*** Treputnev V.V. Electrical heat accumulators for heating and heat water supply. *News of heat supply*, 2010, no.4, pp. 116-118. (Rus).

***9.*** Andrjushhenko A.M., Panasjuk O.V. *Systema teplopostachannja* [System of heat supply]. Patent UA, no.57479, 2011. (Ukr).

***10.*** Available at: http://www.nerc.gov.ua/?id=11889 (accessed 02 December 2017). (Ukr).

*Received 08.01.2018*

*A.M. Andryushchenko*[1],
*V.R. Nikulshin*[1], *Doctor of Technical Science, Professor,*
*A.E. Denysova*[1], *Doctor of Technical Science, Professor,*
[1] Odessa National Polytechnic University,
1, Shevchenko Avenue, Odessa, 65044, Ukraine,
e-mail: amandr@ukr.net; vnikul@paco.net;
alladenysova@gmail.com

*How to cite this article:*
Andryushchenko A.M., Nikulshin V.R., Denysova A.E. Advantages of electrical heating systems with night heat accumulation in Ukrainian conditions. *Electrical engineering & electromechanics*, 2018, no.2, pp. 24-30. **doi: 10.20998/2074-272X.2018.2.04.**

UDC 620.179.16: 620.179.17 **doi: 10.20998/2074-272X.2018.2.05**

S.Yu. Plesnetsov, O.N. Petrishchev, R.P. Mygushchenko, G.M. Suchkov, S.V. Sotnik, O.Yu. Kropachek

# POWERFUL SOURCES OF PULSE HIGH-FREQUENCY ELECTROMECHANICAL TRANSDUCERS FOR MEASUREMENT, TESTING AND DIAGNOSTICS

***Aim. Development of powerful current radio pulses generators (CRPG) for powering high-frequency electromechanical transducers based on IGBT transistors. Methodology. To carry out the research, the statements of the magnetic and electromagnetic fields interaction with electric and ferromagnetic material, electric circuits, structure of radio electronic devices theory were used. Results. The main provisions for creating powerful broadband generators for powering electromechanical transducers based on IGBT transistors are determined. It is shown that the generators intended for use in measurements, testing and diagnostics should provide adjustment of the frequency and duration of the output current pulses, and also provide current in the transducer inductor of several hundred amperes. The connection between the power frequency of the resonant electromechanical transducer and the gap between the transducer and the surface of the metal being diagnosed is established. A CRPG variant for powering electromechanical transducers in the frequency range 1 ... 3 MHz and the duration of current pulses of 1 ... 20 periods of the filling frequency is developed and manufactured. The peak current in the inductor of a high-frequency electromechanical transducer has reached 450 A. Novelty. For the first time, the possibility of using powerful IGBT transistors in electronic devices working in a key mode in push-pull circuits for feeding high-frequency electromechanical transducers is shown. Practical value. Using the results obtained will allow the creation of new instruments for measurement, control and diagnostics with wider characteristics.*** References 12, figures 6.

*Key words:* **powerful transistors, radio pulse generator, electromagnetic field, conductive and ferromagnetic metal, high-frequency current, inductor.**

***Цель работы. Разработка основных положений по созданию мощных источников импульсов тока для питания высокочастотных электромеханических преобразователей для измерений, контроля и диагностики электротехнических устройств на базе силовых IGBT транзисторов. Методика. Для проведения исследований использовались положения теории взаимодействия магнитных и электромагнитных полей с электропроводным и ферромагнитным материалом, электрических цепей, построения электронных устройств. Результаты. Определены основные положения по созданию мощных широкополосных генераторов для питания электромеханических преобразователей на базе силовых IGBT транзисторов. Показано, что генераторы, предназначенные для использования в измерениях, контроле и диагностике, должны обеспечивать регулировку частоты и длительности импульсов выходного тока, а также обеспечивать ток в катушке преобразователя величиной до 450 А. Установлена связь между частотой питания резонансного электромеханического преобразователя и зазором между преобразователем и поверхностью диагностируемого металла. Разработан и изготовлен вариант ИИТ для питания электромеханических преобразователей в диапазоне частот 1…3 MHz и длительности импульсов тока 1…20 периодов частоты заполнения. Пиковая величина тока в катушке высокочастотного электромеханического преобразователя достигла 450 А. Научная новизна. Впервые показана возможность применения силовых IGBT транзисторов в электронных устройствах, при ключевом режиме работы в двухтактных схемах для питания высокочастотных электромеханических преобразователей. Практическая значимость. Использование полученных результатов позволит создавать новые приборы для измерений, контроля и диагностики с улучшенными характеристиками.*** Библ. 12, рис. 6.

*Ключевые слова:* **силовые транзисторы, генератор импульсов, электромагнитное поле, электропроводный и ферромагнитный металл, высокочастотный ток, катушка индуктивности.**

**Introduction**. Recently, there has been a growing tendency to use pulse high-frequency electromechanical transducers (PHFEMT) [1-4] for measurement, control and diagnostics of electrically conductive and ferromagnetic metal products. PHFEMT can transform electromagnetic energy into high-frequency mechanical (ultrasonic). This transformation is traditionally called electromagnetic-acoustic (EMA) transformation. The physical nature of EMA transformation can be explained with the help of Fig. 1 (1 – the source of a constant polarization field; 2 – high-frequency inductor; 3 – product; 4 – power lines of a constant magnetic field; 5 – field lines of high-frequency electromagnetic field; 6 – vortex current in the surface skin layer of the product). Conductors with flat inductor current are located in parallel with the conductive or ferromagnetic metal surface (OT – object of testing). The current layer has a linear density $I = I_0 e^{j\omega t}$, which induces a current $I_f = -I_0$ and creates a uniform magnetic field with the amplitude

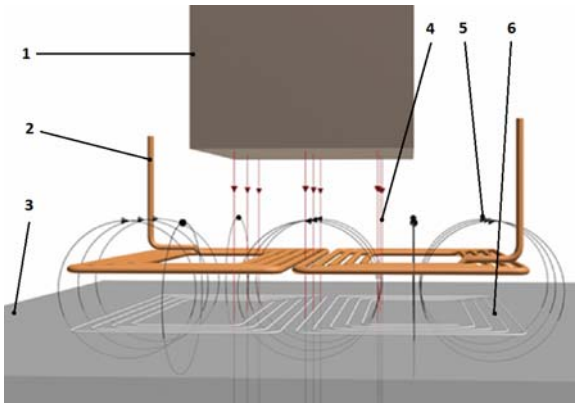


Fig.1 The diagram explains the physical effects of electromagnetic field transformation into high-frequency mechanical (ultrasonic) oscillations

$|H| \propto I_0$, where $j = \sqrt{-1}$, $\omega$ – the current frequency in the EMAT inductor. A constant polarization magnetic field

with induction $\overline{B} = \overline{x}_0 B_x + \overline{y}_0 B_y$ is applied to the surface layer of the OT under the inductor. According to [5], alternating stresses are formed in the surface skin layer of the OT, due to the interaction of the magnetic and electromagnetic fields. The total voltage $T_{xx}$ is written in the form

$$\left|T_{xx}\right| = \left|T_{xx}^{E} + T_{xx}^{M} + T_{xx}^{C}\right| = HB_y \left|1 - \frac{\mu - 1}{\mu} - j\alpha\beta_t^2\right|, \quad (1)$$

where $T_{xx}^{E}$ – the stresses formed due to the electrodynamic effect (Lorentz forces); $T_{xx}^{M}$ – voltages formed due to magnetic interaction; $T_{xx}^{C}$ – the stresses formed due to magnetostrictive effects; $\beta_t$ – generalized parameter that is equal to the ratio of the wave numbers of mechanical and electromagnetic waves $\beta_t^2 = \dfrac{\overline{\omega}}{c_t^2 \mu_0 \mu \sigma}$; $H$ – the intensity of the alternating magnetic field; $\mu_0$– the magnetic constant $4\pi \cdot 10^{-7}$ H/m; $\mu$ – the relative magnetic permeability; $c_t$ – the propagation velocity of the high-frequency elastic shear perturbation in the OT material; $\omega$ – the frequency of high-frequency elastic mechanical oscillations, which coincides with the frequency of the high-frequency current in the EMA transducer's inductor; $\alpha$ – the magnetostrictive constant; $j = \sqrt{-1}$ ; $\sigma$ – electric conductivity of the OT material.

Analysis of the equation (1) shows that the magnitude of the mechanical variable stresses depends on the induction of the polarization magnetic field and the current magnitude in the inductor. When diagnosing ferromagnetic materials, it is very difficult to generate an induction value of the magnetic field in the excitation zone of high-frequency mechanical oscillations of more than 1 T. On the other hand, it is not advisable to significantly increase the induction of the polarization magnetic field, since the EMAT attractive force to the ferromagnetic product will be significant. As a result, it is difficult to scan the OT during diagnostics.

Pulse current in the EMAT inductor can theoretically be increased without special restrictions up to tens of kiloamperes, for example by means of mechanical interrupters. However, it is impossible to use such generators in devices, especially in small ones. In addition, the problem arises when forming high-frequency current pulses in the range from tenths to tens of MHz.

This problem can be solved by increasing the peak power of current pulse sources (CPS) [6-11]. The authors in [6, 7] propose to use powerful short unipolar pulses for powering the PHFEMT, which are not difficult to obtain, for example, with the help of thyristors. However, such pulses have a wide frequency spectrum, which reduces their efficiency at given values of diagnostic frequencies. In articles [8-11], it is proposed to apply a pulse packet of certain duration and with a specified filling frequency to feed PHFEMT. In this case, the output voltage in the device [8] does not exceed 300 V, which is unacceptable. The generator [9] allows obtaining significant pulse currents in the load. However, it is made on high-voltage high-frequency electron tubes GMI-83, which require cumbersome high-voltage power supplies. Such generators consume a lot of electricity. The device is dangerous for maintenance staff. The power sources given in [10, 11] are more promising, but they do not allow increasing the output power. Therefore, the development of high power CPS is of great interest.

**The aim of the paper** is to develop the main regulations for the creation of powerful current pulse sources for feeding high-frequency electromechanical transducers for measuring, monitoring and diagnostics of electrical devices based on IGBT transistors.

**Research and analysis of the developed results.** Analysis of known literature sources [1-11] allowed formulating requirements for CPS, which should provide EMAT feeding, for example, described in [1-4], in the most constantly used frequency range. It should be formed in EMAT with an input resistance from fractions of up to several Ω current pulse packets with a filling frequency from 1 to 3 MHz. The period's number of the pulse filling frequency should be adjustable in the range 1 ... 20 pcs. The maximum peak amplitude of the current in the transducer conductors should reach several hundred amperes. The repetition frequency of the probing pulses should be regulated in the range from 0.01 to 1 kHz, depending on the OT scanning speed.

The authors based on the analysis of the power electronics elements characteristics came to the conclusion that it is expedient to use powerful IGBT transistors in the output stages. To test this assumption, experimental studies were performed of the capabilities of several modern powerful comparatively high-frequency IGBT transistors at high frequencies. It is determined that they do not allow creating a sinusoidal output signal. At the same time, it is shown that in the claimed frequency range, some IGBT transistor models switch with sufficient time intervals in push-pull circuits.

To implement the developed technical solution, it is proposed to form the CPS output pulse in the form of a meander, and the sinusoidal component allocation is carried out using the EMAT resonant circuit or a separate filter. This approach makes it possible to provide an acceptable thermal operating mode of the transistors, especially at high probing frequencies, and to obtain significant amounts of excited currents in the load. The expediency of using parallel switching up to 5 transistors in each arm of a push-pull circuit allows increasing the current in the transducer or increasing the voltage due to the use of high-frequency broadband transformers. The pre-switches in front of the output stages must be powerful enough to quickly fill the gate of the IGBT transistors of the CPS output stage. To quickly switch off the output transistors, the resistance of the pre-output transistors in the open state should be minimal.

The expediency of manufacturing CPS in the form of two main blocks – a signal generator with adjustable parameters and a high-frequency broadband power amplifier is specified.

On the basis of this approach CPS has been developed, which allows fulfilling the requirements necessary for feeding EMAT with modern monitoring, measuring and diagnostic tools. As an example of such a development Fig. 2 shows the electrical circuit diagram of a high-power high-frequency broadband generator.

The signal generator with adjustable parameters is made on a microprocessor U4 of the AT90S1200 type.

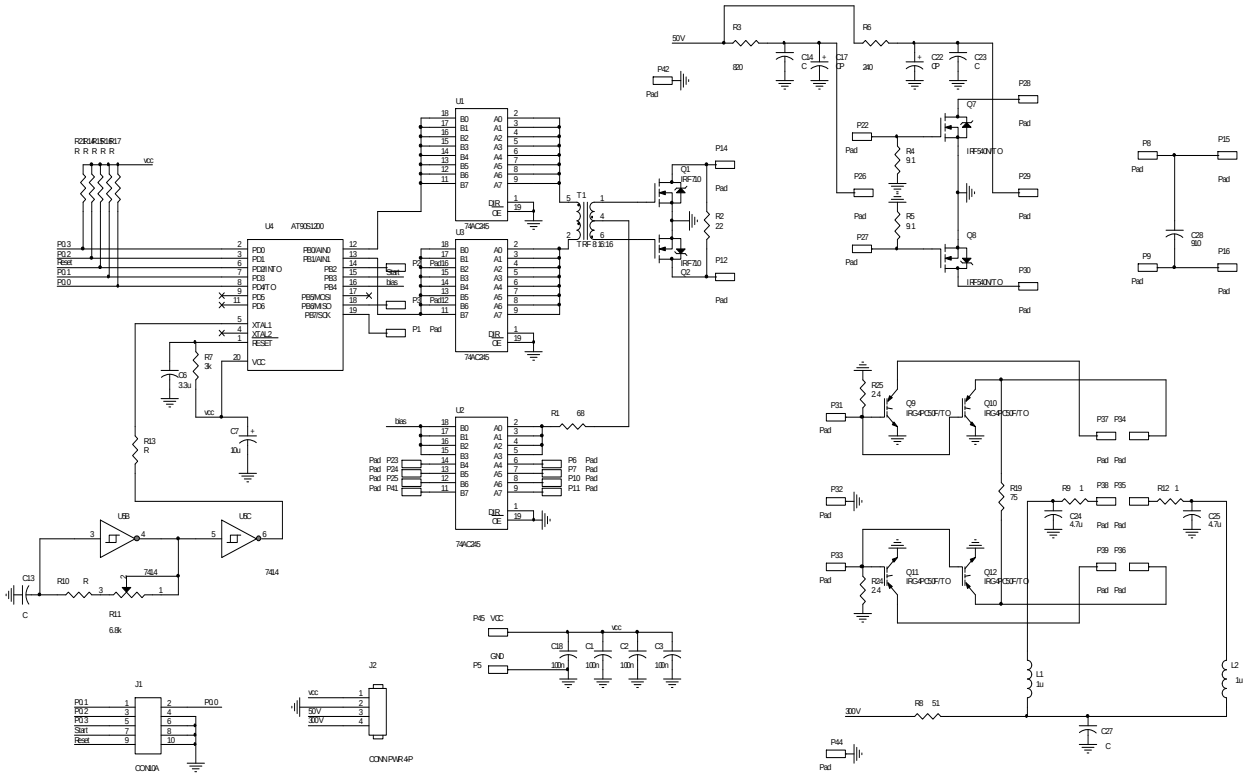

Fig. 2. Electric schematic diagram of CPS for feeding high-frequency electromechanical transducers

It forms two sequences of rectangular pulses IN1 and IN2 with an amplitude of 5V with a pulse ratio of 2 (meander) and the phase opposites that are required to power the subsequent CPS stages. The frequency, pulse ration and the number of pulses are controlled by the buttons PQ0-PQ3 and Reset. Each of the two signals from the microprocessor's output goes to the inputs of the buffered repeaters U1 and U3, executed on the chips of 74AC245 type. Buffered repeaters are used to amplify the current output signal, to provide steep edges, form rectangular pulse sequences IN1 and IN2, and to protect the microprocessor in case of short circuits in the amplifier circuit. To increase the output current, 8 inputs and 8 outputs of each buffered repeater are connected in parallel. The time diagrams of the output signals generators are shown in Fig. 3, where: T1 – the sequence period of rectangular pulses; T2 – total duration of the pulse packet; T3 – the interval period of pulse packet; T4 – the duration of the bias pulse.

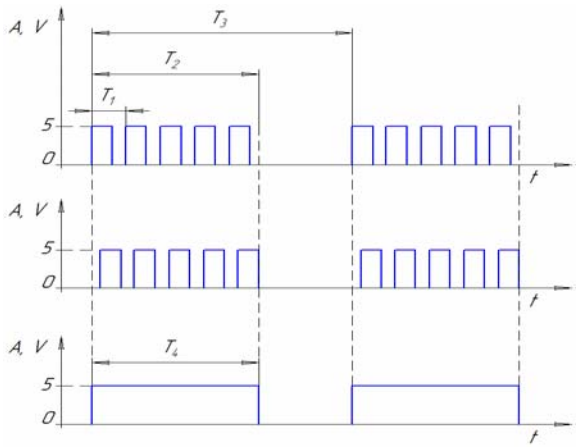


Fig. 3. Time diagram of the output signals generators

The outputs of the buffered repeaters U1 and U3 are loaded on the input winding of the high-frequency wideband transformer T1. From the transformer output T1, rectangular pulses in antiphase go to the transistors gates Q1 and Q2, switched on in a push-pull circuit. Switching on transistors at the same time ensures the sequential opening of only one of them and closing of the other one. Simultaneously, a bias pulse is applied to the middle point of the output winding of the transformer T1. It comes from the microprocessor U4 through the buffer U2 (74AC245), providing a rapid opening of the transistors Q1 and Q2 and their subsequent closing after ending the pulse packet. The duration of the bias pulse T4 is equal to the duration of the T2 packet.

From the outputs of transistors Q1 and Q2, square wave pulses of the packet signal are fed to the input of a high-frequency broadband transformer similar to T1 (not shown in the diagram). Rectangular pulses from the output of the second transformer go to the transistors gates Q7 and Q8 (IRF540N), also included in the push-pull circuit. The stage on transistors Q7 and Q8 serves to amplify rectangular pulses in voltage and current sufficient for the key output stage operation on IGBT transistors Q9 and Q10, Q11 and Q12 (IRG4PC50F), included in pairs in each arm of the push-pull circuit. Parallel switching on two IGBT transistors in each arm allowed increasing the limiting switching current and reducing losses by lowering the resistance of the arm in the open state. The output stage is connected to the previous one using a broadband high-frequency transformer similar to T1 (not shown in the diagram). The output stage is also loaded on a broadband high-frequency transformer (not shown in the diagram), which output is connected to the EMAT, for example [1].

Power units of the generator's stages are not shown in the diagram. To test the developed CPS characteristics, tests were performed when it was connected to the active load and when the EMAT load was operating in a resonance mode.

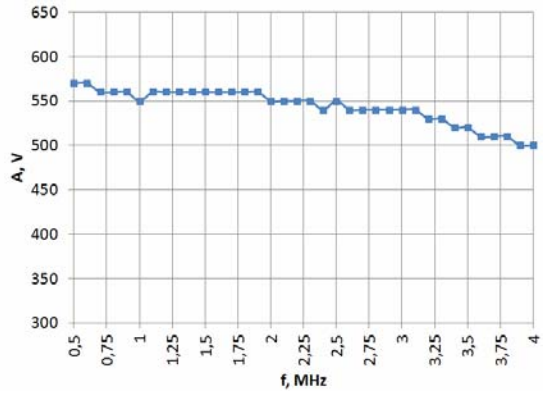


Fig.4. Amplitude-frequency response of CPS with an active load equal to 0.5 Ω

Fig. 4 shows the amplitude-frequency response of CPS with an active load equal to 0.5 Ω in the frequency range exceeding the range of 1 ... 3 MHz. The measurements were performed using an oscilloscope SDS7202.

Data analysis (Fig. 4) shows that the amplitude-frequency response of CPS in the frequency range 1 ... 3 MHz is close to uniform. This means that the use of IGBT transistors in the switching mode in the output push-pull stages allows covering the traditionally used frequency range for measurements, monitoring and diagnostics. In this case, the peak current in the active load exceeds 100 A.

Studying generator's operation when connecting resonant EMAT, the following procedure was used. The high-frequency electromechanical transducer [1] was mounted on a metal (high-carbon steel) with various gaps between the inductor and the metal. The CPS frequency controller fed EMAT into resonance. It is taken into account that the basis of any EMAT is a high-frequency inductor and that the inductance of this inductor is different for different gaps. Consequently, the resonant frequency of the transducer will also be different. This position was confirmed by the data in Fig. 5, which showed the amplitude-frequency response of CPS together with EMAT resonant type. In this case, the high-frequency inductor was connected in parallel with an additional capacitor of $10^4$ pF. The inductance of the high-frequency inductor, taking into account power cables and CPS output parameters, was about 1 ... 2 μH. The backlash was established with the help of gaskets made of glass-textile of various thicknesses. The measurements were performed using an oscilloscope SDS7202.

Data analysis (Fig. 5) shows that when the gap is reduced, the EMAT resonance frequency increases approximately in inverse proportion to the frequency of the power current: with a gap of 7 mm – about 1.3 MHz; with a gap of 4.5 mm – about 1.6 MHz; with a gap of 2 mm – about 2.05 MHz and with a gap of 1 mm – about 2.45 MHz. These data confirm that CPS must necessarily have a frequency regulation of the power current. Its own amplitude-frequency response should be close to linear in order to ensure the same power conditions for the transducer. Especially these requirements are important for automatic or automated measurements, monitoring and diagnostics, when it is impossible to maintain the exact gap size (usually several millimeters).

It is obvious that the CPS current feeding the EMAT can not instantaneously bring into operation the parallel resonant circuit of the electromechanical transducer. This requires several periods of the generator current frequency, Fig. 6. At the same time, the required number of periods for EMAT output to the operating mode also depends on the gap size. Consequently, it is necessary to regulate the periods number of the filling frequency for the pulse packet of the CRPG.

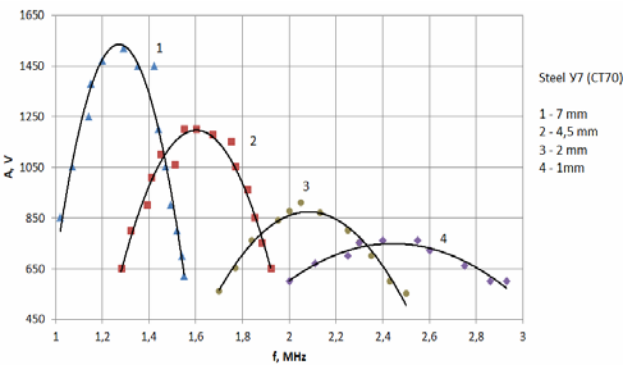


Fig. 5. The amplitude-frequency response of a high-frequency resonant electromechanical transducer [10] connected to CPS at distances (gaps) between a high-frequency conductor and an electrically conductive ferromagnetic OT surface: 1 – 7 mm; 2 – 4.5 mm; 3 – 2 mm; 4 – 1 mm

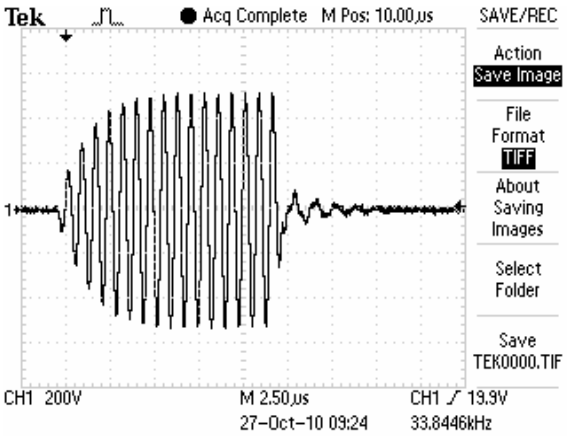


Fig. 6. A typical voltage on the EMAT [1] when feeding CPS

It is known that the current in the resonant circuit exceeds the current coming from the power source [12]. To evaluate its value, a shunt with a resistance of 0.01 Ω was built into the parallel resonant EMAT circuit. During resonance, its voltage was 4.5 V. Consequently, the current in the EMAT high-frequency conductor was about 450 A. The requirement to increase the degree of electromagnetic energy transformation into high-frequency mechanical one by increasing the current in the EMAT inductor developed by CPS on the basis of IGBT transistors is satisfied.

**Conclusions.**

1. The main regulations for the creation of powerful current pulse sources for feeding high-frequency electromechanical transducers for measuring, monitoring and diagnostics of electrical devices based on IGBT transistors are developed.

2. A practical implementation of a powerful current pulse generator based on IGBT transistors of the IRG4PC50F type is proposed, which provides currents of up to 450 A in the frequency range 1 ... 3 MHz with a pulse packet duration of 1 ... 20 in the inductor of a high-frequency electromechanical transducer.

3. It is shown that CPS provides a significant increase in the current of a high-frequency inductor when feeding the resonant EMA transducers, thereby increasing electromagnetic energy transformation into high-frequency mechanical one in electrically conductive and ferromagnetic materials.

4. The necessity to regulate the frequency and duration of power pulses for high-frequency electromechanical transducers intended for measurements, monitoring and diagnostics is determined and experimentally confirmed.

5. It is experimentally determined that the gap increase between the high-frequency EMAT inductor and the surface of an electrically conductive ferromagnetic metal leads to a decrease in the resonant frequency of the transducer, approximately in inverse proportion to the current frequency. This effect is due to the influence of metal properties on the inductance of the high-frequency EMAT inductor located with a gap above the product surface.

REFERENCES


***1.*** Miguschenko R.P., Suchkov G.M., Radev H.K., Petrischev O.N., Desyatnichenko A.V. Electromagnetic acoustic transducer for ultrasonic thickness gauging of ferromagnetic metal items without removing dielectric coating. *Technical electrodynamics*, 2016, no.2, pp. 78-82. (Rus).

***2.*** Suchkov G.M., Taranenko Yu.K., Khomyak Yu.V. A non-contact multifunctional ultrasonic transducer for measurements and non-destructive testing. *Measurement Techniques*, 2016, vol.59, no.9, pp. 990-993. **doi: 10.1007/s11018-016-1081-3.**

***3.*** Boughedda H., Hacib T., Chelabi M., Acikgoz H., Le Bihan Y. Electromagnetic acoustic transducer for cracks detection in conductive material. *2015 4th International Conference on Electrical Engineering (ICEE)*, Dec. 2015, pp. 1-4, **doi: 10.1109/INTEE.2015.7416717.**

***4.*** Li B. Application of electromagnetic acoustic in steel pipe inspection. *2016 35th Chinese Control Conference (CCC)*, Jul. 2016, pp. 9539-9542. **doi: 10.1109/ChiCC.2016.7554872**.

***5.*** Ermolov I.N. *Teoriya i praktika ultrazvukovogo kontrolya* [Theory and practice of ultrasonic testing]. Moscow, Mashinostroenie Publ., 1981. 240 p. (Rus).

***6.*** Zhukov V.K., Ol'shanskii V.P. Electromagnetic-acoustic equipment UVT-01N for inspecting the wall thickness of drilling pipes. *The Soviet journal of nondestructive testing*, 1986, vol.22, iss.2, pp. 76-80.

***7.*** Bolyukh V.F., Oleksenko S.V., Shchukin I.S. Comparative analysis of linear pulse electromechanical converters electromagnetic and induction types. *Technical electrodynamics*, 2016, no.5, pp. 46-48. (Rus).

***8.*** Viskushenko A.A., Remnev A.M., Smerdov V.Yu. *A High-Voltage Pulse-Packet Shaper*. *Instruments and Experimental Techniques*, 2001, vol.44, iss.1, pp. 58-60. **doi: 10.1023/A:1004128932683.**

***9.*** Pachkovskii L.S., Nevolin O.V. High-power broadband radio-frequency pulse generator to excite ultrasonic vibrations by the contactless electromagnetic-acoustic method. *Sov. J. Nondestr. Test.*, 1977, vol.13, iss.6, pp. 704-706.

***10.*** Suchkov G.M., Petrishchev O.N., Cherednichenko I.V., Fedorov V.V., Desyatnichenko A.V, Khashchina S.V., Maslova M.S. A generator of probing pulses for EMA flaw detectors. *Russian Journal of Nondestructive Testing*, 2012, vol.48, no.9, pp. 537-540. **doi: 10.1134/s1061830912090082**.

***11.*** Miguschenko R.P., Suchkov G.M., Taranenko Yu.K., Petrischev O.N., Desyatnichenko A.V. Generators of current sounding impulses for supplying electromagnetic acoustic transducers. *Quality Control Tools and Techniques*, 2015, no.2(35), pp. 5-11. (Rus).

***12.*** Aseev B.P. *Osnovyi radiotehniki* [Foundations of radiotechnics]. Moscow, Svyazizdat Publ., 1947. 572 p. (Rus).



*Received 02.12.2017*



*S.Yu. Plesnetsov*[1], *Candidate of Technical Science,*
*O.N. Petrishchev*[2], *Doctor of Technical Sciences, Professor,*
*R.P. Mygushchenko*[1], *Doctor of Technical Science,*
*G.M. Suchkov*[1], *Doctor of Technical Sciences, Professor,*
*S.V. Sotnik*[3], *Candidate of Technical Sciences,*
*O.Yu. Kropachek*[1], *Candidate of Technical Science,*
[1] National Technical University «Kharkiv Polytechnic Institute»,
2, Kyrpychova Str., Kharkiv, 61002, Ukraine,
e-mail: krskd.kpi@gmail.com, hpi.suchkov@gmail.com
[2] National Technical University of Ukraine «Igor Sikorsky Kyiv Polytechnic Institute»,
37, Prosp. Peremohy, Kyiv, Ukraine, 03056,
e-mail: om.petrischev@aae.kpi.ua
[3] Kharkiv National University of Radio Electronics,
14, Nauka Ave., Kharkiv, Ukraine, 61166,
e-mail: svetlana.sotnik@nure.ua



*How to cite this article:*
Plesnetsov S.Yu., Petrishchev O.N., Mygushchenko R.P., Suchkov G.M., Sotnik S.V., Kropachek O.Yu. Powerful sources of pulse high-frequency electromechanical transducers for measurement, testing and diagnostics. *Electrical engineering & electromechanics*, 2018, no.2, pp. 31-35. **doi: 10.20998/2074-272X.2018.2.05.**

UDC 621.3.01 **doi: 10.20998/2074-272X.2018.2.06**

B.I. Kuznetsov, T.B. Nikitina, I.V. Bovdyj, A.V. Voloshko, E.V. Vinichenko, B.B. Kobilyanskiy

# DEVELOPMENT AND INVESTIGATION OF LAYOUT OF ACTIVE SCREENING SYSTEM OF THE MAGNETIC FIELD GENERATED BY GROUP OF OVERHEAD TRANSMISSION LINES

***Purpose.*** *Development and field experimental research of layout of the single-circuit active screening system of the magnetic field generated by group of high voltage transmission lines in residential area is given.* ***Methodology.*** *Mathematical model of magnetic field, generated by group of high voltage transmission lines in residential area, based of the experimental values of magnetic field flux density in given points on the basis of optimization problem solving is improved. The objective of the synthesis of the single circuit active screening system is to determine their number, configuration, spatial arrangement, wiring diagrams and compensation cables currents, setting algorithm of the control systems as well as the resulting value of the magnetic flux density at the points of the protected space. Synthesis of the full-scale model of active screening system is reduced to the problem of multiobjective nonlinear programming with constraints in which calculation of the objective functions and constraints are carried out on the basis of the Maxwell equations solutions in the quasi-stationary approximation. The problem is solved by a stochastic multiswarm multi-agent particles optimization.* ***Results.*** *The single-circuit active screening system synthesis results for reduction of a magnetic field generated by group of high voltage transmission lines in residential area is given. Field experimental researches of the single-circuit active screening system of the magnetic field generated by group of high voltage transmission lines in residential area with various control algorithms is given.* ***Originality.*** *For the first time out the development and field experimental studies of the single-circuit active screening system of the magnetic field generated by group of high voltage transmission lines in residential area are carried out.* ***Practical value.*** *Practical recommendations on reasonable choice of the spatial arrangement of compensating cables of single-circuit active screening systems of the magnetic field generated by group of high voltage transmission lines is given. Results of field experimental investigations of the single-circuit active screening system of the magnetic field generated by group of high voltage transmission lines in residential area are given***.** References 12, figures 5.

*Key words*: **overhead transmission lines, power frequency technogenic magnetic field, layout of single-circuit active screening system, field experimental investigations.**

***Разработан макет одноконтурной системы активного экранирования магнитного поля, создаваемого в жилом помещении группой ЛЭП. Пространственное расположение и геометрические размеры компенсирующей обмотки, а также параметры регуляторов определены на основе решения задачи многокритериальной оптимизации. Проведены полевые экспериментальные исследования макета системы с разомкнутым и замкнутым управлением. Показано, что эффективность системы при разомкнутом и замкнутом управлении примерно одинаковая и составляет более 4 единиц. Приведены результаты сравнения экспериментальных и расчетных значений индукции магнитного поля в зоне экранирования. Показано, что экспериментальные и расчетные значения индукции магнитного поля отличаются не более чем на 20 %.*** Библ. 12, рис. 5.

*Ключевые слова*: **воздушные линии электропередачи, магнитное поле промышленной частоты, макет одноконтурной система активного экранирования, полевые экспериментальные исследования.**

**Introduction**. The flux density of the magnetic field (MF) of the power frequency outside the guard zones of high voltage power transmission lines (TL) in some cases exceeds the boundary permissible level of 0.5 μT [1], which poses a threat to the health of the population and requires taking certain measures to reduce MF of the existing TL in line of cities of Ukraine. Economically the most suitable for Ukraine are [2] methods of active contour screening of operating TL realizing by means of active screening systems (ASS) [3-10].

**Analysis of existing active screening systems.** In [10], a method for the synthesis of the ASS of the MF was developed, and in [11] experimental studies of the ASS layout with a different number of compensating windings and MF sensors operating according to various control algorithms were carried out [8, 9]. With respect to the geometric dimensions of real systems, these layouts are manufactured on a scale of 1 to 10, which causes additional errors in the layout of the ASS, caused, in particular, by the finite dimensions of the MF sensors commensurate with the dimensions of the compensating windings of the layout. In addition, studies of ASS layouts were carried out for MF, generated by a single TL. In this connection, the problem arises of verification of the synthesis method [10] of the ASS of the MF, created by a group of TL, on a full-scale ASS layout.

**The goal of the work** are development and field experimental investigations of a full-scale layoot of a single-circuit active screening system of a magnetic field created by a group of overhead transmission lines in residential premises.

**Development of the layout of a single-circuit ASS.** Fig. 1 shows the layout of a group of TLs generating MF, the flux density of which must be reduced in residential premises (hereinafter «in the screening zone»).

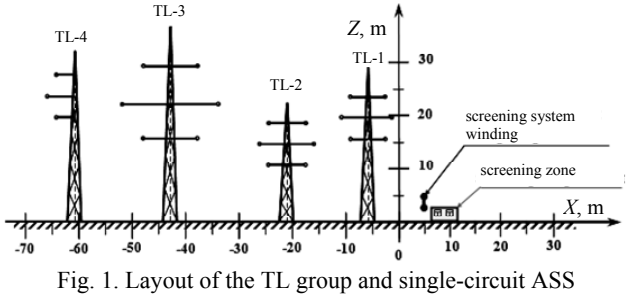


Fig. 1. Layout of the TL group and single-circuit ASS

The initial MF in the screening zone is generated by two double-circuit 110 kV TLs (TL-1 and TL-2), a two-circuit 330 kV TL (TL-3) and a single-circuit 330 kV TL (TL-4). Fig. 1 also shows the zone in which the MF is to be screened. On the basis of experimental studies, it was found that in the screening zone, the MF has an insignificant polarization [12], which makes it possible to use a single-circuit ASS with one compensation winding. In the synthesis of the ASS layout, constraints on the geometric dimensions and the location of the supports of its compensation winding were taken into account.

Fig. 2,*a* shows the calculation scheme of the layout of the single-circuit ASS, screening zone and compensating winding.

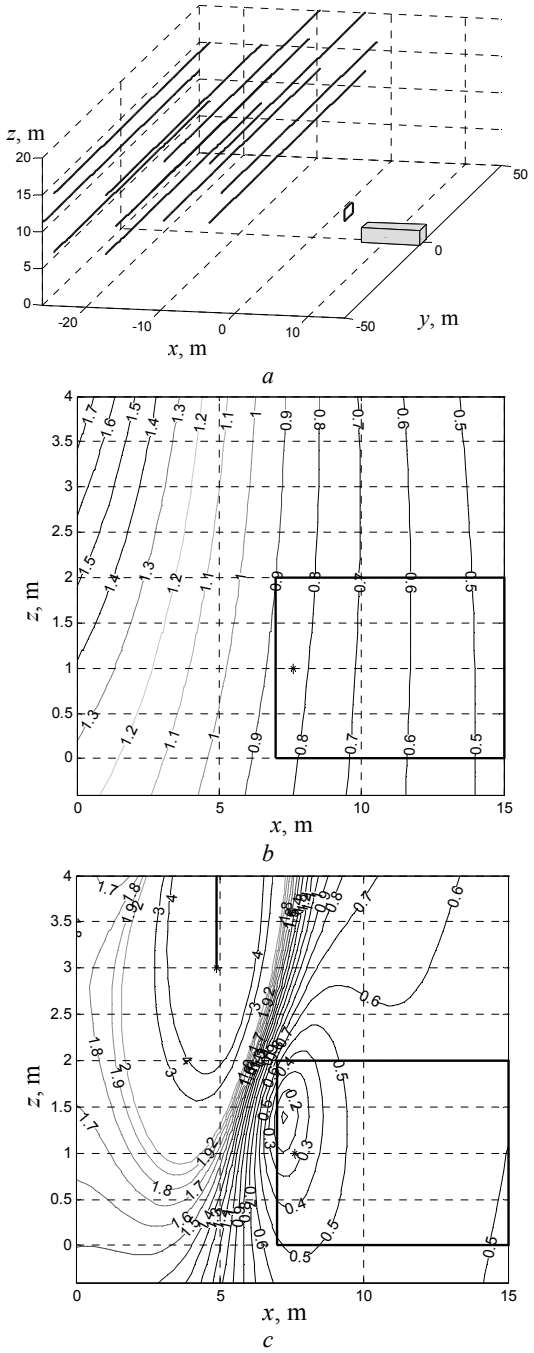


Fig 2. The calculation scheme of the layout of a single-loop ASS (*a*), distribution of the MF initial (*b*) and with the switched on ASS (*c*)

Fig. 2,*b* shows the distribution of the flux density of the initial MF, created by a group of TL, and Fig. 2,*c* – flux density distribution of MF with switched on ASS. The initial flux density of the MF in the space under consideration is 0.9 μT, and with the switched on ASS, the level of the flux density of the magnetic field does not exceed 0.4 μT.

Fig. 3 shows the spatio-temporal characteristics (STC) of MF, created by: *1* – a group of TLs; *2* – compensating winding, and *3* – total magnetic field with the system switched on. As can be seen from this figure, in the space under consideration, the initial MF produced by the TL group has a negligible polarization, so that its STC represents a strongly elongated ellipse, and the ellipse coefficient (ratio of the smaller semiaxis of the ellipse to the larger semiaxis) is about 0.4, which is confirmed by the experimental research.

STC of the MF, created by the winding of a single-circuit ASS is a line and, consequently, this MF has no polarization. With this winding, the larger semiaxis of the STC ellipse of the original MF is compensated, so that the STC of the resultant MF remaining after the operation of the ASS is an ellipse with an ellipse coefficient equal to 0.8.

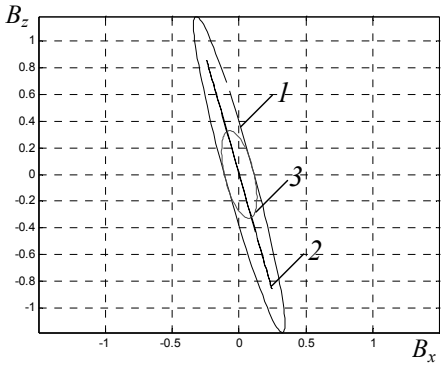


Fig. 3. Spatio-temporal characteristics of the MF created by: a group of TLs (*1*); compensating winding (*2*), and total MF with switched on ASS (*3*)

**Implementation of the layout of a single-circuit ASS.** The layout of a single-circuit ASS contains [10] one square winding, the upper part of which is located at a height of 5.1 m, and the lower one – at a height of 3.1 m. The winding contains 20 turns and is powered by an amplifier of the TDA7294 type. The inductive sensor is used as the flux density sensor of the MF, and the flux density measurement of the MF is performed by a magnetometer of the EMF-828 type from Lutron. The ASS is powered by an autonomous source.

The winding control system is built on the principle of subordinate regulation and contains an internal current regulator and an external regulator of the flux density of the MF.

**Results of field experimental studies of the open-loop single-circuit ASS layout.** To realize the open control of the ASS, the MF sensor was installed in the immediate vicinity of the TL wires and at some distance from the screening zone. With the help of such a MF sensor, the flux density of the magnetic field produced by only the TL is measured and, consequently, the output

voltage of such a MF sensor is proportional to the current of one of the phases of the TL wire or their superposition. Thus, an indirect measurement of the currents of the TL generating the initial MF is carried out, and the ASS on the basis of such a MF sensor, on the principle of its construction, is open.

Fig. 4 shows the experimental flux density distributions of: *a*) the initial MF, created by the TL group and *b*) – *d*) the total MF with the switched on ASS.

The initial flux density of MF in the space under consideration is 1.15 μT, which is more than twice the boundary permissible level in 0.5 μT [1].

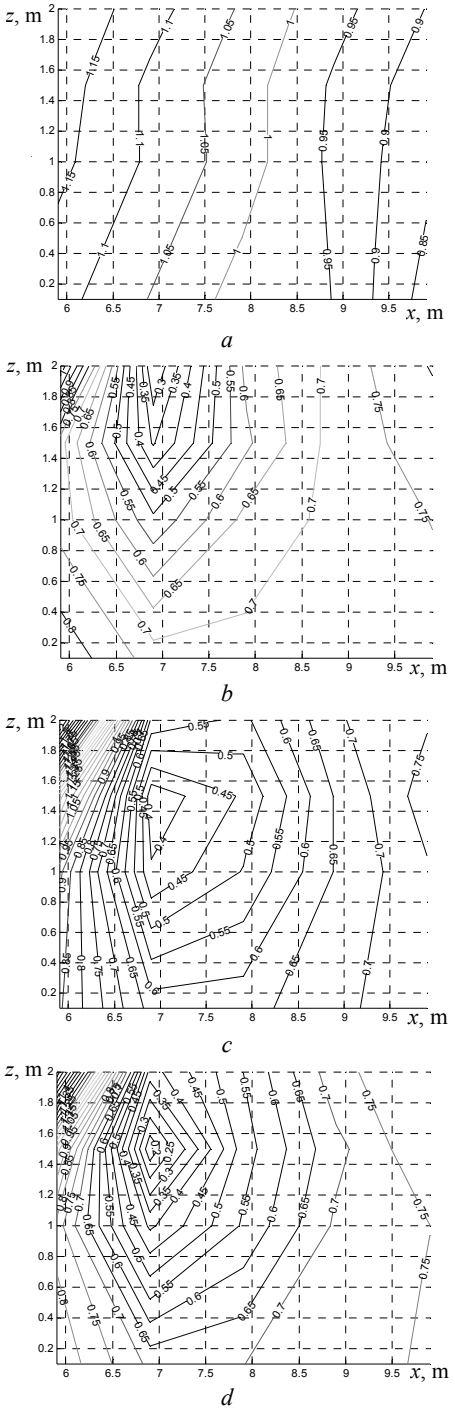


Fig. 4. Lines of equal level of the magnetic flux density module of: *a*) the initial magnetic field produced by the TL group and *b*) – *d*) the total magnetic field with the switched on open ASS

The adjustment of the open ASS was performed in such a way as to minimize the flux density of the MF at a given point in the space where it is necessary to screen the original MF. In particular, Fig. 4,*b* – *d* show the distributions of the total MF with the switched on ASS at its adjustment to different points of the screening zone. Note that in the adjustment points of the ASS, the flux density of the MF has a minimum value, practically the same for any adjustment point, and is 0.2 μT.

**Field experimental studies of the layout of a closed single-circuit ASS.** To implement closed-loop control, the MF sensor was installed directly in the screening zone.

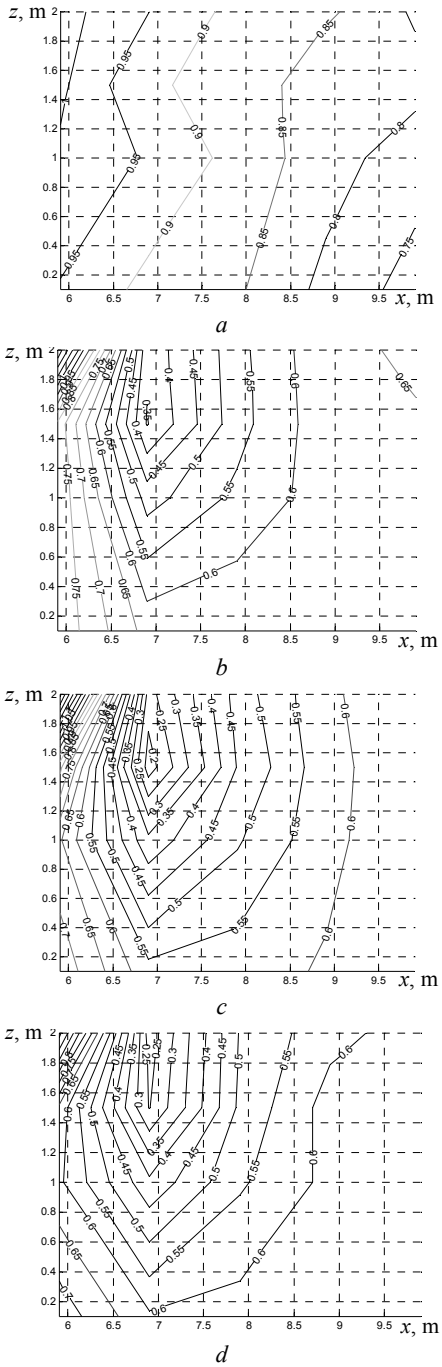


Fig. 5. Lines of equal level of the magnetic flux density module of: *a*) the initial magnetic field produced by the TL group and *b*) – *d*) the total magnetic field with the switched on closed ASS

Here, with the help of such a MF sensor, the flux density of the total MF, created in the screening zone by the wires of the TL and the compensation winding, is measured, and the ASS on the basis of such a sensor becomes closed on the basis of its construction principle.

Fig. 5 shows the magnetic flux density distributions of: *a*) the initial MF, created by the TL group and *b*) – *d*) the total MF with the switched on enclosed ASS at a different position of the MF sensor. With the help of a closed ASS, the flux density of the MF at the point of installation of the MF sensor is minimized. In this case, the minimum value of the flux density in the three considered variants is 0.2 μT, but the distribution of the magnetic field in the screening zone depends significantly on the position of the MF sensor.

The initial flux density of the MF in the space under consideration is 0.95 μT, and when the closed ASS is switched on, the level of the flux density of the magnetic field does not exceed 0.4 μT.

Note that the efficiency of the closed system depends on the location in the screening zone of the MF sensor. Moreover, with one compensation winding, an important issue is also the spatial orientation of this MF sensor, which ensures the maximum efficiency of a closed system.

In general, a closed ASS minimizes the level of the magnetic field at the location of the MF sensor. Therefore, one of the possible approaches to the problem of determining the location of the MF sensor is its placement at a point in space in which the flux density value of the MF calculated in the synthesis of the ASS assumes a minimum value. In this case, a closed ASS provides the maximum screening efficiency in a given space.

The advantage of a closed ASS is also the possibility of compensating both the external MF, generated by TL, and the internal MF, generated, for example, by household electric appliances located near the screening zone, by electric floors, etc. In addition, when the parameters of a closed ASS change, its efficiency varies insignificantly, i.e. the closed system has more robustness in comparison with the open system. However, with significant changes in parameters, a closed system may lose stability and, therefore, become inoperable. In addition, the measurement of the magnetic field at the point at which the level of the total MF has a minimum value leads to an increase in measurement noise and, consequently, to a deterioration in the efficiency of the closed system operation.

The advantage of an open ASS is the use of an MF sensor located near the TL wires, where the level of the flux density of the initial MF is sufficiently large and, therefore, can be measured with a high signal-to-noise ratio. Therefore, in an open system, the noise level can be substantially smaller than the noise of measuring the MF in a closed system. In addition, in the open system when the parameters of the system are changed, its stable operation is always ensured, although the efficiency of its operation can be reduced due to undercompensation or overcompensation of the initial MF.

A comparison of the results of the MF distribution of the synthesized single-circuit ASS, shown in Fig. 2,*c*, with the experimental MF distributions of the open and closed single-circuit ASS shown in Fig. 4,*b-d* and Fig. 5,*b – d* showed that they differ by not more than 20 %.

**Conclusions.**

1. A full-scale layout of a single-circuit system for active screening of a magnetic field created in the screening zone by a group of overhead transmission lines is developed, taking into account the limitations on the spatial arrangement and geometric dimensions of the compensating winding.

2. Field experimental studies of the layout of a single-circuit active screening system of magnetic field with open and closed control algorithms are carried out. It is shown that the efficiency of an open and closed system is approximately the same and is more than 4 units.

3. Comparison of the results of experimental and calculated values of the magnetic field flux density in the screening zone shows that their spread does not exceed 20%, which confirms the adequacy of the developed method for synthesizing the active screening system layout and the possibility of using it for creating real active screening systems.

REFERENCES


***1.*** Rozov V., Grinchenko V. Simulation and analysis of power frequency electromagnetic field in buildings closed to overhead lines. *2017 IEEE First Ukraine Conference on Electrical and Computer Engineering (UKRCON)*. Kyiv, Ukraine, pp. 500-503. **doi: 10.1109/UKRCON.2017.8100538**.

***2.*** Voloshko O.V. Synthesis of active shielding systems of power transmission lines magnetic field. *Visnyk of the National Academy of Sciences of Ukraine*, 2017, no.7, pp. 64-73. (Ukr). **doi: 10.15407/visn2017.07.064**.

***3.*** Active Magnetic Shielding (Field Cancellation). Available at: http://www.emfservices.com/afcs.html (accessed 10 September 2012).

***4.*** Beltran H., Fuster V., García M. Magnetic field reduction screening system for a magnetic field source used in industrial applications. *9 Congreso Hispano Luso de Ingeniería Eléctrica (9 CHLIE)*, Marbella (Málaga, Spain), 2005, pp. 84-99.

***5.*** Celozzi S., Garzia F. Active shielding for power-frequency magnetic field reduction using genetic algorithms optimization. *IEE Proceedings – Science, Measurement and Technology*, 2004, Vol.151, no.1, pp. 2-7. **doi: 10.1049/ip-smt:20040002**.

***6.*** Shenkman A., Sonkin N., Kamensky V. Active protection from electromagnetic field hazards of a high voltage power line. *HAIT Journal of Science and Engineering. Series B: Applied Sciences and Engineering*, Vol. 2, Issues 1-2, pp. 254-265.

***7.*** Celozzi S. Active compensation and partial shields for the power-frequency magnetic field reduction. *Conference Paper of IEEE International Symposium on Electromagnetic Compatibility*. Minneapolis (USA), 2002, Vol.1, pp. 222-226. **doi: 10.1109/isemc.2002.1032478.**

***8.*** Shydlovskyi A.K., Rozov V.Yu. The system of automatic compensation of external magnetic fields of energy-objects. *Technical electrodynamics*, 1996, no.1, pp. 3-9. (Rus).

***9.*** Rozov V.Y., Assyirov D.A. Method of external magnetic field active shielding of technical objects. *Technical electrodynamics. Thematic issue «Problems of modern electrical engineering»*, 2006, chapter 3, pp. 13-16. (Rus).

***10.*** Kuznetsov B.I., Turenko A.N., Nikitina T.B., Voloshko A.V., Kolomiets V.V. Method of synthesis of closed-loop

systems of active shielding magnetic field of power transmission lines. *Technical electrodynamics*, 2016, no.4, pp. 8-10. (Rus).
***11.*** Kuznetsov B.I., Nikitina T.B., Voloshko A.V., Bovdyj I.V., Vinichenko E.V., Kobilyanskiy B.B. Experimental research of magnetic field sensors spatial arrangement influence on efficiency of closed loop of active screening system of magnetic field of power line. *Electrical engineering & electromechanics*, 2017, no.1, pp. 16-20. **doi: 10.20998/2074-272X.2017.1.03.**
***12.*** Rozov V.Yu., Reutskyi S.Yu. Pyliugina O.Yu. The method of calculation of the magnetic field of three-phase power lines. *Technical electrodynamics*, 2014, no.5, pp. 11-13. (Rus).

*Received 15.12.2017*

*B.I. Kuznetsov*[1], *Doctor of Technical Science, Professor,*
*T.B. Nikitina*[2], *Doctor of Technical Science, Professor,*
*I.V. Bovdyj*[1], *Candidate of Technical Science,*
*A.V. Voloshko*[1], *Candidate of Technical Science,*
*E.V. Vinichenko*[1], *Candidate of Technical Science,*
*B.B. Kobilyanskiy*[1], *Candidate of Technical Science, Associate Professor,*
[1] State Institution «Institute of Technical Problems of Magnetism of the NAS of Ukraine»,
19, Industrialna Str., Kharkiv, 61106, Ukraine,
phone +380 50 5766900,
e-mail: kuznetsov.boris.i@gmail.com
[2] Kharkov National Automobile and Highway University,
25, Yaroslava Mudrogo Str., Kharkov, 61002, Ukraine,
e-mail: tatjana55555@gmail.com

*How to cite this article:*
Kuznetsov B.I., Nikitina T.B., Bovdyj I.V., Voloshko A.V., Vinichenko E.V., Kobilyanskiy B.B. Development and investigation of layout of active screening system of the magnetic field generated by group of overhead transmission lines. *Electrical engineering & electromechanics*, 2018, no.2, pp. 36-40. **doi: 10.20998/2074-272X.2018.2.06.**

UDC 621.319 **doi: 10.20998/2074-272X.2018.2.07**

G.V. Bezprozvannych, V.M. Zolotaryov, Yu.A. Antonets

# EFFECT OF THE THICKNESS OF INSULATION OF PROTECTED WIRES OF HIGH-VOLTAGE OVERHEAD TRANSMISSION LINES TO THEIR CURRENT CARRYING CAPACITY

***Introduction. The main direction of technical policy in the design, construction and technical re-equipment of transmission lines is the modernization of electrical networks and increase their energy efficiency in order to increase the throughput and reliability. Problem. Existing calculation methods do not take into account the influence of insulation thickness on the long-term current load of the wires according to the values of the maximum permissible working temperature of the conductors. Purpose. The investigation of the influence of insulation thickness of the protected wires of high-voltage*** **electric transmission lines** ***on their current carrying capacity. Methodology. The long operating temperature of the wire when the rated load current flows is determined based on the heat balance equation. Results. A method has been developed for determining the optimum thickness of polyethylene cross linked and oxide insulation to provide the lowest thermal resistance to the heat transfer of protected wires, the use of which allows increasing the current carrying capacity by 20 % compared to bare wires. It is shown that the internal temperature drop in cross linked polyethylene insulation is an order of magnitude smaller in comparison with the oxide insulation at identical values of the dielectric loss tangent. Originality. The calculations take into account the presence on the surface of a non-insulated aluminum conductor of a natural dense film based on aluminum oxide, which protects it from further contact with air. The capacitance of a single phase conductor with insulation is determined on the basis of the calculation of the electric field in a piecewise homogeneous medium by the method of secondary sources.*** References 12, tables 3, figures 5.

*Key words:* **bare conductor, protected wire, cross-linked polyethylene insulation, oxide insulation, thermal resistance, optimal insulation thickness, heat balance, effective heat transfer coefficient, current carrying capacity.**

***Разработана методика определения оптимальной толщины полиэтиленовой сшитой и оксидной изоляции для обеспечения наименьшего теплового сопротивления теплопередаче защищенных и неизолированных проводов. Обоснована применимость разработанной методики для оптимизации толщины изоляции защищенных проводов напряжением 20 кВ. Показана возможность повышения пропускной способности по току защищенных проводов на 20 % по сравнению с неизолированными проводами за счет оптимизации толщины их изоляции. Установлено, что внутренний перепад температуры в сшитой полиэтиленовой изоляции на порядок меньше в сравнении с оксидной изоляции при одинаковых значениях тангенса угла диэлектрических потерь***. Библ. 12, табл. 3, рис. 5.

*Ключевые слова:* **неизолированные провода, защищенные провода, сшитая полиэтиленовая изоляция, оксидная изоляция, тепловое сопротивление, оптимальная толщина изоляции, тепловой баланс, эффективный коэффициент теплопередачи, пропускная способность по току.**

**Introduction.** The main direction of the technical policy in the design, construction and technical re-equipment of transmission lines (TLs) is the modernization of electric networks and increase of their energy efficiency with the purpose of increasing the capacity and reliability, reducing losses on the basis of an innovative approach to the development and modernization of the existing power transmission complex [1]. Technical re-equipment, reconstruction of electric networks and their development should be carried out on the domestic regulatory framework, taking into account the recommendations of the International Electrotechnical Commission and regional peculiarities regarding the conditions of reliability and environmental safety, taking into account the real cost of land and maximum use of basic materials and equipment of own production.

One of the main directions of work in the construction of high-voltage TLs with increased current carrying capacity is the creation of new types of wires: high-temperature non-insulated ones based on aluminum alloys [2] and protected [3, 4]. The use of high-temperature wires with increased current carrying capacity in two times at an increase in cost, practically by an order of magnitude, is most effectively for high-voltage TLs of 110 kV and above [2].

As a progressive alternative to standard non-insulated aluminum wires for high-voltage TLs of voltage class 6-110 kV, it is possible to consider protected wires (PW). The design of a protected wire is a single-stranded multiwire conductor covered with a protective sheath [3, 4]. The conductor is made of aluminum alloy, the protective layer is made of light-stabilized cross-linked polyethylene. The permissible long operating temperature of cross-linked polyethylene insulation corresponds to 90 °C [3, 4]. The operating temperature of non-insulated aluminum wires does not exceed 75 °C [5].

The use of PW provides an increase in the current carrying capacity of high-voltage transmission lines in comparison with non-insulated aluminum wires [3, 5] (Table 1).

Table 1

Current carrying capacity of aluminum non-insulated and protected wires based on cross-linked polyethylene insulation with thickness of 2.3 mm of high-voltage TL with voltage of 20 kV (ambient air temperature 25 °C)

| Strand cross-section $S$, mm$^2$ | 70 | 120 | 150 | 185 | 240 |
|---|---|---|---|---|---|
| Continuous load current of bare wire $I$, A | 235 | 330 | 370 | 430 | 500 |
| Continuous load current of PW $I$, A | 310 | 430 | 485 | 560 | 600 |

**Problem definition.** The continuous operating current flowing through the solid conductor is determined on the basis of the thermal calculation [6] and depends on: the active resistance of the strand $R_g$, the strand temperature $T_g$ and the ambient temperature $T_c$, the thermal insulation resistance $R_{ts}$ and the environment (air) resistance $R_{oc}$, the dielectric loss power in insulation $P_d = U_f^2 \omega C \mathrm{tg}\delta$ [7]

$$I = \sqrt{\frac{T_g - T_c - P_d(R_{ts} + R_{oc})}{R_g \cdot (R_{ts} + R_{oc})}}, \quad (1)$$

where $U_f$ is the phase voltage, $\omega$ is the angular frequency, $C$ – is the own capacitance of wire, $\mathrm{tg}\delta$ is the tangent of the dielectric loss angle of insulation.

Existing calculation methods [4, 7] do not take into account the influence of insulation thickness on the continuous current load of the wires by the values of the maximum permissible working temperature of the conductors (strands). The need to analyze the effect of the thickness of cross-linked polyethylene insulation on the long-term permissible working temperature of protected wires is an urgent task, because it allows you to optimize the size of the wire.

**The goal of the paper** is investigation of the influence of the insulation thickness of the protected wires of high-voltage TLs on their current carrying capacity.

**Method for calculating the heat balance.** The continuous operating temperature of the wire when the rated load current flows is determined on the basis of the heat balance equation between the extracted $P_v$ and the dissipated $P_{otd}$ power [8]

$$P_v = P_{otd} . \quad (2)$$

The heat extract power is determined by the thermal resistance of the insulation $R_{ts}$, the temperature of the heated strand $T_g$ and the surface temperature of the wire $T_p$ [8]

$$P_v = \frac{T_g - T_p}{R_{ts}} . \quad (3)$$

For a wire in the air, the dissipated heat power $P_{otd}$ depends on the thermal resistance of the ambient air $R_{oc}$ and the surface temperature of the wire $T_p$ and the medium temperature $T_c$ [8]

$$P_{otd} = \frac{T_p - T_c}{R_{t0}} . \quad (4)$$

The thermal insulation resistance $R_{ts}$, the thermal resistance of the ambient air $R_{oc}$ and the total thermal resistance $R_t$ are defined as [8]

$$R_{ts} = \frac{1}{2\lambda} \ln\left(\frac{d_2}{d_{21}}\right), \quad R_{t0} = \frac{1}{\alpha_{ef} S_{ts}}, \quad R_t = R_{ts} + R_{t0}, \quad (5)$$

where $\lambda$ is the insulation heat conductivity; $d_1$, $d_2 = d_1 + 2\Delta_{ins}$, $S_{ts} = \pi \cdot d_2 \cdot l_{pr}$ are the strand diameter, the insulated wire diameter, the insulation thickness and the cooling surface of a wire of length $l_{pr}$, respectively; $\alpha_{ef} = \alpha_c + \alpha_{rad}$ is the effective heat transfer coefficient to the environment due to convection of $\alpha_c$ and radiation $\alpha_{rad}$ [8, 9].

**Optimum insulation thickness for minimum heat transfer resistance.** The calculations take into account the presence on the surface of a non-insulated aluminum conductor of a natural dense film based on aluminum oxide, which protects it from further contact with air. The film thickness is unity – hundreds of nm, depending on the service life and environmental conditions [9].

Fig. 1 shows the dependence of the thermal insulation resistance $R_{ts}$ (curve 1), the heat transfer to the environment $R_{oc}$ (curve 2) and the total thermal resistance $R_t$ (curve 3) on the ratio of the diameter of the insulated wire $d_2$ to the diameter of the aluminum strand $d_1$: $K_{kp} = d_2/d_1$. For PW with an increase in the thickness of the cross-linked polyethylene insulation $\Delta_{ins}$ with an unchanged diameter of the strand $d_1$, the thermal insulation resistance $R_{ts}$ increases (Fig. 1,*a*, curve 1 for $\lambda$ = 0.25 W/m·K), and the thermal resistance $R_{oc}$ of the ambient air decreases (Fig. 1,*a*: curve 2 for $R_{oc}$ = = 17 W/m$^2$·K). The total thermal resistance $R_t$ (curve 3) has a minimum value at the intersection of the curves $R_{ts}$ and $R_{oc}$ corresponding to the critical (optimal) value $K_{kp}$. At $K > K_{kp}$, the thermal resistance to heat transfer increases, at $K < K_{kp}$ – decreases. The critical values of $K_{kp}$ are 1.5 (Fig. 1,*a*) and 70 (Fig. 1,*b*) for a protected wire made of cross-linked light-stabilized polyethylene insulation and a wire with oxide insulation, respectively.

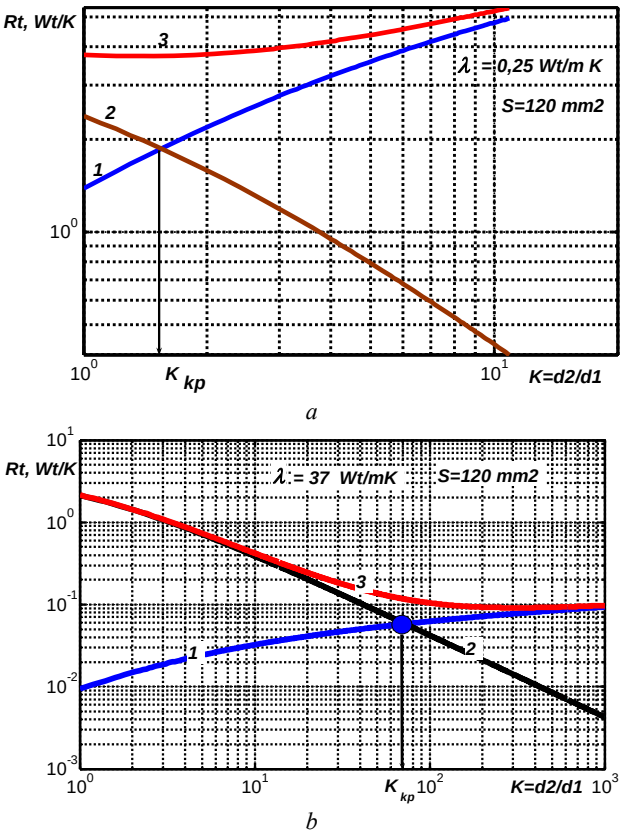


Fig. 1. To the determination of the optimum thickness of insulation of a protected wire and a wire with an oxide dielectric film at the cross-section of the strand 120 mm$^2$

The thickness of the wire insulation, corresponding to the minimum thermal resistance of heat transfer, is *optimal*. For a protected wire and an oxide-insulated wire, the optimum insulation thickness is $\Delta_{ins\,opt}$ =3.2 mm and 434 mm, respectively.

Critical values $K_{kp}$ for PW at corresponding strand cross-sections are: $K_{kp}$ =1.9 (70 mm$^2$), $K_{kp}$ =1.5 (120 mm$^2$), $K_{kp}$ =1.5 (150 mm$^2$), $K_{kp}$ =1.4 (185 mm$^2$), $K_{kp}$ =1.2 (240 mm$^2$).

**Effect of insulation thickness on the thermal stability of protected wires.** On the basis of the presented technique, a thermal calculation has been performed for a continuous current load (see Table 1) of the protected and bare wires of a high-voltage TL with voltage of 20 kV (Table 2). At this stage of the calculation, the dielectric losses power $P_d$ in insulation is not taken into account. The effective heat transfer coefficient (Fig. 2) is determined using the criterial equation of natural convection and the Stefan-Boltzmann equation [8, 9].

Table 2

Effect of insulation thickness on heat resistance of PW of high-voltage TL with voltage of 20 kV

| Aluminum strand cross-section $S$, mm$^2$ | | | | |
|---|---|---|---|---|
| 70 | 120 | 150 | 185 | 240 |
| Continuous current load $I$, A | | | | |
| 310 | 430 | 485 | 560 | 600 |
| **1. Ambient air temperature 25 °C** | | | | |
| 1.1. PW of cross-linked light-stabilized polyethylene insulation | | | | |
| The temperature of the aluminum strand $T_g$, °C: in the numerator – for the optimal insulation thickness, in the denominator – by 33 % less than the optimal | | | | |
| **81/85** | **80/84** | **80/82** | **80/81** | **75/77** |
| The temperature of the wire surface $T_p$, °C: in the numerator - for the optimal insulation thickness, in the denominator – by 33 % less than the optimal | | | | |
| **75/80** | **75/80** | **75/77** | **75/77** | **75/76** |
| 1.2. Bare aluminum wire | | | | |
| The strand temperature $T_g$, °C: in the numerator – for bare, in the denominator – with the oxide film of thickness of 100 nm | | | | |
| **105/105** | **95/95** | **92/92** | **90/90** | **82/82** |
| **2. Ambient air temperature 30 °C** | | | | |
| 2.1. PW of cross-linked light-stabilized polyethylene insulation | | | | |
| The temperature of the aluminum strand $T_g$, °C: in the numerator - for the optimal insulation thickness, in the denominator - by 33 % less than the optimal | | | | |
| **85/90** | **85/85** | **85/85** | **85/87** | **77/79** |
| The temperature of the wire surface $T_p$, °C: in the numerator – for the optimal insulation thickness, in the denominator – by 33 % less than the optimal | | | | |
| **80/85** | **80/85** | **80/82** | **80/82** | **76/78** |
| 2.2. Bare aluminum wire | | | | |
| The strand temperature $T_g$, °C: in the numerator – for bare, in the denominator – with the oxide film of thickness of 100 nm | | | | |
| **120/120** | **105/105** | **95/95** | **95/95** | **87/87** |

Fig. 2 shows the results of calculating the effective heat transfer coefficient (Fig. 2,*a*) and the thermal resistance of the surrounding medium (Fig. 2,*b*) of a protected and bare wire with different sections of the aluminum strand. An increase in the cooling surface of a protected wire in comparison with a bare wire with identical strand cross-sections leads to a decrease in the effective coefficient of heat transfer and thermal resistance (Fig. 2,*a*,*b*): curves 1 and 1' – for a protected wire with a cross-section of 120 mm$^2$ and 150 mm$^2$, 2 and 2' – for bare wire of cross-section of 120 mm$^2$ and 150 mm$^2$, respectively.

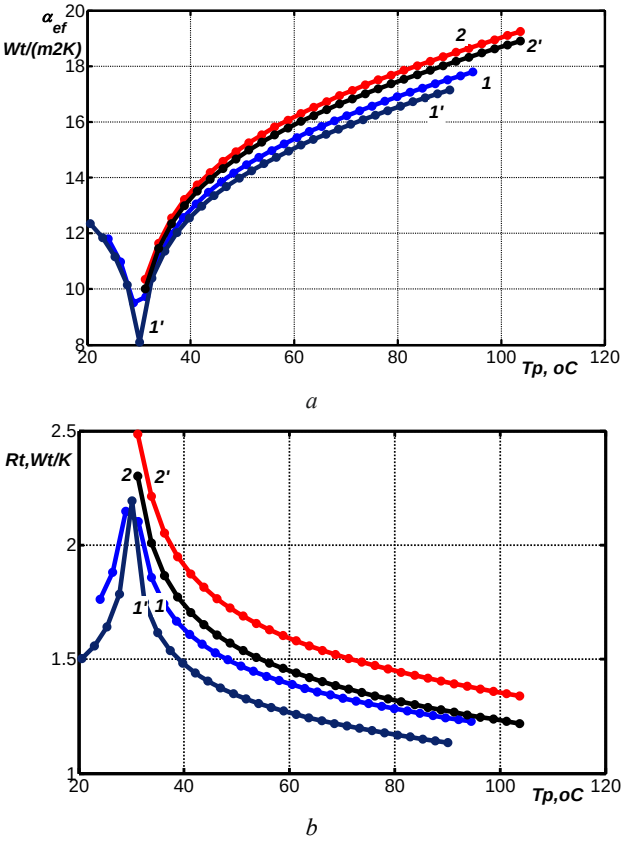


Fig. 2. The effect of the wire cooling surface on the temperature dependencies of the effective heat transfer coefficient (*a*) and thermal resistance of the environment (air) (*b*)

The results of the thermal calculation show that the protected wires, whose insulation thickness is 33 % less than the optimal one, provide current carrying capacity at an increased ambient temperature of 30 °C: the strand temperature does not exceed the permissible working temperature of the cross-linked polyethylene insulation (see Table 2, curve 4 of Fig. 3,*a*).

Reducing the thickness of cross-linked polyethylene insulation makes it possible to reduce the mass-dimensions of the protected wire.

In Fig. 3,*a* curve 1 corresponds to the extracted power, curves 2, 3, 4 and 5 – dissipated power: curves 2 and 4 correspond to the optimal insulation thickness, curves 3, 5 – 33 % less than optimal at ambient air temperature of 25 °C (curves 2, 3) and 30 °C (curves 4, 5).

The wire temperature $T_g$ of bare wires exceeds the permissible working temperature by 30 °C – 45 °C (for a 70 mm$^2$ wire) and 7 °C – 12 °C (for a 240 mm$^2$ wire) (see Table 2 and Fig. 3,*b*).

The presence on the bare wire surface of an oxide film of 100 nm thick does not affect the heat balance

condition: the temperature on the wire surface remains constant.

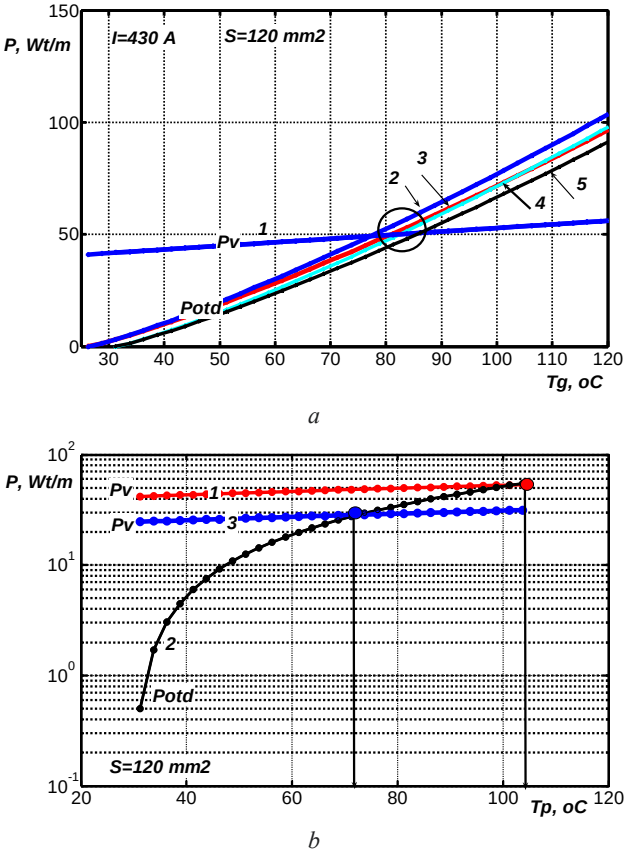


Fig. 3. Heat balance in a protected (*a*) and bare (*b*) wire

The requirement to limit the working temperature of bare wires is due to the process of possible annealing of cold-drawn aluminum wires, an increase in plastic elongation and, as a consequence, sagging arrows. At load current of 430 A, the curves of the dissipated $P_{otd}$ (curve 2) and the extracted power $P_v$ (curve 1) intersect at a point corresponding to a temperature of 105 °C (Fig. 3,*b*). Reduction of the load current up to 330 A, i.e. by 20 %, leads to the intersection of $P_v$ (curve 3) and $P_{otd}$ (curve 2) at a point corresponding to a working temperature of 75 °C (Fig. 3,*b*).

**Effect of dielectric losses in insulation on the current carrying capacity of the protected wire.** The internal temperature drop in insulation (see (1)) $\Delta T_{ins} = P_d(R_{ts} + R_{oc})$ is determined by the dielectric losses power $P_d = U_f^2 \omega C \mathrm{tg}\delta$, which depends on the electrical characteristics of insulation: the dielectric losses angle tangent and the relative permittivity determining the wire capacity. The capacity of a single phase conductor with insulation is determined on the basis of the calculation of the electric field calculation in a piecewise homogeneous medium by the method of secondary sources [11], which reduces to solving a system of linear algebraic equations (SLAE). The first *Ne* rows of SLAE follow from the Fredholm integral equation of the first kind for potentials on the surface of a current-carrying strand (electrode). The following *Nd* rows are from the Fredholm integral equation of the second kind for jumps in the normal component of the field strength $E_n$, undergoing a break at the interfaces of dielectric media with relative dielectric permittivities $\varepsilon_1$ и $\varepsilon_2$ to satisfy the condition: $\varepsilon_1 \cdot E_{1n} = \varepsilon_2 \cdot E_{2n}$. The written form of the combined SLAE has the form [12]

$$\overline{A} \cdot \overline{\sigma} = \overline{U}\ , \qquad (6)$$

where $\overline{\sigma}$ is the matrix-column of unknown calculated densities of secondary charges, C/m$^2$; $\overline{U}$ is the matrix-column, the first *Ne* elements of which reflect the given potentials of the nodes lying on the electrode, and the remaining ones are equal to zero (the potentials of the nodes lying on the interface of dielectric media); $\overline{A}$ is the square matrix of coefficient.

The total number of nodes (the number of unknown of the charge density) is $N = Ne + Nd$. Solving SLAE (6) by a numerical method, the calculated density (in vacuum) of secondary charges is determined. The field strength for the electrode surface is determined by the calculated charge density $E_i = \sigma_i / \varepsilon_0$ and for the interfaces of dielectric media $E_i = \frac{\sigma_i}{2\varepsilon_0}(1 + \frac{1}{\alpha})$, where $\alpha$ is the parameter related to the permittivity of adjacent media: $\alpha = (\varepsilon_2 - \varepsilon_1)/(\varepsilon_2 + \varepsilon_1)$ [12]. The true density $\sigma'$ of charges on the surface of the strand, which is insulated by a dielectric with relative dielectric permittivity $\varepsilon_2$, is greater by $\varepsilon_2$ times [12]. The desired capacitance is defined as the ratio of the true charge to the specified phase voltage. The wires are in the air with dielectric permittivity $\varepsilon_1 = 1$.

Fig. 4 shows the sweep of the electric field strength as a function of the length of the *SDL* generator (*SDL* corresponds to the reduction of «*sum of DL*» – the sum of a plurality of small length sections) for a PW and a 20 kV bare wire with a strand cross-section of 120 mm$^2$. Curve 1 – the optimal thickness of insulation (3.2 mm) and curve 2 – 33 % less than the optimal (2.3 mm) for a protected wire made of cross-linked polyethylene insulation (relative dielectric permittivity $\varepsilon_2$ = 2.3). Curve 3 – for a wire with oxide insulation thickness of 100 nm (relative dielectric permittivity $\varepsilon_2$ = 9: for a continuous oxide film obtained, for example, by high-voltage oxidation, the value of the relative dielectric permittivity is $\varepsilon$ = 8-10 at a frequency of 50 Hz). Section I – distribution of the field strength along the surface of the strand, section II – along the insulation surface. The relative permittivity greatly influences on the distribution of the electric field strength (compare curves 1, 2 and 3, Fig. 4): the electric field strength on the surface of the wire with the oxide film is 30 % higher in comparison with the PW with the cross-linked polyethylene insulation.

Table 3 shows the results of calculating the intrinsic capacitance of the wires for different sections and the thickness of the insulation.

The results of the calculations show (Fig. 5) that adjacent phase protective wires located by a triangular at a distance of 50 cm from each other lead to a decrease in the intrinsic capacity of the wires: 18 % for the wire at the apex of the triangle ($C_1$ = 9.7 pF/m); 8 % for two other ($C_2$ = 10.6 pF/m and $C_3$ = 10.6 pF/m).

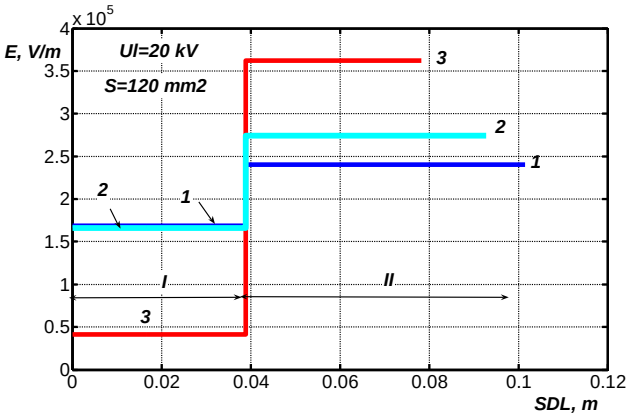


Fig. 4. The effect of the relative dielectric permittivity and insulation thickness on the distribution of the electric field strength over the wire surface

Table 3

Effect of insulation thickness on intrinsic capacitance of wires of high-voltage TL of voltage of 20 kV

| Aluminum strand cross-section $S$, mm$^2$ | | | | |
|---|---|---|---|---|
| 70 | 120 | 150 | 185 | 240 |
| **1. Protected wire capacitance $C$, pF/m** optimal insulation thickness | | | | |
| 11.1 | 11.5 | 11.7 | 11.9 | 12.1 |
| insulation thickness by 33% less than the optimal | | | | |
| 10.9 | 11.4 | 11.5 | 11.7 | 12.0 |
| **2. Wire capacitance $C$, pF/m** oxide insulation thickness 100 nm | | | | |
| 10.5 | 11.0 | 11.3 | 11.5 | 11.8 |

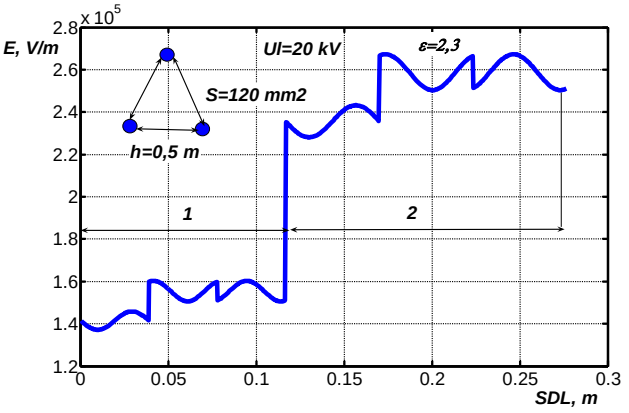


Fig. 5. The effect of near located protected wires on the distribution of the electric field strength along the surfaces of the strands (curve 1) and cross-linked polyethylene insulation (curve 2)

The dielectric losses power in XLPE insulation is $0.5 \cdot 10^{-3}$ W/m, 0.005 W/m for tg$\delta$ = 0.1 % and 1 %, respectively. The thermal resistance of the wire is 1 m·°C/W at core temperature of 90 °C and ambient air temperature of 30 °C (see Fig. 2,*b*). The internal temperature drop in the insulation $\Delta T_{ins} = P_d(R_{ts} + R_{oc})$ (see formula (1)) is 0.12 % and 1.2 % for the corresponding values of tg$\delta$ in comparison with the total temperature difference between the strand and ambient air $\Delta T = T_g - T_c$. For wire with oxide insulation $\Delta T_{ins}$ =10 % (tg$\delta$ =1 %), which causes a reduction in the permissible current load in the bare wire.

**Conclusions.**

1. For the first time, a method has been developed for determining the optimum thickness of polyethylene cross-linked and oxide insulation to provide the lowest thermal resistance to the heat transfer of protected wires, the use of which makes it possible to increase the current carrying capacity by 20% compared to bare wires.

2. The applicability of the developed technique for optimizing the thickness of insulation, both separated protected wires of various types, and for high-voltage transmission lines based on them, is justified, provided that the minimum distance between phase wires of the transmission line is limited to 0.5 m.

3. The results of the studies performed, provided they are appropriately experimentally substantiated, can become the scientific basis for the creation of a new class of compact high-voltage transmission lines with increased current carrying capacity.

REFERENCES


***1.*** *Enterprise standard. Technical policy of SE «NEK» UKRENERGO» in the field of development and operation of in trunk and interstate electric networks*. SOU NEC 20.261. Kyiv, 2017. 84 p. (Ukr).

***2.*** *Catalog of LLC «Sim-Ross-Lamifil». Energy-efficient wires of a new generation for power lines.* 2014. 26 p. (Rus).

***3.*** *DSTU 4743: 2007. Provody samoutrymni izolovani ta zakhyshcheni dlia povitrianykh linii elektroperedavannia. Zahalni tekhnichni umovy* [State Standard of Ukraine DSTU 4743: 2007. Wires self-supporting insulated and protected for overhead transmission lines. General specifications]. Kyiv, 2007. 26 p. (Ukr).

***4.*** Shcherba A.A., Peretyatko Yu.V., Zolotaryov V.V. *Samonesushchie izolirovannye i vysokovol'tnye zashchishchennye provoda* [Self-supporting insulated and high-voltage protected wires]. Institute of Electrodynamics of the NAS of Ukraine, National Technical University of Ukraine «KPI», Private Joint-stock company Yuzhcable works Publ., 2008. 271 p. (Rus).

***5.*** *Guide for qualifying high temperature conductors for use on overhead transmission lines*. CIGRÉ TB 426. 2010. 44 p.

***6.*** *IEC 60287-1-1:2006* Electric cables – Calculation of the current rating – Part 1-1: Current rating equations (100 % load factor) and calculation of losses. General specifications.

***7.*** Bezprozvannych G.V., Naboka B.G., Moskvitin E.S. Substantiation of electrophysical characteristics of high-voltage power cable semiconducting screens with stitched insulation. *Electrical engineering & electromechanics*, 2010, no.3, pp. 44-47. (Rus). **doi: 10.20998/2074-272X.2010.3.10.**

***8.*** Bezprozvannych G.V., Naboka B.G. *Matematicheskie modeli i metody rascheta elektroizoliatsionnykh konstruktsii* [Mathematical models and methods of calculation of electrical designs]. Kharkiv, NTU «KhPI» Publ., 2012. 108 p. (Rus).

***9.*** Carslaw H.S., Jaeger J.C. *Conduction of heat in solids*. *Second Ed*. Clarendon Press, London, 2003. 510 p.
***10.*** Hunter M., Fowle P. Natural and thermally formed oxide films on aluminium. *Journal of the Electrochemical Society*, 1956, vol.103, no.9, pp. 482-485. **doi: 10.1149/1.2430389.**
***11.*** Naboka B.G. *Raschety elektrostaticheskikh polei v elektroizoliatsionnoi tekhnike: uchebnoe posobie dlia studentov elektroenergeticheskikh spetsial'nostei* [Settlements electrostatic fields in the insulating technique: a textbook for students of electric power specialties]. Kiev, IEDL Publ., 1995. 120 p. (Rus).
***12.*** Bezprozvannych A.V. High electric field and partial discharges in bundled cables. *Technical electrodynamics*, 2010, no.1, pp. 23-29. (Rus).

*Received 25.01.2018*

*G.V. Bezprozvannych*[1]*, Doctor of Technical Science, Professor,*
*V.M. Zolotaryov*[2]*, Doctor of Technical Science, Professor,*
*Yu.A. Antonets*[2]*, Candidate of Technical Science,*
[1] National Technical University «Kharkiv Polytechnic Institute»,
2, Kyrpychova Str., Kharkiv, 61002, Ukraine,
phone +380 57 7076010,
e-mail: bezprozvannych@kpi.kharkov.ua
[2] Private Joint-stock company Yuzhcable works,
7, Avtogennaya Str., Kharkiv, 61099, Ukraine,
phone +380 57 7545312,
e-mail: zavod@yuzhcable.com.ua, antonets@yuzhcable.com.ua

*How to cite this article:*
Bezprozvannych G.V., Zolotaryov V.M., Antonets Yu.A. Effect of the thickness of insulation of protected wires of high-voltage overhead transmission lines to their current carrying capacity. *Electrical engineering & electromechanics*, 2018, no.2, pp. 41-46. **doi: 10.20998/2074-272X.2018.2.07.**

UDC 621.365.5 **doi: 10.20998/2074-272X.2018.2.08**

V.M. Zolotaryov, M.A. Shcherba, R.V. Belyanin, R.P. Mygushchenko, I.M. Korzhov

# ELECTROMECHANICAL TRANSIENT PROCESSES DURING SUPPLY VOLTAGE CHANGING IN THE SYSTEM OF POLYMER INSULATION COVERING OF THE CURRENT-CARRYING CORE OF ULTRA HIGH VOLTAGE CABLES

***Aim.*** ***The article is devoted to the analysis of the electromechanical transient processes in a system of three frequency-controlled electric drives based on asynchronous motors that control current-carrying core motion, as well as to the study of the effect of such processes on the modes applying three-layer polymer insulation to the current-carrying core.*** ***Technique.*** ***The study was conducted based on the concepts of electromechanics, electromagnetic field theory, mathematical physics, mathematical modeling.*** ***Results.*** ***A mathematical model has been developed to analyze transients in an electromechanical system consisting of three frequency-controlled electric drives providing current-carrying core motion of ultra-high voltage cables in an inclined extrusion line. The coordination of the electromechanical parameters of the system drives has been carried out and the permissible changes in the supply voltage at the limiting mass while moving current-carrying core of ultra-high voltage cables with applied polymer insulation have been estimated.*** ***Scientific novelty.*** ***For the first time it is determined that with the limiting mass of the current-carrying core, the electromechanical system allows to stabilize the current-carrying core speed with the required accuracy at short-term decreases in the supply voltage by no more than 27 % of its amplitude value. It is also shown that this system is resistant to short-term increases in voltage by 32 % for 0.2 s.*** ***Practical significance.*** ***Using the developed model, it is possible to calculate the change in the configuration and speed of the slack current-carrying core when applying polymer insulation, depending on the specific mass of the current-carrying core per unit length, its tension at the bottom, the torque of the traction motor and the supply voltage to achieve stable operation of the system and accurate working of the set parameters.*** References 12, figures 7.

*Key words:* **electromechanical transient processes, ultra-high voltage cable, mathematical modeling, frequency-controlled electric drives, polymer insulation covering.**

***Цель.*** ***Целью статьи является проведение анализа электромеханических переходных процессов в системе из трех частотно регулируемых электроприводов на базе асинхронных двигателей, которые управляют движением токопроводящей жилы, а также исследование влияния таких процессов на режимы нанесения на жилу трехслойной полимерной изоляции.*** ***Методика.*** ***Для проведения исследований использовались положения электромеханики, теории электромагнитного поля, математической физики, математического моделирования.*** ***Результаты.*** ***Разработана математическая модель, позволяющая анализировать переходные процессы в электромеханической системе, состоящей из трех частотно регулируемых электроприводов, обеспечивающих движение токопроводящей жилы сверхвысоковольтного кабеля в наклонной экструзионной линии. Проведено согласование электромеханических параметров приводов системы и выполнена оценка допустимых изменений напряжения питающей сети при предельной массе движущейся жилы сверхвысоковольтного кабеля с нанесённой на нее полимерной изоляцией.*** ***Научная новизна.*** ***Впервые определено, что при предельной массе токопроводящей жилы электромеханическая система позволяет стабилизировать скорость перемещения жилы с необходимой точностью при кратковременных уменьшениях питающего напряжения не более чем на 27 % от его амплитудного значения. Также показано, что данная система является устойчивой к кратковременному увеличению напряжения на 32 % в течение 0,2 с.*** ***Практическое значение.*** ***Использование разработанной модели позволяет рассчитывать изменение конфигурации и скорости движения провисающей токопроводящей жилы при нанесении на нее полимерной изоляции, в зависимости от удельной массы жилы на единицу длины, ее натяжения в нижней точке, момента тягового электродвигателя и величины питающего напряжения для достижения стабильной работы системы и точной отработки заданных параметров.*** Библ. 12, рис. 7.

*Ключевые слова*: **электромеханические переходные процессы, сверхвысоковольтный кабель, математическое моделирование, частотно регулируемые электроприводы, нанесение полимерной изоляции.**

**Introduction.** The modern phase of technological development for applying polymer insulation to current-carrying cores of power-driven cables is characterized by the use of adjustable AC electric drives. These drives are made on the basis of asynchronous motors with frequency control, which have high dynamic and energy performance. At the same time, when two or more adjustable drives are used in one system, the solution to the problem of their electrical and mechanical parameters coordination becomes much more complicated. When choosing the optimal structure of the control unit of the whole system, it becomes necessary to model complex electrodynamic processes, which now is most appropriate to implement using the Matlab/Simulink/Sim-PowerSystems package.

This approach helps to investigate the laws of frequency regulation and determine the most appropriate system regimes for its stability, speed and other indicators [10]. When operating these drives systems, there is also the task of studying their operation stability when changing the supply network parameters, which is especially important in case of maximum mechanical loads of the drives and their power supply from the power supply system with a limited installed capacity of the servicing substation. The use of computer modeling to solve this type of problems makes it possible to significantly reduce the material costs and timing of such systems design.

This research provides an estimation of the operation stability of electromechanical system with vector control of frequency-controlled electric drives considering short-term changes in the supply network voltage. It is known [10] that the vector control advantages are the high accuracy of diagram optimization at a set speed, the preserva-

tion of the necessary torque magnitude at low rotational speeds, the smooth operation of the motor and the rapid reaction to load jumps due to the high dynamics of regulation. At the same time, the quantitative analysis of the stability and accuracy of the specified parameters optimization - motion speed and the torque shaft of the drive, are currently insufficiently studied.

**The aim of the paper** is to analyze the electromechanical transients in a system consisting of three frequency-controlled electric drives based on asynchronous motors that control the current-carrying core motion, as well as the effect of such processes on the modes of applying three-layer polymer insulation to the current-carrying core.

The paper studies such freelance regimes as the appearance of short-term voltage failures in the supplying three-phase network and short-term increases in this voltage. The study is carried out to coordinate the electromechanical parameters of the system two drives and to evaluate the permissible level of the voltage failure in the supply network at the limiting mass of the moving cable.

The material is based on the computer modeling results of electrical system that includes two induction motors with vector control, using the scientific statements presented in [7, 11]. Synthesis of the virtual model uses the tools of the Matlab / Simulink computer modeling software package [8], which contains special blocks and demonstration samples dealing directly with the elements and systems of the automated electric drive. The principles of constructing and exploring individual blocks of virtual models are presented in [6, 7], and the control systems of electric drives in the monograph [5].

**Description of the inclined line**. The inclined extrusion line (Fig. 1,*a*) is in the form of a metal vulcanization pipe, inside of which extrusion and vulcanization (cross-linking) of a polyethylene insulation layer as well as two polymeric semiconductive layers are applied on the current-carrying core of high-voltage and ultrahigh voltage cables. In such a line, the insulation of aluminum and copper current-carrying cores of power cables is made with a cross section of 35-2000 mm$^2$ for a voltage of 10-330 kV. The current-carrying core consists of many twisted and compacted current-carrying cores, which can be divided into 5-7 separately sealed and isolated sectors. A polymeric semiconductive layer 0.4-3 mm thick is applied to the current-carrying core, on which an insulating layer of high-quality polyethylene with a thickness of up to 28 mm and another layer of semiconductive polyethylene with a thickness of 0.4-3.5 mm are applied. All three layers are simultaneously applied by extrusion using a triple extrusion head and vulcanized in a vulcanization pipe of continuous vulcanization at 450 °C in a medium compressed to 16 atm. nitrogen in the gaseous state. This is necessary to ensure the insulation quality, namely to exclude the presence of conductive microcircuits larger than 50 μm and groups of closely located microinclusions [4, 12].

The cable current-carrying core with polyethylene insulation and semi-conductive shielding layers applied must move at a speed of 0.3-50 m/min inside the vulcanization pipe 172 m long. The motion is carried out as a result of the effort up to $4.5 \cdot 10^4$ N electric drive No. 1 (Fig. 1,*b*).

The principle of line operation, its scheme is shown in Fig. 1 as follows. The current-carrying core wounded on the feeding device cylinder, is passed through the electric drive No. 1 through a triple extrusion head, into which polyethylene insulation melts and a semiconductive polymer are simultaneously fed. The head has three extruders of different capacities: the first (with the highest capacity) for applying a polyethylene insulation layer, and the second for forming semiconductive polymer layers.

In order for the liquid layer of molten polyethylene to be less displaced relative to the current-carrying core axis, a twisting mechanism is additionally applied. It twists the current-carrying core in the direction of its wires approximately at a pitch equal to one current-carrying core turn around its axis for 30 linear meters of its length. This makes it possible to obtain a cylindrical item with a crust of solidified polyethylene on its surface and avoid the displacement of the polymeric semiconducting and insulating layers relative to the current-carrying core axis, i.e. avoid the polymer layers eccentricity.

The possibility of such technology implementation is provided by a special configuration of the inclined vulcanization pipe. The initial part of the pipe, where the current-carrying core polymer layers are still sufficiently liquid, is practically vertical. Then the pipe bends and in its final part, where the current-carrying core polymer layers are sufficiently hardened, becomes almost horizontal. The bending and cross-section of the pipe are selected from the conditions of inadmissibility of touching its internal surface by polymeric layers of the current-carrying core with all changes in its cross-section, mass, polymeric layers thickness and linear displacement speed.

A current-carrying core with polymeric layers must move in the central part of the vulcanization pipe and can be considered as a heavy material thread. The angle $\alpha$ between the abscissa axis and the line connecting the beginning and the point with coordinates ($x$, $y$), as is known from mechanics, can be determined from the expression:

$$tg\alpha = \frac{gx}{H}, \qquad (1)$$

where $g$ is the weight of heavy material thread per unit length and $H$ is the tension at the lowest point.

Since the manufacture of insulated cable standards of different cross-sections and at different voltages the value of g varies, the profile of the sag thread also varies:

$$y = \frac{1}{c}x^2, \qquad (2)$$

where $c = H/g$ is sag constant.

From the equations given, it is clear that the sag constant $c$ should be unchanged to keep the thread profile. Such profile invariance can be made by adjusting the tension force $H$ and correspondingly adjusting the motor shaft of the drive No. 2 (Fig. 1,*b*), driving the track-type traction device at a constant technological speed $V$ of the current-carrying core motion in the vulcanization pipe. The invariance of the current-carrying core speed is ensured by adjusting the torque of the traction motor. These relationships are the basis for the motion control system of the current-carrying core inside the vulcanization pipe, which bend is determined from the sagging equations of the current-carrying core as a material heavy thread.

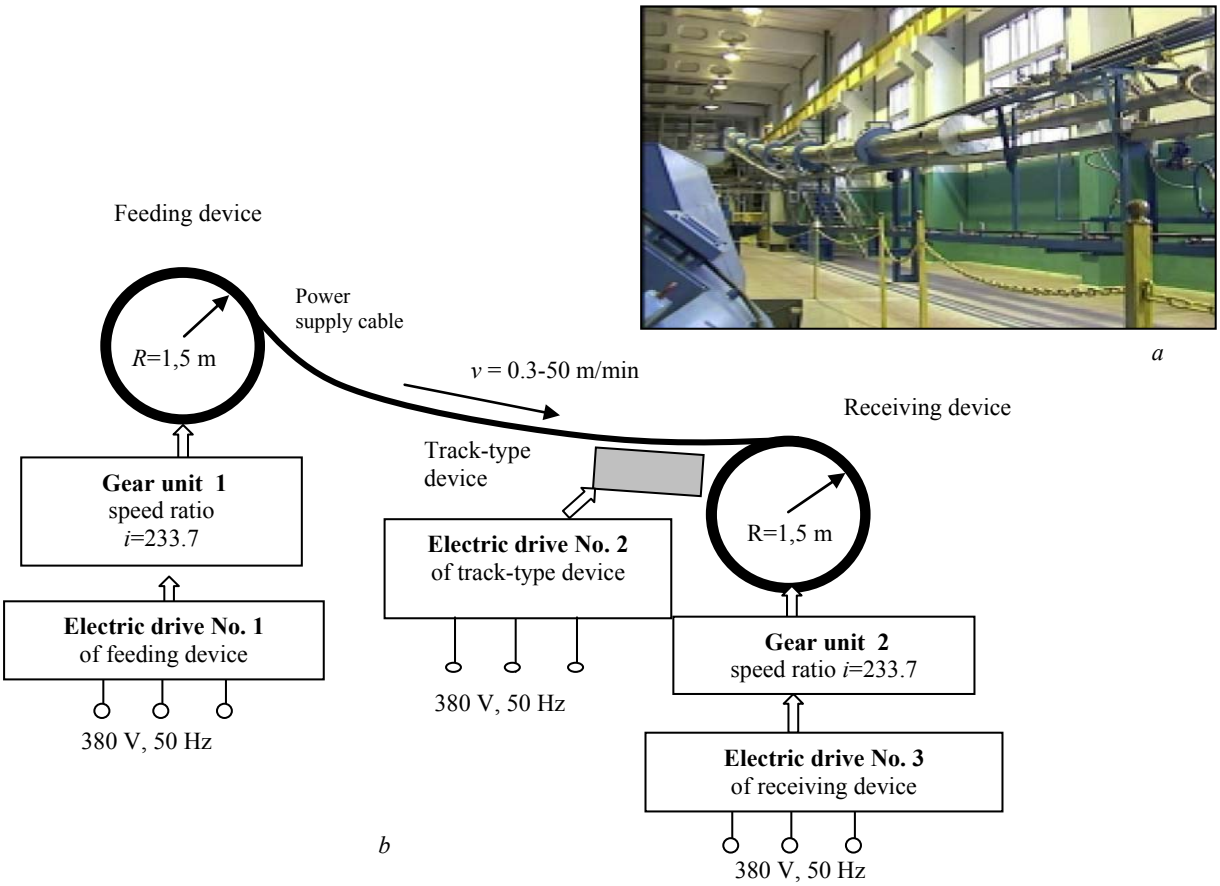


Fig. 1. Inclined extrusion line of applying and vulcanizing a polyethylene insulation layer and two semiconductive layers on current-carrying core of high and ultrahigh voltage cables, *a* – photo of PJSC «Yuzhcable Works» and *b* – its block diagram

**Problem statement and the development of mathematical model of electromechanical system.** The electromechanical system is studied. It is schematically shown in Fig. 1,*b* and contains three electric drives, based on asynchronous motors with vector control.

Drives No. 1 and No. 3 set in motion the cylinder of the deeding and receiving devices and ensure the cable motion at a constant speed *V* set by the technological conditions. Drive No. 2 sets in motion the track-type traction device and provides the required cable tension *H* when it moves inside the vulcanization pipe. All drives are built based on direct control of the torque and flow of an asynchronous motor (DTC method), described in [1, 3, 9].

In this paper, as in [7], a mathematical model was developed using the Matlab / Simulink software package [8] to study the electromagnetic processes in electromechanical system shown in Fig. 1. This system model with two electric drives with vector control is shown in Fig. 2.

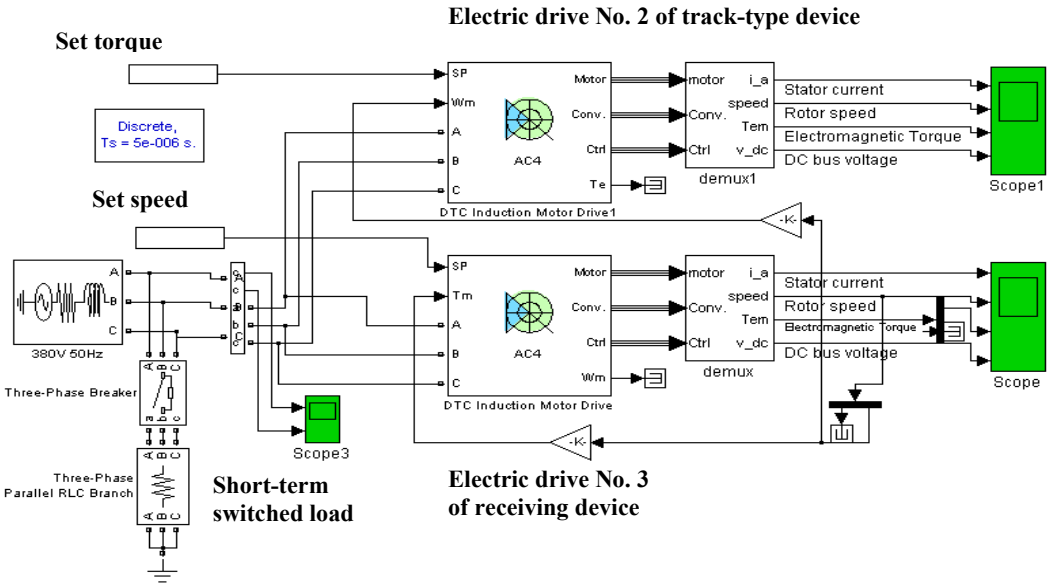


Fig. 2. Mathematical model of a system with two electric drives with vector control

In this model, the effect of two drives No. 1 and No. 3, providing a set speed of the cable motion, is replaced by the equivalent action of one drive, so a system consisting of two drives is considered in the modeling. The model has a drive's receiving device, providing a set speed of shaft rotation of the asynchronous motor, and, consequently, a set speed of cable pulling. Also, there is a drive of the track-type device No. 2, which creates a set torque on the motor shaft, and, consequently, a set tension of the cable. Both drives are connected to a three-phase power supply. To model a short-term voltage failure mode, an additional active three-phase load is connected to this source with a key. To visualize the calculation results, the blocks of virtual oscilloscopes *Display* of the *Simulink* package are used, the inputs of which are connected to the corresponding communication lines.

Each of the two drive units, as in [7], model the electric drive operation based on an induction motor with vector control. This model contains an uncontrolled three-phase rectifier, a three-phase inverter with pulse-width modulated current (PWM), an asynchronous motor, a speed controller and an inverter control unit. In order to avoid overvoltage at the rectifier output when the motor is switched on in the electric power generation mode, a special chopper block is located between the rectifier and the inverter, which provides the connection of a resistor shunting the storage capacitance when the voltage across the set value exceeds it. The block diagram of the drive realized by the DTC method is given in [2, 3, 8].

The asynchronous machine model is used and consisted of an electrical part represented by a fourth-order state space model and a mechanical part model in the form of a second-order system. All electric variables and machine parameters were driven to the stator.

The initial equations of the electrical part of the machine are recorded for a two-phase coordinate system (the *d-q* axis) and have the form:

$$V_{qs} = R_s i_{qs} + \frac{d}{dt}\varphi_{qs} - \omega\varphi_{ds}, \quad (3)$$

$$V_{ds} = R_s i_{ds} + \frac{d}{dt}\varphi_{ds} - \omega\varphi_{qs}, \quad (4)$$

$$V'_{qr} = R'_r i'_{qr} + \frac{d}{dt}\varphi'_{qr} + (\omega - \omega_r)\varphi'_{dr}, \quad (5)$$

$$V'_{dr} = R'_r i'_{dr} + \frac{d}{dt}\varphi'_{dr} - (\omega - \omega_r)\varphi'_{qr}, \quad (6)$$

$$T_e = 1{,}5(\varphi_{ds} i_{ds} - \varphi_{qs} i_{ds}), \quad (7)$$

where: $\varphi_{qs} = L_s i_{qs} + L_m i'_{qr}$, $\varphi_{ds} = L_s i_{qs} + L_m i'_{dr}$, (8, 9)

$$\varphi'_{qr} = L'_r i'_{qr} + L_m i_{qs}, \quad \varphi'_{dr} = L'_r i_{dr} + L_m i_{ds}, \quad (10, 11)$$

$$L_s = L_{ls} + L_m, \qquad L'_r = L'_{lr} + L_m. \quad (12, 13)$$

The mechanical part of the machine was described by two equations:

$$\frac{d}{dt}\omega = \frac{1}{J}(T_e - F\omega - T_m), \quad \frac{d}{dt}\theta = \omega. \quad (14, 15)$$

The following symbols are used in the equations: $R_s$, $L_{ls}$ and $R'_r$, $L_{lr}$ are the resistance and inductance of stator and rotor scattering; $L_m$ is the inductance of the magnetizing circuit; $L_s$, $L'_r$ are the total inductances of the stator and rotor; $V_{qs}$, $i_{qs}$ and $V'_{qr}$, $i'_{qr}$ are the projections of the stator and rotor stresses and currents on the *q* axis; $V_{ds}$, $i_{ds}$ and $V'_{dr}$, $i'_{dr}$ are the projections of the stator and rotor voltages and currents on the *d* axis; $\varphi_{ds}$, $\varphi_{qs}$ and $\varphi'_{dr}$, $\varphi'_{qr}$, are the projections of the stator and rotor flux linkages on the *d* and *q axes*; $\omega$ is the angular velocity of the rotor; $\theta$ is the angular velocity of the rotor; $J$ is the rotor inertia torque; $T_e$ is the motor electromagnetic torque; $T_m$ is the static load moment; $F$ is the friction coefficient.

This mathematical model has become the basis for the one developed in the Simulink and for the virtual model of the asynchronous machine used in this paper. A number of parameters were calculated from the machine's passport data on the basis of the method described in [6]. At that, the asynchronous motor RA160MA4 (11 kW, 1460 rpm) was used in the drive's receiving device, and RA132S2 (5.5 kW, 1455 rpm) was used in the drive of the tracked chassis.

**The analysis of modeling results.** Fig. 3 shows the timing diagrams of the main characteristics of the drive's receiving device for the studied time period – 2 s, corresponding to the start-up mode. The diagrams are in good agreement with the results given in [7]. The Fig. 3 shows the time-dependent current of the stator motor winding, the rotor speed, the electromagnetic torque on the motor shaft, and the reference voltage at the inverter input considering stable parameters of the supply network or network with infinitely large power.

Based on the modeling results, it can be noted that the current in the stator of the receiving device's motor changes in amplitude and frequency during start-up, and at the initial area the frequency is low and gradually increases as the motor accelerates. It is this trigger mode that is characterized by low energy consumption. The motor is monotonously accelerated to a set speed of 1200 rpm for a time equal to 1.35 s and then accurately reproduces this predetermined rotation frequency in the subsequent time interval.

At the next stage of the research, dynamic processes in the drives were modeled with a short-time increase during 0.4 s of the supply voltage from an amplitude value of 380 V to various values up to 500 V. Such a mode was modeled by connecting the drive to an additional voltage source of increased amplitude in a time point of 1.4 s (after reaching the steady state). The results of calculating these processes for the drive's receiving device are shown in Fig. 4.

Based on calculation results it follows that, although the inverter input voltage increases from 580 V to 800 V, rotor speed does not change. That is, the studied system of the two drives is stable to short-time increases in the input voltage in the wide range.

At the next stage, dynamic processes in the drives were modeled for a short-time (0.4 s) network voltage failure from the amplitude value $u_0$ to the value $u_0 - \Delta u$, with $\Delta u/u_0 = 0.54$. This mode was modeled by connecting to a power supply with a limited power of an additional three-phase load.

The calculating results of these processes for the drive's receiving device are shown in Fig. 5 for the phase voltage and in Fig. 6 for the stator current, the rotor speed, the electromagnetic torque and the inverter input voltage.

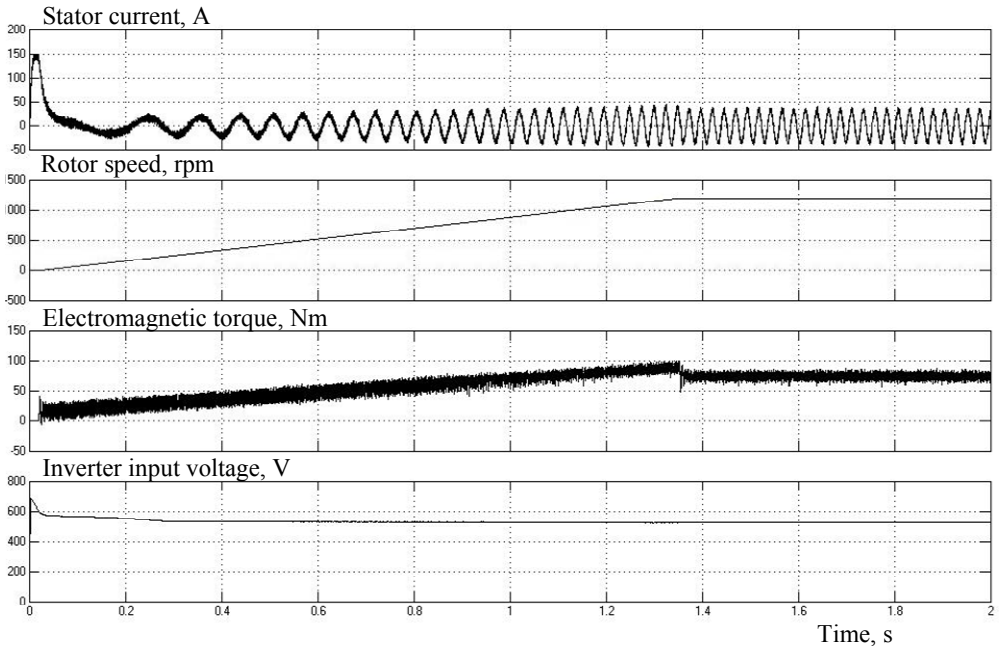


Fig. 3. Timing diagrams of the main characteristics of the drive's receiving device for a period of time corresponding to the start-up mode

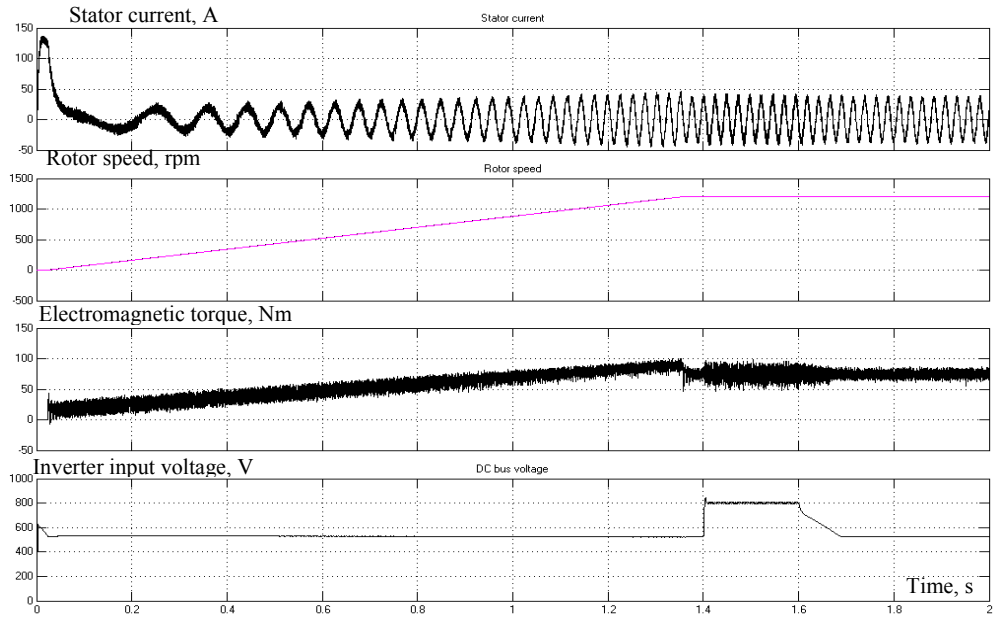


Fig. 4. Dynamic processes in the drive's receiving device at a short-term increase in the supply voltage

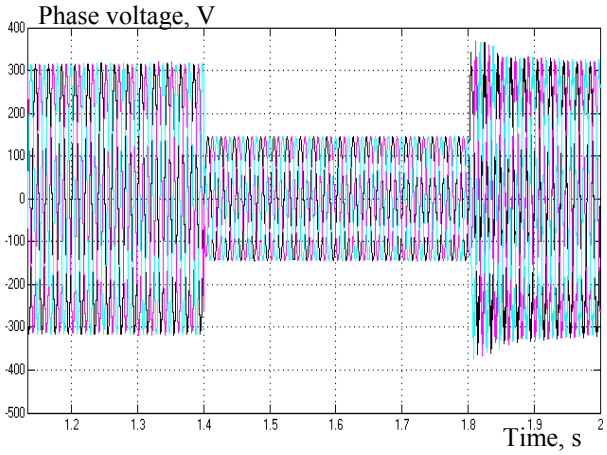


Fig. 5. Dependence of the phase voltage network on time

Fig. 6 shows that the voltage failure (time interval 1.4 – 1.8 s) at the inverter input decreases, current level in the stator motor winding decreases, but vector control system increases the electromagnetic torque in order to work at the set speed. It can be seen that with this voltage failure, the electromechanical system, despite the torque increase, cannot work at the set rotor speed, which decreases at the end of this time interval by an amount $\Delta n \approx 430$ rpm.

In order to obtain a quantitative dependence of the relative decrease in the rotor speed $\Delta n/n_0$ on the relative decrease in the network voltage $\Delta u/u_0$, calculations were carried out for different values of the load additionally connected to the network. These dependences are shown in Fig. 7.

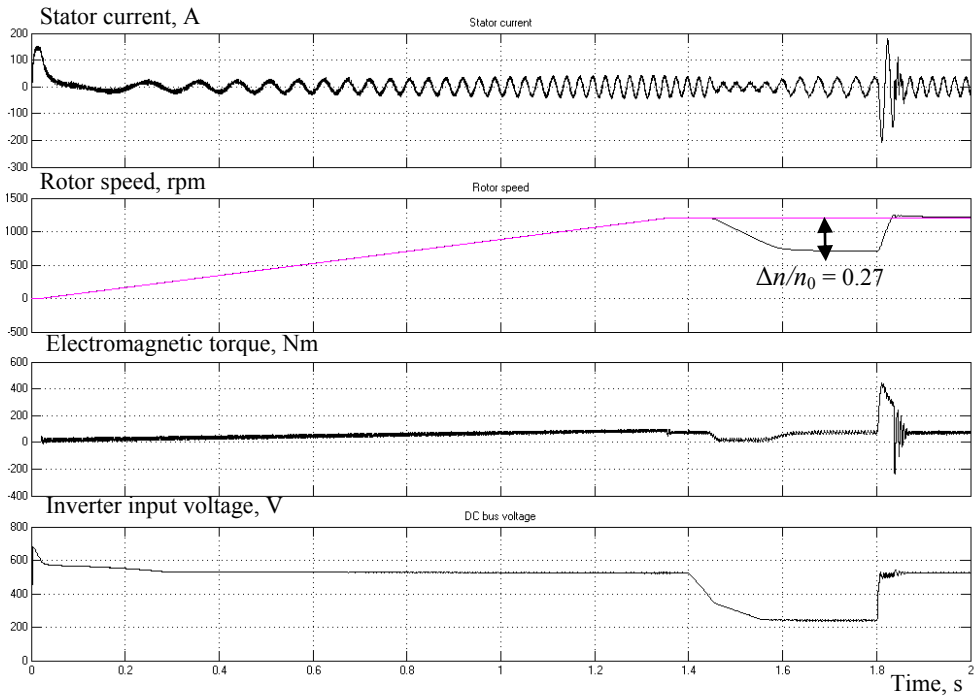


Fig. 6. Dynamic processes in the drive's receiving device at a short-term failure of the supply voltage

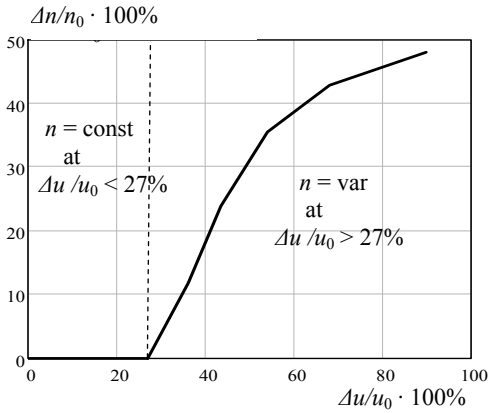


Fig. 7. Dependence of the relative decrease in the rotor speed $\Delta n/n_0$ of the electromechancal system on the relative decrease in the network voltage $\Delta u/u_0$

As can be seen from this figure, there is a threshold value for the voltage failure $\Delta u/u_0 \cdot 100\ \% = 27\ \%$, below which the drive ensures stabilization of the set speed with high accuracy. When this value is exceeded, the relative rotor speed $\Delta n/n_0$ increases, that is, the drive does not provide stabilization of the set speed. The obtained data on the threshold value of the voltage failure allow us to formulate the requirements for the parameters of power supply systems, taking into account their possible connection to additional power loads.

**Conclusions.**

1. A mathematical model has been developed to study the dynamic processes in the electromechanical system used in the production line for the extrusion coating of polyethylene insulation and semiconductive polymer layers on the current-carrying core of ultrahigh-voltage cables. The investigated system includes electric drives on the basis of frequency-controlled asynchronous motors and their load - moving current-carrying core with necessary speed and tension.

2. The coordination of electrical and mechanical parameters of the system is carried out and the analysis of its dynamic processes is made. It is determined that with a critical mass of the current-carrying core, the electromechanical system allows stabilizing the current-carrying core speed with the necessary accuracy at short-time failures in the supply voltage of no more than 27 % of its amplitude value. This is one of the basic requirements for the parameters of power supply systems, taking into account their possible connection to additional power loads.

3. It is also shown that this system is stable to a short-term voltage increase for 0.2 s from a value of 380 V to 500 V.

REFERENCES

***1.*** Anuchin A., Shpak D., Aliamkin D., Briz F. Adaptive observer for field oriented control systems of induction motors. *57th International Scientific Conference on Power and Electrical Engineering of Riga Technical University (RTUCON)*, 2016, pp. 1-4. **doi: 10.1109/RTUCON.2016.7763157**.

***2.*** Krause P.C., Wasynczuk O., Scott D.S. *Analysis of Electric Machinery and Drive Systems*. Wiley-IEEE Press, 2013. 680 p.

***3.*** Trzynadlowski A. *Control of Induction Motors*. Academic Press, 2001. 225 p.

***4.*** Bezprozvannych A.V., Kessaev A.G., Shcherba M.A. Frequency dependence of dielectric loss tangent on the degree of humidification of polyethylene cable insulation. *Technical Electrodynamics*, 2016, no.3, pp. 18-24. (Rus).

***5.*** German-Galkin S.G. *Matlab/Simulink. Proektirovanie mekhatronnykh sistem na PK* [Matlab/Simulink. Designing mechatronic systems on a PC]. St. Petersburg, Korona-Vek Publ., 2008. 368 p. (Rus).

***6.*** German-Galkin S.G., Cardonov G.A. *Elektricheskie mashiny. Laboratornye raboty na PK* [Electric machines. Lab. work on a PC]. St. Petersburg: Korona print Publ., 2003. 256 p. (Rus).

***7.*** Zolotaryov V.M., Shcherba A.A., Podoltsev A.D. Modelling of dynamic processes in electromechanical system for the control of superhigh-voltage cable movement in slant extrusion-type line. *Technical Electrodynamics*, 2010, no.3, pp. 44-51. (Rus).

***8.*** *Description of the application SimPowerSystems*. Available at: www.mathworks.com (accessed 11 May 2017).
***9.*** Peresada S.M. *Nelineinoe i adaptivnoe upravlenie v elektromekhanicheskikh sistemakh s vektorno-upravliaemymi elektrodvigateliami*. Diss. dokt. techn. nauk [Nonlinear and adaptive control in electromechanical systems with vector-controlled electric motors. Doc. tech. sci. diss.]. Kyiv, 2007. 472 p. (Rus).
***10.*** Pivnyak G.G., Volkov A.V. *Sovremennye chastotno-reguliruemye asinkhronnye elektroprivody s chastotno-impul'snoi moduliatsiei* [Modern frequency-controlled asynchronous electric drives with frequency-pulse modulation]. Dnipropetrovsk, NGU Publ., 2006. 468 p. (Rus).
***11.*** Chermalykh V.M., Chermalykh A.V., Maidansky I.Ya. Investigation of the dynamics and energy parameters of an asynchronous electric drive with vector control by the virtual simulation method. *Bulletin of NTU «KhPI»*, 2008, no.30, pp. 41-45. (Rus).
***12.*** Shcherba M.A., Podoltsev O.D. Electric field and current density distribution near water inclusions of polymer insulation of high-voltage cables in view of its nonlinear properties. *Technical Electrodynamics*, 2016, no.1, pp. 11-19. (Rus).

*Received 15.11.2017*

*V.M. Zolotaryov*[1]*, Doctor of Technical Science,*
*M.A. Shcherba*[2]*, Candidate of Technical Science,*
*R.V. Belyanin*[1]*,*
*R.P. Mygushchenko*[3]*, Doctor of Technical Science,*
*I.M. Korzhov*[3]*,*
[1] Private Joint-stock company Yuzhcable works,
7, Avtogennaya Str., Kharkiv, 61099, Ukraine,
phone +380 57 7545228, e-mail: zavod@yuzhcable.com.ua
[2] The Institute of Electrodynamics of the NAS of Ukraine,
56, prospekt Peremogy, Kiev-57, 03680, Ukraine,
phone +380 44 3662460, e-mail: m.shcherba@gmail.com
[3] National Technical University «Kharkiv Polytechnic Institute»,
2, Kyrpychova Str., Kharkiv, 61002, Ukraine,
phone +380 57 7076116, e-mail: mrp1@ukr.net

*How to cite this article:*
Zolotaryov V.M., Shcherba M.A., Belyanin R.V., Mygushchenko R.P., Korzhov I.M. Electromechanical transient processes during supply voltage changing in the system of polymer insulation covering of the current-carrying core of ultra high voltage cables. *Electrical engineering & electromechanics*, 2018, no.2, pp. 47-53. **doi: 10.20998/2074-272X.2018.2.08.**

UDC 621.318 **doi: 10.20998/2074-272X.2018.2.09**

E.A. Chaplygin, M.V. Barbashova, A.Yu. Koval

# NUMERICAL ESTIMATES OF ELECTRODYNAMICS PROCESSES IN THE INDUCTOR SYSTEM WITH AN ATTRACTIVE SCREEN AND A FLAT RECTANGULAR SOLENOID

***Purpose. To carry out numerical estimates of currents and forces in the investigated inductor system with an attractive screen (ISAS) and determine the effectiveness of the force attraction. Methodology. The calculated relationships and graphical constructions were obtained using the initial data of the system: induced current in the screen and sheet metal; the distributed force of attraction (Ampère force); the repulsive force acting on the sheet metal (Lorentz force); amplitude values of the force of attraction and repulsion; phase dependence of the force of attraction, the repulsive force and the total resulting force. Results. The results of calculations in the form of graphical dependencies of electrodynamic processes in the region under the conductors of a rectangular solenoid of inductor system with an attracting screen are presented. The graphs of forces and currents in region of dent are obtained. In the paper the analysis of electrodynamics processes for whole area under the winding of inductor system with an attractive screen is shown. The flowing this processes in the region of dent a given geometry is presented. Originality. The considered inductor system with an attractive screen and a rectangular solenoid is improved, in comparison with the previous developed ISAS. It has a working area under the lines of parallel conductors in the cross section of a rectangular solenoid, and this allows to place a predetermined portion of the sheet metal anywhere within the working region. Comparison of the indicators of electrodynamics processes in the considered variants of calculation shows an approximate growth of almost 1.5 times the power indicators in the area of the accepted dent in comparison with similar values for the entire area under the winding of the ISAS. Practical value. The results obtained are important for the practice of real estimates of the excited forces of attraction. With a decrease in the dent, the amplitude of the electrodynamics forces being excited is growing proportionally (for example, when the depth decreases by 3 mm, the forces increase more than 2 times). The highest efficiency of force attraction is for sheet metal regions, the dimensions do not exceed the transverse dimensions of the winding branches of the exciting solenoid.*** References 8, figure 7.

*Key words:* **magnetic-pulsed treatment, inductor system, attractive screen, rectangular solenoid, electrodynamics processes.**

***Проведены численные оценки и анализ полученных результатов для токов и сил в исследуемой индукторной системе с притягивающим экраном и прямоугольным соленоидом. Выявлено, что при уменьшении глубины вмятины в металле, амплитуда, возбуждаемых электродинамических усилий, растёт. Анализ показал, что значение сил отталкивания, интегральное во времени, ниже развиваемых сил притяжения. При достаточно низких рабочих частотах действующих полей, рассмотренная система работает, как инструмент магнитно-импульсного притяжения тонкостенных листовых металлов.*** Библ. 8, рис. 7.

*Ключевые слова:* **магнитно-импульсная обработка, индукторная система, притягивающий экран, прямоугольный соленоид, электродинамические процессы.**

**Introduction.** The development of any area of modern industry is focused on the accelerated introduction of innovations. This applies to the metalworking area. The needs of society also indicate that it is necessary to promote a greater development of manufacturing industries. Magnetic-pulse processing of metals (MPPM) has recently become quite common in the application of various manufacturing operations [1, 2]. In this regard, the improvement of systems and tools that improve the efficiency of existing devices or the creation of absolutely new ones for the modern level of development of MPPM is actual.

**Analysis of major achievements and publications.** The main component of any system of magnetic-impulse attraction of thin-walled metal sheets is the inductor system. Its improvement is a solution to the problem of increasing the effectiveness of instruments of magnetic pulse technology. In order to obtain high homogeneity of the excited field and forces in the working area of the MPPM tool, inductor systems with an attractive screen (ISAS) were created. The principle of operation is based on the mutual attraction of conductors with identically directed currents (Ampere law) [3-6].

**The goal of the work** is to carry out numerical estimates of electrodynamics forces in the «inductor system with an attractive screen» under investigation to determine the effectiveness of the force attraction.

**Problem definition.** The ISAS system consists of a source of a magnetic field (a flat rectangular solenoid), an auxiliary conducting screen and an object of processing. The field of the solenoid excites unidirectional Foucault eddy currents in the screen and sheet metal. Due to the rigidly fixed screen, the attraction experiences only the processing object. Force magnetic-pulse action leads to a stretching of the specified area on its surface. The working zone of the ISAS under consideration is the area under the branches of the parallel conductors, that is, the specified section of the sheet metal processed object, which has a depression (for example, a dent), which must be deformed (attracted).

Initial data (Fig. 1). *Solenoid:*

a) number of turns in each branch – $N = 10$;

b) branch width – $(b - a) = 0.05$ mm;

c) width of turn and interturn insulation – $g = \frac{(b-a)}{2N-1} \approx 0{,}0026$ m;

d) internal solenoid window – $a = 0.025$ m;

e) current in the inductor generated at the capacitive storage discharge – $C = 1200$ μF with voltage – $U_m \approx 2000$ V at frequency – $f = 1500$ Hz, is assumed – $J_m \approx 22620$ A (respectively, the linear density of the exciting current – $j_m \approx 8.6 \cdot 10^6$ A/m).

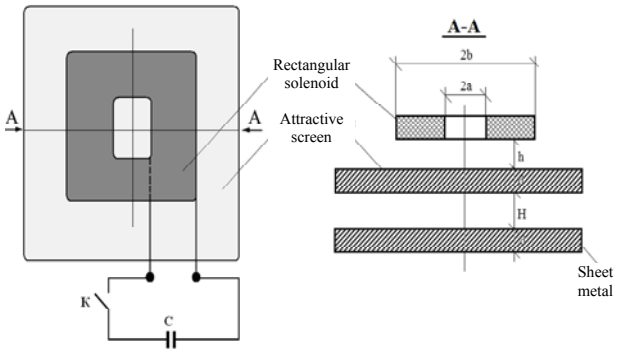


Fig. 1. Schematic representation of ISAS, $C$ – capacitance, $K$ – switch

*Screen and sheet metal:*

a) thickness – $d = 0.0075$ m;

b) conductivity – $\gamma = 0.4 \cdot 10^7$ $(\Omega \cdot \text{m})^{-1}$ (steel).

*The system geometry:*

a) distance between the working surface of the solenoid and the screen – $h = 0.0005$ m;

b) dent depth – $H = 0.005$ m, its length – $D = 0.03$ m.

**Calculation relations:**

a) from the expression obtained in [7] we obtain the formula for the current induced in the screen:

$$j_{\text{e}}(\psi, y) = \left(\frac{J_m}{g}\right)\frac{\left(\mu_0 \gamma \omega d^2\right)}{2}\frac{dj_i(\psi)}{d\psi} \times \times \int_0^{\infty} f(x) e^{-x \cdot \frac{h}{d}} \left(1 - e^{-x}\right) \sin\left(x \frac{y}{d}\right) dx \quad (1)$$

where $J_m$ is the amplitude of the current in the solenoid, $\psi = \omega t$ is the phase of the induced current in the pulse, $j_i(\psi)$ is the phase function of the current in the solenoid, $f(x) = \frac{2}{\pi} \cdot \frac{1}{x^3} \int_0^{\infty} f(\alpha) \cdot \sin(\alpha) d\alpha$, $f(\alpha)$ is the lateral distribution function of the exciting current

$$f(\alpha) = \begin{cases} 1, \alpha \in [\frac{a}{d}, \frac{b}{d}], \\ 0, \alpha \notin [\frac{a}{d}, \frac{b}{d}], \end{cases}$$

$$f(x) = \frac{2}{\pi x^3} \cdot \left( \sum_{k=1}^{N} \left[ \cos\left( x \cdot \left( \frac{a}{d} + 2(k-1)\frac{g}{d} \right) \right) - \right. \right.$$

$$\left. \left. - \cos\left( x \cdot \left( \frac{a}{d} + (2k-1)\frac{g}{d} \right) \right) \right] \right);$$

b) from the relation obtained in [7] we obtain a formula for the current induced in sheet metal:

$$j_{\text{lm}}(\psi, y) = \left(\frac{J_m}{g}\right)\frac{\left(\omega \mu_0 \gamma d^2\right)}{2}\frac{dj_i(\psi)}{d\psi} \times \times \int_0^{\infty} f(x) e^{-x \frac{(h+d+H)}{d}} \left(1 - e^{-x}\right) \sin\left(x \frac{y}{d}\right) dx ; \quad (2)$$

c) from the relation obtained in [7] we find the distributed force of attraction (Ampere force),

$$F_{\text{attr}}(\psi, y) = \frac{\mu_0}{2\pi} \cdot j_{\text{e}}(\psi, y) \cdot j_{\text{lm}}(\psi, y) \cdot \frac{D}{H}; \quad (3)$$

where $D$ is the dimension (length), $H$ is the dent depth, $j_{\text{e,lm}}(\psi,y)$ is the current density induced in the screen and sheet metal in accordance with (1), (2);

d) the repulsive force (the Lorentz force!) acting on the sheet metal is determined from the expression in [7]:

$$F_{\text{rep}}(\psi, y) = \frac{\mu_0}{2\pi} \cdot j_i(\psi, y) \cdot j_{\text{lm}}(\psi, y) \cdot \frac{D}{\left(h + d + H\right)}, \quad (4)$$

where $j_i(\psi,y)$ is the current density in the solenoid,

$$j_i(\psi, y) = \begin{cases} \left(\frac{J_m}{g}\right) \cdot j_i(\psi), & \text{at } |y| \in [a, b], \\ 0, & \text{at } |y| \notin [a, b], \end{cases}$$

$j_i(\psi)$ is the phase dependence of the current in the solenoid, $j_{\text{lm}}(\psi,y)$ is the current density induced in sheet metal in accordance with (2);

e) amplitude-for-phase value of the attractive force

$$F_{\text{attr}}^{\max}(y) = F_{\text{attr}}(\psi, y)\big|_{\psi=\psi_{\max}} = = \frac{\mu_0}{2\pi} \cdot j_{\text{e}}(\psi, y)\big|_{\psi=\psi_{\max}} \cdot j_{\text{lm}}(\psi, y)\big|_{\psi=\psi_{\max}} \cdot \frac{D}{H}; \quad (5)$$

f) phase dependence of the attractive force averaged in the transverse dimension on the interval $y \in [-b, b]$

$$\overline{F}_{\text{attr}}(\psi) = \frac{1}{2b} \int_{-b}^{b} F_{\text{attr}}(\psi, y)\, dy; \quad (6)$$

g) amplitude value of repulsive force

$$F_{\text{rep}}^{\max}(y) = F_{\text{rep}}(\psi, y)\big|_{\psi=\psi_{\max}} = = \frac{\mu_0}{2\pi} j_i(\psi, y) j_{\text{lm}}(\psi, y)\big|_{\psi=\psi_{\max}} \frac{D}{\left(h + d + H\right)}; \quad (7)$$

h) phase dependence of the repulsive force averaged in the transverse dimension on the interval $y \in [-b, b]$

$$\overline{F}_{\text{rep}}(\psi) = \frac{1}{2b} \int_{-b}^{b} F_{\text{rep}}(\psi, y)\, dy; \quad (8)$$

i) phase dependence of the resultant force, found as a phase superposition of repulsive and attractive forces averaged in the transverse dimension along the width of the ISAS in the interval $y \in [-b, b]$

$$\overline{F}_{\text{sum}}(\psi) = \overline{F}_{\text{attr}}(\psi) + \overline{F}_{\text{rep}}(\psi). \quad (9)$$

The characteristic phase dependence of the exciting aperiodic signal can be described by a function of the form [8]:

$$j_i(\psi) = \begin{cases} \sin\psi, & \psi \le \frac{\pi}{2}, \\ \exp\left(-\beta \cdot \left(\psi - \frac{\pi}{2}\right)\right), \psi \ge \frac{\pi}{2}, \beta \approx 0{,}75. \end{cases} \quad (10)$$

In addition, we illustrate graphical dependencies with additional averaged numerical estimates:

a) the value of the attractive force averaged in the transverse dimension on the interval $y \in [-b, b]$ and in phase $\psi \in [0, 2\pi]$

$$\overline{F}_{attr} = \frac{1}{2\pi}\int_0^{2\pi} \overline{F}_{\text{attr}}(\psi)d\psi = \frac{1}{(2\pi \cdot 2b)}\int_0^{2\pi}\int_{-b}^{b} F_{\text{attr}}(\psi, y)dyd\psi. \quad (11)$$

b) the value of the repulsive force averaged in the transverse dimension on the interval $y \in [-b, b]$ and in phase $\psi \in [0, 2\pi]$

$$\overline{F}_{\text{rep}} = \frac{1}{2\pi}\int_0^{2\pi} \overline{F}_{\text{rep}}(\psi)d\psi = \frac{1}{(2\pi \cdot 2b)}\int_0^{2\pi}\int_{-b}^{b} F_{\text{rep}}(\psi, y)dyd\psi. \quad (12)$$

c) the value of the resultant force (the superposition of the attractive force – Ampere and the repulsive force - Lorentz) averaged in the transverse dimension on the interval – $y \in [-b, b]$ and in phase – $\psi \in [0, 2\pi]$

$$\overline{F}_{\text{sum}} = \frac{1}{2\pi}\int_0^{2\pi} \overline{F}_{\text{sum}}(\psi)\, d\psi = \frac{1}{(2\pi \cdot 2b)} \times \times \int_0^{2\pi}\int_{-b}^{b} F_{\text{sum}}(\psi, y)\, dyd\psi. \quad (13)$$

We note that formula (13) illustrates the quantitative increase in the efficiency of the magnetic-pulse attraction taking into account the phase of the proceeding process. Numerical estimates can be averaged over any interesting spatial or phase interval. For example, when considering processes in the region directly under a separate inductor current lead, the averaging interval – $y \cup [a, (a + b)]$.

**Results of calculations.**

1. Electrodynamics processes in the region under the conductors of a rectangular solenoid of ISAS (Fig. 2-7).

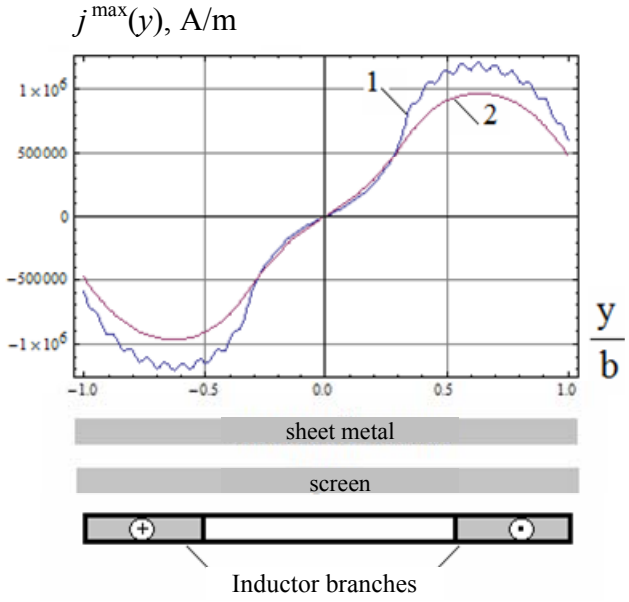


Fig. 2. The picture of the spatial distribution of induced currents, 1 – screen metal, 2 – sheet metal

With a decrease in the depth of the dent, the amplitude of the excited electrodynamics forces increases in practice, in proportion. Thus, with a decrease in depth from 0.005 m to 0.002 m, the forces increase by more than a factor of ~ 2.

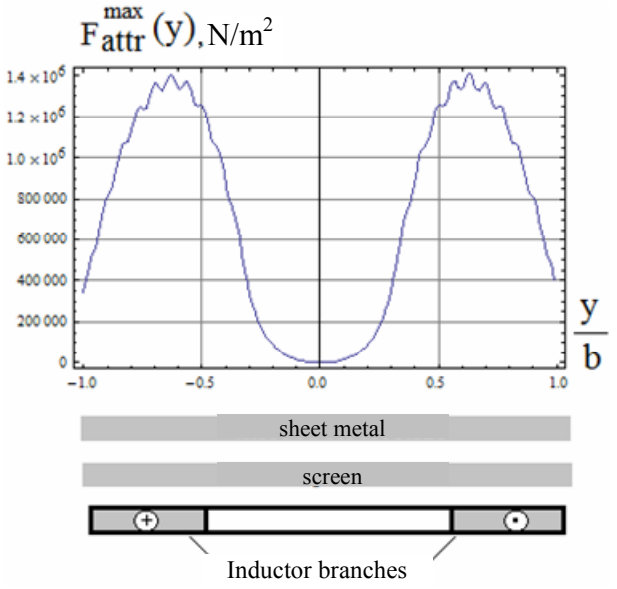


Fig. 3. The spatial pattern of the distributed force of attraction (Ampere), the average value on the width of the ISAS – $\overline{F}_{\text{attr}} \approx 0.78 \cdot 10^6$ N/m²

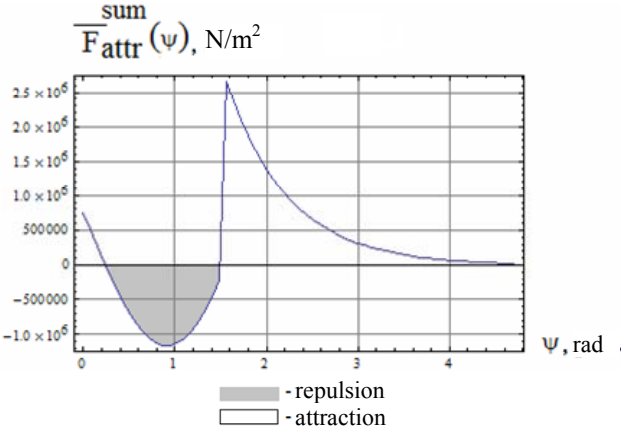


Fig. 4. The phase dependence of the resultant force (superposition of Ampere and Lorentz) acting on the sheet metal in the ISAS, the average value over the time of action – $\overline{F}_{\text{attr}}^{\text{sum}} \approx 0.245 \cdot 10^6$ N/m²

The main results of the calculations are as follows:

- calculated data are integral indicators of electrodynamics processes, characterizing their flow over the entire area of the inductor system, excited by a multiturn flat rectangular solenoid with current amplitude in the winding of ~ 22.6 kA with storage capacitor voltage of ~ 2 kV and storage energy of ~ 2.4 kJ;
- the temporal dependencies of the exciting and induced currents are different, which ultimately causes the oscillation of the Lorentz force, that is, the appearance of repulsion and attraction intervals;
- the prevalence of repulsive forces over the forces of attraction is short-term and occurs exclusively in the initial phase of the process of force action;
- averaging of the excited forces over the action time shows more than an order of magnitude (~ 15 times) the

excess of attraction over repulsion (attraction – $\overline{F}_{attr} \approx \approx 0.282 \cdot 10^6$ N/m$^2$, repulsion – $\overline{F}_{rep} \approx -0.0182 \cdot 10^6$ N/m$^2$);

- in the integral (averaging over the action time and the spatial variable), the ISAS examined over its entire area provides a magnetic-pulse attraction with force – $\overline{F}^{sum}_{attr} \approx 0.245 \cdot 10^6$ N/m$^2$.

2. Currents and forces in the area of the dent.

Geometry of the dent area (assumed area of force action): $D \times D \times H = 0.03$ m×0.03 m×0.05 m.

The specified sheet metal area is placed under the plane of the conductors of any of the branches of a rectangular solenoid, which excites the «inductor system with an attractive screen» (ISAS).

For the assumed region of force action, averaging over the transverse spatial variable is performed in the interval $\psi \in [0, D]$.

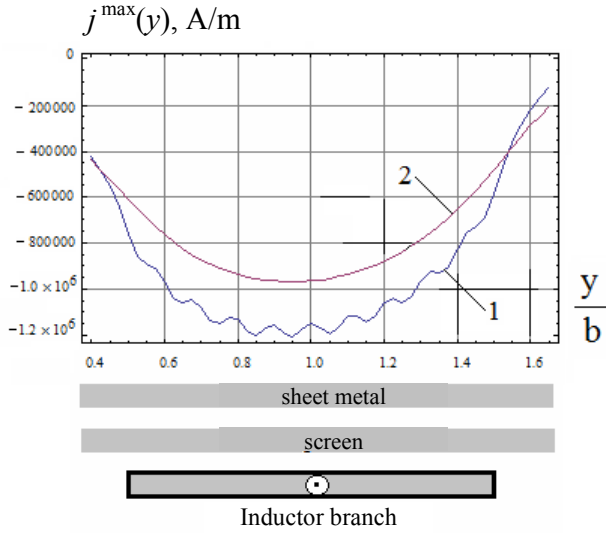


Fig. 5. The picture of the spatial distribution of induced currents, 1 – screen metal, 2 – sheet metal

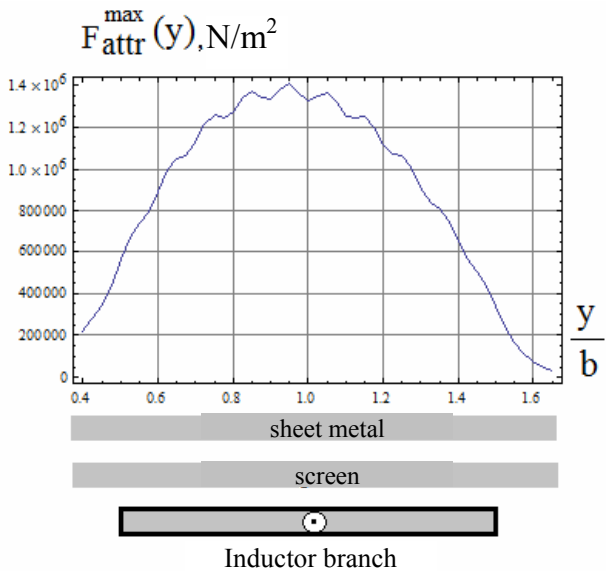


Fig. 6. The spatial pattern of the distributed force of attraction (Ampere), the average value on the width of the ISAS – $\overline{F}_{attr} \approx 0.92 \cdot 10^6$ N/m$^2$

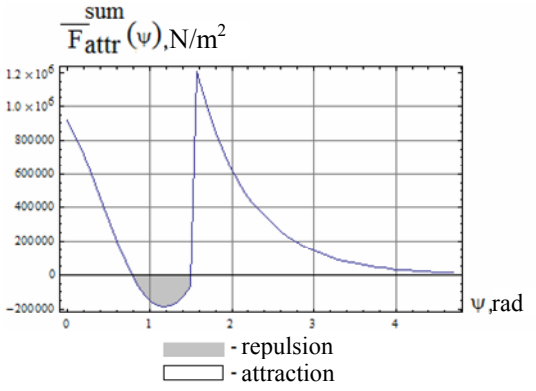


Fig. 7. The phase dependence of the resultant force (superposition of Ampere and Lorentz!) acting on the sheet metal in the ISAS, the average value over the time of action – $\overline{F}^{sum}_{attr} \approx 0.345 \cdot 10^6$ N/m$^2$

Discussion of the results of calculations:

- calculated data are local indicators of electrodynamics processes that characterize their flow in the region of a dent of a given geometry, in contrast to previous results obtained for the entire area under the ISAS winding;
- as before, the prevalence of repulsive forces over the forces of attraction is short-term and occurs exclusively in the initial phase of the process of force action;
- averaging of the excited forces by time of action shows a significant excess of attraction over repulsion (attraction – $\overline{F}_{attr} \approx 0.35 \cdot 10^6$ N/m$^2$, repulsion – $\overline{F}_{rep} \approx -0.056 \cdot 10^6$ N/m$^2$);
- in the integral (averaging over the action time and the spatial variable), the ISAS considered on its entire area provides a magnetic-pulse attraction with a distributed force – $\overline{F}^{sum}_{attr} \approx 0.345 \cdot 10^6$ N/m$^2$;
- in general, the comparison of the indicators of electrodynamics processes in the considered variants of the calculation shows an approximate growth in 1.3-1.5 times of the force indicators in the area of the accepted dent on the surface of the sheet metal in comparison with similar values for the whole area under the winding of the ISAS inductor.

**Conclusions.**

1. A numerical analysis of electrodynamics processes in an inductor system with an attractive screen and a source of a magnetic field − a flat rectangular solenoid is carried out in the work.

2. Numerical estimates have shown that when the depth of the dent decreases, the amplitude of the electrodynamics forces excited increases in practice in proportion.

3. The greatest efficiency of force attraction occurs for sheet metal regions, the dimensions of which do not exceed the transverse dimensions of the winding branches of the exciting solenoid.

4. The integral value of the repulsive forces in time is much lower than the developed attractive forces (less than ~ 5 %).

5. In general, at sufficiently low operating frequencies of acting fields (~ 1500 Hz), the «inductor system with an

attractive screen» considered operates as an instrument of magnetic-pulse attraction of thin-walled sheet metals. Local distributed forces of attraction in the region of given areas (for example, dents with limited dimensions!) at current in the inductor of ~ 22 kA can reach values of the order of ~ $0.345 \cdot 10^6$ N/m$^2$.

REFERENCES


***1.*** Batygin Yu.V., Lavinskiy V.I., Khimenko L.T. *Impul'snyye magnitnyye polya dlya progressivnykh tekhnologiy. Tom 1. Izdaniye vtoroye, pererabotannoye i dopolnennoye*. [Pulsed magnetic fields for advanced technologies. Vol.1. 2nd edition, revised and enlarged.] Kharkov, MOST-Tornado Publ., 2003. 284 p. (Rus).

***2.*** Yuriy V. Batygin, Sergey F. Golovashchenko, Andrey V. Gnatov. Pulsed electromagnetic attraction of sheet metals – fundamentals and perspective applications. *Journal of Materials Processing Technology*, 2013, vol.213, no.3, pp. 444-452. **doi: 10.1016/j.jmatprotec.2012.10.003**.

***3.*** Psyk V., Risch D., Kinsey B.L., Tekkaya A.E., Kleiner M. Electromagnetic forming – A review. *Journal of Materials Processing Technology*, 2011, vol.211, no.5, pp.787-829. **doi: 10.1016/j.jmatprotec.2010.12.012**.

***4.*** Gnatov A., Argun S. New method of car body panel external straightening. Tools of method. *International Journal of Vehicular Technology*, 2015, vol.2015, pp. 1-7. **doi: 10.1155/2015/192958**.

***5.*** Batygin Yuri V., Sergey F. Golovashchenko, Andrey V. Gnatov. Pulsed electromagnetic attraction of nonmagnetic sheet metals. *Journal of Materials Processing Technology*, 2014, vol.214, iss.2, pp. 390-401. **doi: 10.1016/j.jmatprotec.2013.09.018**.

***6.*** Batygin Yu.V., Golovashchenko S.F., Gnatov A.V., Chaplygin E.A. Pulsed Electromagnetic Attraction Processes for Sheet Metal Components. *Proceedings of the 6th International Conference High Speed Forming 2014*, May 26-29, 2014, Daejeon, Korea, pp. 253-260.

***7.*** Batygin Yu.V., Chaplygin E.A., Shinderuk S.A., Gavrilova O.E. Inductor system with attracting screen and rectangular solenoid. *Automobile Transport*, 2017, no.41, pp. 146-154. (Rus).

***8.*** Chitode J.S. *Signal an systems*. Pune, India, Technical Publications, 2009. 767 p.



*Received 25.12.2017*



*E.A. Chaplygin*[1]*, Candidate of Technical Sciences, Associate Professor,*
*M.V. Barbashova*[1]*, Candidate of Technical Sciences,*
*A.Yu. Koval*[1]*, student,*
[1] Kharkiv National Automobile and Highway University,
25, Yaroslava Mudrogo Str., Kharkov, 61002, Ukraine,
phone +380 57 7073727,
e-mail: chaplygin.e.a@gmail.com; barbashova1987@gmail.com



*How to cite this article:*
Chaplygin E.A., Barbashova M.V., Koval A.Yu. Numerical estimates of electrodynamics processes in the inductor system with an attractive screen and a flat rectangular solenoid. *Electrical engineering & electromechanics*, 2018, no.2, pp. 54-58. **doi: 10.20998/2074-272X.2018.2.09.**

UDC 629.424 **doi: 10.20998/2074-272X.2018.2.10**

S.G. Buriakovskyi, A.S. Maslii, V.V. Panchenko, D.P. Pomazan, I.V. Denis

# THE RESEARCH OF THE OPERATION MODES OF THE DIESEL LOCOMOTIVE CHME3 ON THE IMITATION MODEL

***Introduction. Fuel consumption by diesel locomotive during operation depends significantly on many factors, among which the main is the mode of driving a train. Purpose. Research on the mathematical model of the modes of driving a train on the site of Kharkiv-Merefa with the purpose of the main oscillograms of the operation of the locomotive on the site. Methodology. A mathematical model of the operation of the main units of the locomotive CHME3 in the Matlab environment was developed. The model of the diesel engine is based on the calculated indicator diagram of its operation, which is approximated by a continuous dependence. The control panel operates on a system of conditions, the purpose of which is to maintain the set speed. Results. In the course of the simulation, statistical data were obtained on the fuel consumption of the diesel locomotive when it operated on a section with a train of constant mass. Based on the data obtained, a three-dimensional surface is constructed showing the dependence of the fuel consumption on the time of the site's exploration and the maximum speed on the site. Practical value. The dependence obtained can be used to optimize the driving behavior of trains along a section. The apparent dependence of fuel consumption on the driver's behavior is the basis for the further development of automatic locomotive speed control systems.*** References 8, figures 6.

*Key words:* **diesel locomotive, imitation model, diesel engine, traction electric drive, road profile, fuel consumption, train mode.**

***Разработана имитационная модель тепловоза ЧМЭ3, которая состоит из дизеля с регулятором числа оборотов коленчатого вала, тягового генератора постоянного тока независимого возбуждения и тягового электрического привода. Проведено тестирование работы имитационной модели на профиле участка пути Харьков - Мерефа, при этом основными ограничениями являются время движения, для данного перегона не должно превышать 45 мин., а также максимальная допустимая скорость, которая для грузовых поездов составляет 80 км/ч. Получена трехмерная поверхность, которая показывает зависимость расхода топлива локомотива от режима ведения поезда машинистом при выполнении одинаковой работы, то есть одинакового времени движения по перегону.*** Библ. 8, рис. 6.

*Ключевые слова:* **тепловоз, имитационная модель, дизель, тяговый электропривод, профиль пути, расход топлива, режим ведения поезда.**

**Introduction.** Efficient use of fuel and energy resources is one of the most important tasks facing the Ukrainian economy. The Law of Ukraine «On Energy Saving» defines the energy efficiency of the economy as one of the main strategic guidelines for long-term state energy policy [1].

Railway transport is one of the largest energy consumers in the country. Energy efficiency in modern conditions is the most important factor in increasing the competitiveness of Ukrainian railways in the domestic and international transport services market. In 2010, the Cabinet of Ministers of Ukraine approved the Transport Strategy of Ukraine for the period up to 2020, aimed, in particular, at optimizing energy consumption in the unconditional performance of cargo transportation services and energy security of the company.

The main share of expenses of fuel and energy resources in the company accounts for traction of trains. Today it is 82 % of the total consumption of electricity and 90 % of diesel fuel [2]. Therefore, emphasis in energy saving is made, first of all, on the main type of activity - the transportation process. In this regard, the issue of energy efficiency is very relevant for the railways and requires further research.

**Analysis of literary data and problem definition.** An overview [3] shows that CHME3 locomotives make up 97 % of the entire fleet of shunting locomotives in the Ukrainian railways. In addition to maneuvering at stations, these locomotives are often used for transportation, as well as in the suburban traffic. In the conditions of the introduction of high-speed traffic, the optimization of the modes of data types of trains by sections is of particular importance. In conditions of increasing the speed of the passage of the site we should not forget about the cost of fuel and energy resources.

As noted in [4], the conditions of the locomotive operation while driving the trains are characterized by a continuous change in traction and speed, and to this also there are sections of the paths with insufficient grip. In this case, the power of the locomotive depends on many circumstances, it varies depending on the speed being implemented, the selected position of the controller of the driver and the degree of weakening of the excitation field. These circumstances allow us to implement very diverse modes of control of traction rolling stock, which often differ from those taken in the traction calculations and specified in the regime cards.

For various modes of operation, the rational driving conditions are essential. It does not allow to recommend one mode of driving a train as optimal for all practically possible traffic conditions in the area, because even on the same site, these conditions often change. In addition, the characteristics of electric machines and specific locomotives, depending on their technical state, may differ in certain respects from the corresponding passport data.

All this creates difficulties in the development and practical use of rational modes of driving trains. However, experience shows that even in the presence of regime maps and the implementation of recommended modes of driving trains, technically justified for some average operating conditions, actual costs of electricity and fuel from different drivers on

the same sites are different, deviations can be both greater and to a lesser extent than the established norm (up to 10 %).

Based on the above mentioned, one can conclude that studying the modes of driving a train is very important. Imitation modeling is the most appropriate way of research, since it enables to obtain important statistics with sufficient accuracy [5].

**The goal and tasks of the research.** The goal of the work is to investigate various modes of driving a train by CHME3 diesel locomotive for their optimality in terms of time of passage of a site and fuel consumption.

To achieve this goal we need:

- to develop an imitation model of all components of the locomotive involved in the creation and implementation of traction force;
- to select and simulate the section of the path on which the research will be conducted;
- to identify train driving modes and explore each one.

**Presentation of the main material.** The diesel generator set together with the electrical part of the research object consists of the following basic structural elements: control panel, diesel with regulator of crankshaft speed, traction generator of direct current of the independent excitation and traction electric drive. The block diagram of such object of research is shown in Fig. 1.

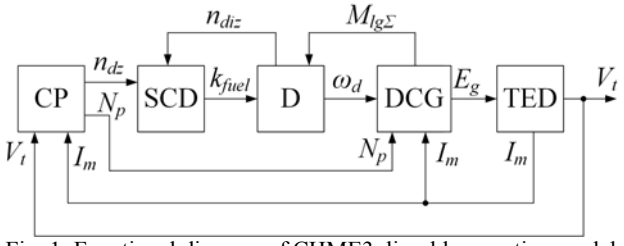


Fig. 1. Functional diagram of CHME3 diesel locomotive model: CP - control panel; SCD - diesel speed regulator; D - diesel; DCG - DC generator with exciter; TED - traction electric drive

The input parameters for the CP unit are the train speed $V_t$ and the motor current $I_m$, on the value of which depend the driver's controller position number $N_p$ and the specified number of diesel turns $n_{dz}$ which is the input value for the SCD block. Depending on $n_{dz}$ and $n_{diz}$, SCD determines the required amount of fuel $k_{fuel}$. On the basis of $k_{fuel}$ and loading torque $M_{lg\Sigma}$, DCG receives from D the value $\omega_d$. The value $E_g$ which is the input parameter of the TED block, is calculated by DCG depending on $N_p$ and $I_m$. At the output of TED, the value $V_p$ is formed.

The control panel CP of the diesel locomotive CHME3 has 8 positions of the voltage change on the traction motors and two positions of the field weakening. At each position, with the help of automatic regulators, the steady values of the frequency of rotation of the crankshaft of the diesel engine and of the voltage on the terminals of the exciter are maintained [6].

The modeled control panel switches the position of the driver's controller depending on two coordinates, namely: the current of engines and the speed of the train. The operation of the unit that simulates the panel is carried out under the following conditions:

$$N_p = \begin{cases} N_p - 1 \ \textit{if} \ I_m > I_n \ \vee \ V_t > V_s \\ N_p \ \textit{if} \ I_m < I_n \ \wedge \ V_s - 5 \le V_t \le V_s \\ N_p + 1 \ \textit{if} \ I_m < I_n \ \wedge \ V_t < V_s - 5 \end{cases}, \quad (1)$$

where $N_p$ is the position number of the driver's controller, $I_m$ is the current of the motor, $I_n$ is the rated current of the motor, $V_t$ is the current train's speed, $V_S$ is the specified train's speed.

To exclude the possibility of too frequent switching of positions, analysis of the need for switching occurs at intervals of 1 s. To exclude a large number of switches in steady state, when the actual speed is close to the given, there is a dead zone of 5 km/h in which there is no switching, and the movement is carried out on the previously selected position.

The block diagram realizing the condition (1) is shown in Fig. 2, where PS is the position selection block. The selected position number, also, is converted to a given speed of the diesel engine $n_{dz}$.

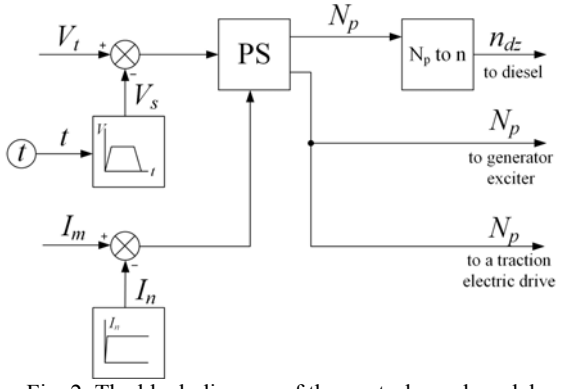


Fig. 2. The block diagram of the control panel model

All diesel engines according to the nature of their operation are very sensitive to load changes. An increase in diesel loading causes a reduction in the speed of the crankshaft («drawdown»), which can lead to the stopping of the diesel engine, and a decrease in the load is accompanied by a sharp increase in the rotational speed of the shaft, that is, the diesel engine can go to «spacing» [7].

In order to maintain constant rotational speed of the shaft under variable load conditions, a special regulator is required which automatically controls the fuel pumps. Mounted on a diesel K6S310DR a centrifugal inverted indirect action regulator protects it from overload performing the functions of the power regulator. The combined regulator can be represented as the PI regulator of the rotation speed of the crankshaft of the diesel engine, the input value of which is the amount of fuel that needs to be fed into the cylinder.

As the basis of the simulation model of the diesel, indicator diagram of its operation is used. The process taking place in the cylinder of the piston engine can be presented as a indicator diagram. Indicator diagram is the extreme reflection of pressure change of gas in the cylinder of the piston engine depending on the piston displacement or the turn angle of the crank [8]. For the K6S310DR diesel engine, the indicator diagram of its operation is calculated and built. The indicator diagram is

built as a dependence of the change in pressure $P$ in the engine's cylinder on the change in volumes $V$ during the piston's displacement.

For the diesel model, the use of the diagram in the axes $P$ and $V$ is rather uncomfortable, so the diagram is transformed into a diagram in the axes $F$ and $S$, where $F$ is the force acting on the piston, $S$ is the displacement of the piston. The dependence diagram of the force acting on the piston on the displacement is shown in Fig. 3.

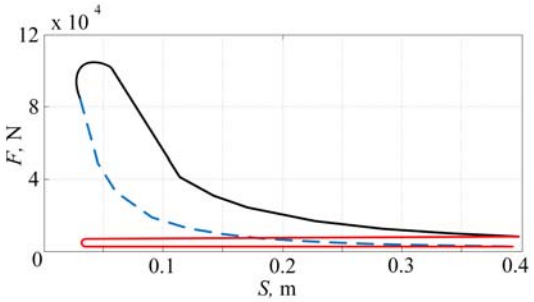


Fig. 3. Operation diagram of the diesel engine K6S310DR

The locomotive has a generator that is a ten-pole DC motor with independent excitation. The power supply of the independent excitation winding of the generator is carried out from the exciter - a machine of direct current connected by a shaft with auxiliary generator.

The block that simulates the traction electric drive includes, in addition to the traction electric motor, blocks that simulate the train's motion in the section and braking of a train.

The model of the resistance blocks of the train's movement is made according to the empirical formulas for the locomotive and cars. The profile of the section Kharkiv-Merefa has been used as a profile of the road. The input parameter for the slope selection block is the path that traveled, which is obtained by integrating the speed of the train.

Input variables for the braking unit operation are the given speed $V_s$, the current train speed $V_t$, and the position number of the locomotive driver's controller $N_p$. To exclude the mode at which braking occurs with operating traction motors, the check of the current position of the handle of the driver's controller is performed. If the position is non-zero, braking does not occur.

The testing of the imitation model was carried out under the parameters given above. Here, the main restrictions were the time of travel, which for the Kharkiv-Merefa section should not exceed 45 minutes, as well as the maximum permissible speed, which for freight trains is 80 km/h. Taking this into account, it is possible to use different intensity of acceleration of the train with the subsequent maintenance of the average speed of the run. Fig. 4 shows two types of train traction tachograms.

In the tachograms shown, $t_d$ is the run-time, which is the same for two tachograms. The change in the intensity of the train's acceleration leads to a change in the maximum speeds that are shown in the diagrams shown as $V_{m1}$, $V_{m2}$. In the software package Matlab, using a m-file, a subroutine was written in which the calculation of the intensity of acceleration and train's braking depending on a given maximum speed was performed, subject to the observance of the driving time of the run. In the study of the operation of the train on the imitation model, tachographs with maximum speeds in the range of 40-80 km/h with step 10 km/h were set. Fig. 5 shows the oscillograms of the shunting diesel locomotive operation with 10 cars, at a maximum speed of 60 km/h.

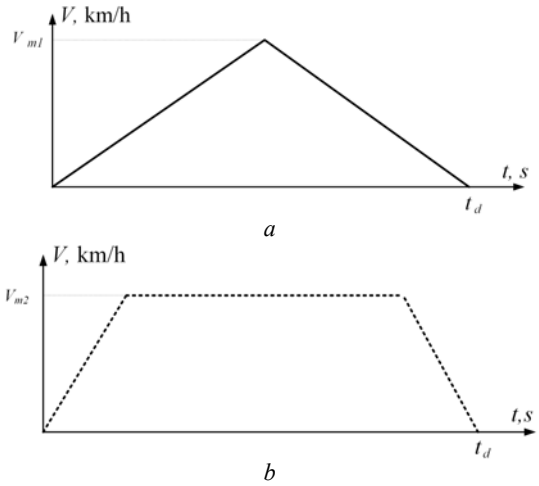


Fig. 4. Types of tachograms of the train acceleration: *a* - triangular; *b* - trapezoidal

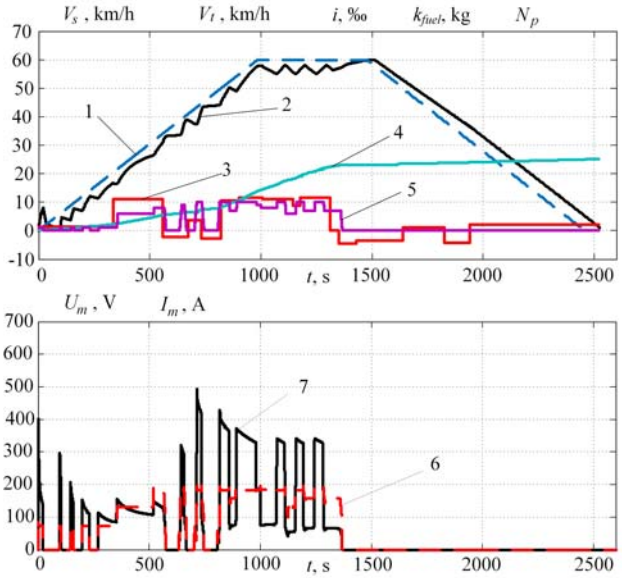


Fig. 5. Oscillograms of the locomotive operation at a maximum speed of 60 km/h: 1 - a tachogram is given; 2 - real speed of the train; 3 - profile of the path; 4 - fuel consumption; 5 - position number of the driver's controller; 6 - voltage on the traction motor; 7 - current of the traction motor

On the obtained oscillograms curve 3 shows the process of set of positions, which varies with different values of maximum speed. Each position corresponds to the change in the voltage on the traction motors (curve 6) and the values of current (curve 7) in them, which was limited to 600 A. The graphs show a tendency to increase fuel consumption with an increase in maximum speed, which requires a more detailed study. Changing the maximum speed of a triangular diagram in the range of 70-95 km/h with step of 5 km/h the results presented in the form of a three-dimensional surface were obtained (Fig. 6).

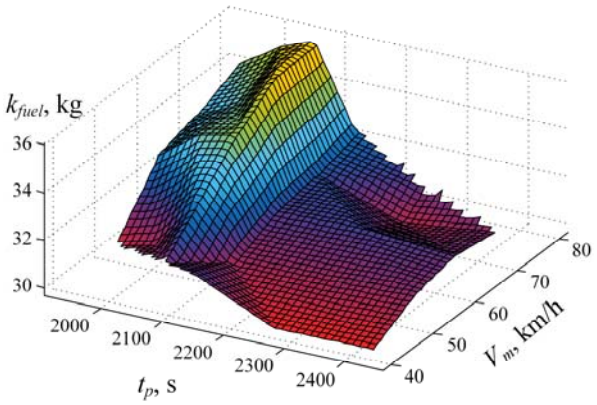

Fig. 6. Changing the fuel consumption depending on the maximum speed of the given diagram

The resulting surface confirms the dependence of the fuel consumption on the locomotive on the train driver's mode of driving (on the time the locomotive operation at a certain position and the intensity of the transition from position to position) when performing the same work, that is, the same time of movement on the run. The smallest fuel consumption, namely 29-31 kg, takes place when the maximum speed is set at 40-50 km/h. Therefore, there is a need to optimize the given train tachogram and develop an automatic control system using a speed regulator that more accurately worked out such a tachogram.

**Conclusions.** An imitation model of the diesel locomotive CHME3, consisting of a control panel, a diesel engine with a crankshaft speed regulator, an independent excitation DC traction generator and a traction electric drive with sequential excitation DC motors, has been developed. An algorithm is created that simulates the work of the driver, that is, it switches the positions of the controller and controls the brakes. The modeling of the diesel engine is based on the indicator diagram of its operation, which is approximated by continuous dependencies. The obtained imitation model allows obtaining important statistical data for conducting analysis of train driving modes.

A number of operation modes investigations have been carried out when changing the tachogram of speed. Changing the maximum speed of a triangular diagram in the range of 70-95 km/h with step of 5 km/h oscillograms of the locomotive operation with a constant loading on the real section of the road Kharkiv-Merefa are obtained.

From the oscillograms it is seen that the current during motion of the site was lower than the nominal, and in peak modes reached 500 A. Time of passage of the site with a given acceleration rate and speed limit on the level 60 km/h was 2530 s.

The model includes a block that calculates fuel consumption by diesel locomotive. Based on the data obtained from the simulation, a three-dimensional surface is constructed, which reflects the dependence of fuel consumption on the time of the passage of the site and the maximum speed. It has been established that the smallest fuel consumption, namely 29-31 kg, occurs when the maximum speed is set at 40-50 km/h.

The results obtained during the study show that there is a need to create an automatic control system using a speed controller that more accurately worked out the given tachogram, as well as optimization of train driving modes.

REFERENCES

***1.*** Available at: http://www.uz.gov.ua/en/about/general_information (accessed 08 May 2017).

***2.*** Efimenko Yu.I., Kovalev V.I., Loginov S.I. *Zheleznyie dorogi. Obschiy kurs* [Railways. General course]. Moscow, UMC ZhDT Publ., 2014. 503 p. (Rus).

***3.*** Kulaev Yu.F. *EkonomIka zalIznichnogo transportu. Navchalniy posibnik* [The Economics of Railway Transport. A Textbook]. Nizhyn, Aspect. Poligraph Publ., 2006. 232 p. (Ukr).

***4.*** Franzitta V., Curto D., Milone D., Trapanese M. Energy Saving in Public Transport Using Renewable Energy. *Sustainability*, 2017, vol.9, no.12, p. 106. **doi: 10.3390/su9010106.**

***5.*** Velten K. *Mathematical Modeling and Simulation*. Wiley-VCH Verlag GmbH & Co. KGaA, Weinheim, Germany, 2008. **doi: 10.1002/9783527627608.**

***6.*** Buryakovs'kyy S.H., Masliy A.S., Pomazan D.P., Denys I.V. Rationale for modernization of diesel locomotives CHME3 using hybrid propulsion system. *Electrification of Transport*, 2016, no.12, pp. 82-86. (Ukr).

***7.*** Xin Q. Engine-vehicle matching analysis in diesel powertrain system design. *Diesel Engine System Design*, 2013, pp. 348-394. **doi: 10.1533/9780857090836.2.348**.

***8.*** *Diesel Engine.* Van Nostrand's Scientific Encyclopedia. John Wiley & Sons, Inc., 2005. **doi: 10.1002/0471743984.vse2527.**

*Received 13.02.2018*

*S.G. Buriakovskyi*[1]*, Doctor of Technical Science,*
*A.S. Maslii*[2]*, Candidate of Technical Science, Associate Professor,*
*V.V. Panchenko*[2]*, Candidate of Technical Science, Associate Professor,*
*D.P. Pomazan*[2]*, Postgraduate Student,*
*I.V. Denis*[3]*,*
[1] Scientific-&-Research Planning-&-Design Institute «Molniya»,
National Technical University «Kharkiv Polytechnic Institute»,
2, Kyrpychova Str., Kharkiv, 61002, Ukraine,
e-mail: sergbyr@i.ua
[2] Ukrainian State University of Railway Transport,
7, Feierbakh Square, Kharkiv, 61050, Ukraine,
e-mail: a.masliy@ukr.net, vlad_panchenko@ukr.net, danil.pomazan@ukr.net
[3] PJSC «CARTEL»,
84a, Dnieper highway Str., Kriviy Rig, 50026, Ukraine,
e-mail: div99@ukr.net

*How to cite this article:*
Buriakovskyi S.G., Maslii A.S., Panchenko V.V., Pomazan D.P., Denis I.V. The research of the operation modes of the diesel locomotive CHME3 on the imitation model. *Electrical engineering & electromechanics*, 2018, no.2, pp. 59-62. **doi: 10.20998/2074-272X.2018.2.10.**

UDC 621.314 **doi: 10.20998/2074-272X.2018.2.11**

M.Yu. Artemenko, L.M. Batrak, S.Y. Polishchuk

# CURRENT FILTERING IN A THREE-PHASE THREE-WIRE POWER SYSTEM AT ASYMMETRIC SINUSOIDAL VOLTAGES

***Purpose. Investigation of the optimal current distribution between source, shunt active filter and reactive compensator of a three-phase three-wire system that provides consumption of a sinusoidal symmetric current under asymmetric source voltages with minimal power losses was provided. Methodology. The tasks were solved by conducting theoretical and experimental studies. The main provisions of the theory of electrical circuits, the apparatus of mathematical analysis, methods for solving linear differential and algebraic equations, elements of matrix and complex calculus and vector algebra are used. During the development, modern methods and software of computer simulation of electrical engineering complexes and dynamic systems were applied: Matlab-Simulink, MATHCAD. Originality. The principle of compensating current distribution between PAF and reactive compensator of a three-phase three-wire power system with asymmetric sinusoidal voltage was proposed at which the input current is equal to the positive-sequence active current and rms value of PAF current is minimal. The feasibility to compensate the inactive sinusoidal Fryze current by reactive elements under arbitrary combination of load and source parameters was proved and expression for direct calculation of the reactive compensator parameters for generation of inactive Fryze current in the source unbalanced mode was obtained. Practical value. The simulative example for transmission line load showed that combined application of PAF and reactive compensator with the specified distribution of compensating currents ensured a reduction of power losses in 3.273 times and rms value of the SAF current is 12.9 % of rms value total compensation current.*** References 10, tables 1, figures 2.

*Key words:* **active and inactive Fryze current, asymmetrical voltage and load, reactive compensator, symmetrical components.**

***Рассмотрены принципы активной фильтрации тока в трехфазной трехпроводной системе электропитания при несимметричном синусоидальном источнике питания, удовлетворяющие требованиям стандарта IEEE Std.1459-2010. Показаны преимущества формирования синусоидального симметричного входного тока при параллельном подключении активного фильтра и реактивного компенсатора. Доказана возможность компенсации неактивного синусоидального тока Фризе реактивными элементами при произвольной комбинации параметров нагрузки и источника. Получена формула прямого расчета параметров реактивного компенсатора для генерации неактивного тока Фризе в несимметричном режиме источника питания. Приводятся результаты численного моделирования.*** Библ. 10, табл. 1, рис. 2.

*Ключевые слова:* **активный и неактивный ток Фризе, несимметричное напряжение и нагрузка, реактивный компенсатор, симметричные составляющие.**

**Introduction.** The unbalanced load of three-phase, three-wire power systems leads to a deterioration in the quality of electricity, which manifests in the emergence of negative sequence currents and pulsations of instantaneous power, which cause additional losses on the active supports of the transmission line and asymmetry of the supply voltages in the nodes of the overall connection of loads. Passive filters on reactive elements are efficiently used to balance the asymmetrical stationary linear load, calculation of which is based on two approaches: compensation of inactive components of input currents [1, 3-5] and elimination of the pulsating component of instantaneous power [2, 6]. However, in the case of asymmetry of voltages, the use of passive reactive compensators of both types leads to the emission into the transmission line of negative sequence currents and even greater voltage asymmetry, which contradicts the approaches outlined in [7]. Effective compensation of these currents is possible only by means of active filtration [8], and parallel active filters (PAF) are dominated successive ones by power of energy losses on their own elements. To further reduce the loss of PAF they are used in combination with reactive compensators [9]. Therefore, it is relevant to study the optimal distribution of asymmetric load currents between a three-phase source, PAF and a reactive compensator, which provides the minimum power loss when consuming sinusoidal symmetric source current.

**Vectors of active currents in phase coordinates.** The periodic process in the section <*A*, *B*, *C*> of the three-wire power supply system is determined by three-coordinate vectors of instantaneous voltage and current values

$$\boldsymbol{u}(t)=\begin{Vmatrix}u_A(t)\\u_B(t)\\u_C(t)\end{Vmatrix}=\sqrt{2}\begin{Vmatrix}U_A\cos(\omega t+\phi_A)\\U_B\cos(\omega t+\phi_A)\\U_C\cos(\omega t+\phi_A)\end{Vmatrix};$$

$$\boldsymbol{i}(t)=\begin{Vmatrix}i_A(t)\\i_B(t)\\i_C(t)\end{Vmatrix}=\boldsymbol{i}(t+2\pi/\omega), \qquad (1)$$

where $\omega$ is the circular frequency of the three-phase source; $u_A$, $u_B$, $u_C$ are the phase voltages deduced from the point of artificial grounding [5], $U_A$, $U_B$, $U_C$ and $\varphi_A$, $\varphi_B$, $\varphi_C$ are their mean square and initial phases; the periodic current vector $\boldsymbol{i}(t)$ contains higher harmonic components in the case of nonlinear loading.

According to the Fryze [1] concept, active current

$$\boldsymbol{i}_A(t)=\frac{P}{U^2}\boldsymbol{u}(t) \qquad (2)$$

provides the same active power $P$ as the total current $\boldsymbol{i}(t)$.

The scalar coefficients of formula (2) can be found in the time domain as integrals

$$P = \frac{1}{T}\int_0^T \boldsymbol{u}^{\wedge}(t)\boldsymbol{i}(t)dt;$$

$$U^2 = \frac{1}{T}\int_0^T \boldsymbol{u}^{\wedge}(t)\boldsymbol{u}(t)dt = U_A^2 + U_B^2 + U_C^2;$$

where $\wedge$ is the sign of transposition, $T = 2\pi/\omega$ is the period.

The current determined by the formula

$$\boldsymbol{i}_N(t) = \boldsymbol{i}(t) - \boldsymbol{i}_A(t), \tag{3}$$

is called inactive [1], it does not carry energy to load, but causes additional losses in the transmission line.

Since the vectors of active and inactive currents are mutually orthogonal, the correct ratio for the mean square values of these currents is:

$$I^2 = \frac{1}{T}\int_0^T \boldsymbol{i}^{\wedge}(t)\boldsymbol{i}(t)dt = I_A^2 + I_N^2.$$

In the case of compensation of inactive current by means of filtration, we will have a decrease in the power loss $\Delta P$ in the transmission line, which can be characterized [10] by the coefficient of gain on the power loss:

$$k_A^{\Delta P} = \frac{\Delta P}{\Delta P_A} = \frac{I^2 r}{I_A^2 r} = \frac{1}{\lambda^2}, \tag{4}$$

where $r$ is the resistance of each wire of the transmission line; $\lambda = P/S = I_A/I$ is the power factor; $S = UI$ is the full power of the three-phase system.

In the sinusoidal mode of the three-phase voltage source, the active current vector also consists of sinusoidal temporal functions, so it is expedient [5] to introduce three-dimensional complex vectors (3D-phasors) of voltage and current in the same way [5].

$$\overline{\boldsymbol{u}} = \frac{\sqrt{2}}{T}\int_0^T \boldsymbol{u}(t)e^{-j\omega t}dt = \begin{Vmatrix} U_A e^{j\varphi_A} \\ U_B e^{j\varphi_A} \\ U_C e^{j\varphi_A} \end{Vmatrix} = \begin{Vmatrix} \dot{U}_A e^{j\varphi_A} \\ \dot{U}_B e^{j\varphi_A} \\ \dot{U}_C e^{j\varphi_A} \end{Vmatrix};$$

$$\bar{\boldsymbol{i}}_1 = \frac{\sqrt{2}}{T}\int_0^T \boldsymbol{i}(t)e^{-j\omega t}dt = \begin{Vmatrix} \dot{I}_A e^{j\psi_A} \\ \dot{I}_B e^{j\psi_A} \\ \dot{I}_C e^{j\psi_A} \end{Vmatrix}. \tag{5}$$

The complex vector $\bar{\boldsymbol{i}}_1$ represents the harmonic component of the fundamental frequency of the vector $\boldsymbol{i}(t)$. In the time domain, it corresponds to a vector of instantaneous values $\boldsymbol{i}_1(t)$, which differs from the vector $\boldsymbol{i}(t)$ on the vector of higher harmonics

$$\boldsymbol{i}_H(t) = \boldsymbol{i}(t) - \boldsymbol{i}_1(t) = \boldsymbol{i}(t) - \sqrt{2}\,\mathrm{Re}\left(\bar{\boldsymbol{i}}_1 e^{j\omega t}\right). \tag{6}$$

However, two complex vectors of (5) completely determine the active Fryze current in the frequency domain:

$$\bar{\boldsymbol{i}}_A = \frac{\sqrt{2}}{T}\int_0^T \boldsymbol{i}_A(t)e^{-j\omega t}dt = \frac{P}{U^2}\overline{\boldsymbol{u}} = \frac{\mathrm{Re}\left(\overline{\boldsymbol{u}}^{\wedge}\bar{\boldsymbol{i}}_1^*\right)}{\overline{\boldsymbol{u}}^{\wedge}\overline{\boldsymbol{u}}^*}\overline{\boldsymbol{u}} = \bar{\boldsymbol{i}}_1 - \boldsymbol{i}_{1N}, \tag{7}$$

where the sign * denotes complex conjugation, $\bar{\boldsymbol{i}}_{1N}$ is the complex vector of inactive current of the main frequency.

In the unbalanced mode of the three-phase source, the vectors $\overline{\boldsymbol{u}}$ and $\bar{\boldsymbol{i}}_A$ contain symmetric components of the negative sequence, which the modern Standard [7] refers to inactive components of the current to be compensated. To meet the requirements of the Standard, the active current must be formed as proportional to the reference voltage vector containing only the symmetric components of the direct sequence. We represent this vector in the frequency domain as proportional to the ort of a symmetric direct sequence [5]

$$\overline{\boldsymbol{u}}_+ = U_+\overline{\boldsymbol{e}}_+ = \frac{U_+}{\sqrt{3}}\begin{Vmatrix} 1 \\ e^{-j2\pi/3} \\ e^{j2\pi/3} \end{Vmatrix} = \frac{U_+}{\sqrt{3}}\begin{Vmatrix} 1 \\ \tilde{a} \\ \dot{a} \end{Vmatrix}, \tag{8}$$

then the active current vector of the direct sequence is given by the expression

$$\bar{\boldsymbol{i}}_{A+} = \frac{P}{\overline{\boldsymbol{u}}_+^{\wedge}\overline{\boldsymbol{u}}_+^*}\overline{\boldsymbol{u}}_+ = \frac{P}{U_+^2}\overline{\boldsymbol{u}}_+, \tag{9}$$

where the coefficient of proportionality is determined from the condition of providing by this current under the action of the voltage vector $\overline{\boldsymbol{u}}$ of the same active power $P$, as the total current $\boldsymbol{i}(t)$.

**Decomposition of load currents in symmetric coordinates.** For a detailed study of the difference between the vectors defined by formulas (7) and (9), we turn to the basis of symmetric coordinates [5]. Since the symmetric component of the zero sequence of each of these vectors is zero, we multiply them on the matrix containing the transposed orts of the symmetric components of the direct and negative sequences

$$\left(\boldsymbol{F}_0^{\wedge}\right)^* = \begin{Vmatrix} \overline{\boldsymbol{e}}_-^{\wedge} \\ \overline{\boldsymbol{e}}_+^{\wedge} \end{Vmatrix} = \frac{1}{\sqrt{3}}\begin{Vmatrix} 1 & \dot{a} & \tilde{a} \\ 1 & \tilde{a} & \dot{a} \end{Vmatrix}.$$

As a result, we obtain the following expressions for complex voltage vectors in symmetric coordinates:

$$\tilde{\boldsymbol{u}}_+ = (\boldsymbol{F}_0^{\wedge})^*\overline{\boldsymbol{u}}_+ = \begin{Vmatrix} \overline{\boldsymbol{e}}_-^{\wedge} \\ \overline{\boldsymbol{e}}_+^{\wedge} \end{Vmatrix} U_+\overline{\boldsymbol{e}}_+ = \begin{Vmatrix} U_+ \\ 0 \end{Vmatrix};$$

$$\tilde{\boldsymbol{u}} = (\boldsymbol{F}_0^{\wedge})^*\overline{\boldsymbol{u}} = (\boldsymbol{F}_0^{\wedge})^* \begin{Vmatrix} \dot{U}_A \\ \dot{U}_B \\ \dot{U}_C \end{Vmatrix} = \begin{Vmatrix} U_+ \\ \dot{U}_- \end{Vmatrix}.$$

The transition from two-coordinate vectors in symmetric coordinates to three-coordinate complex vectors in phase coordinates is carried out by multiplying on the matrix $\boldsymbol{F}_0 = \|\overline{\boldsymbol{e}}_+ \quad \overline{\boldsymbol{e}}_-\|$. Taking into account the relationship between the matrices

$$(\boldsymbol{F}_0^{\wedge})^*\boldsymbol{F}_0 = \begin{Vmatrix} 1 & 0 \\ 0 & 1 \end{Vmatrix} = \boldsymbol{I}_{2\times 2};\ \ \boldsymbol{F}_0(\boldsymbol{F}_0^{\wedge})^* = \boldsymbol{I}_{3\times 3} - \frac{\boldsymbol{j}\boldsymbol{j}^{\wedge}}{3};\ \ \boldsymbol{j} = \begin{Vmatrix} 1 \\ 1 \\ 1 \end{Vmatrix},$$

which stores the mean square values of the quantities in symmetric and phase coordinates, we obtain the following

expressions for complex active current vectors in symmetric coordinates

$$\widetilde{\boldsymbol{i}}_A = \frac{P}{\overline{\boldsymbol{u}}\,\hat{}\,\overline{\boldsymbol{u}}^*}\widetilde{\boldsymbol{u}} = \frac{P}{\widetilde{\boldsymbol{u}}\,\hat{}\,\widetilde{\boldsymbol{u}}^*}\widetilde{\boldsymbol{u}} = \frac{P}{U_+^2+U_-^2}\begin{Vmatrix} U_+ \\ \dot{U}_- \end{Vmatrix};$$

$$\widetilde{\boldsymbol{i}}_{A+} = \frac{P}{U_+^2}\widetilde{\boldsymbol{u}}_+ = \frac{P}{U_+^2}\begin{Vmatrix} U_+ \\ 0 \end{Vmatrix}. \qquad (10)$$

Consumption from an asymmetric sinusoidal Fryze current source does not eliminate the pulsations of active power [5]. Its instantaneous value can be determined [2] using the vector

$$\widetilde{\boldsymbol{i}}_A^{\leftrightarrow} = \frac{P}{U_+^2+U_-^2}\begin{Vmatrix} \dot{U}_- \\ U_+ \end{Vmatrix}$$

by the formula

$$\widetilde{p}_A(t) = \mathrm{Re}\left(\widetilde{\boldsymbol{u}}\,\hat{}\,\widetilde{\boldsymbol{i}}_A^{\leftrightarrow} e^{j2\omega t}\right) = \frac{P\,\mathrm{Re}\left(2U_+\dot{U}_- e^{j2\omega t}\right)}{U_+^2+\dot{U}_-^2} =$$

$$= \frac{2P\delta_-\cos\left(2\omega t+\varphi_-\right)}{1+\delta_-^2},$$

where $\dot{\delta}_- = \dot{U}_-/\dot{U}_+ = \delta_- e^{j\varphi_-}$ is the complex parameter of asymmetry of a three-phase source.

If the input current of the three-phase system is determined by the vector $\widetilde{\boldsymbol{i}}_A$, the instantaneous value of the pulsation of the active power is

$$\widetilde{p}_{A+}(t) = \mathrm{Re}\left(\widetilde{\boldsymbol{u}}\,\hat{}\,\widetilde{\boldsymbol{i}}_{A+}^{\leftrightarrow} e^{j2\omega t}\right) = \frac{P}{U_+^2}\mathrm{Re}\left(\begin{Vmatrix} U_+ & \dot{U}_- \end{Vmatrix}\begin{Vmatrix} 0 \\ U_+ \end{Vmatrix} e^{j2\omega t}\right) =$$

$$= P\delta_-\cos\left(2\omega t+\varphi_-\right).$$

Thus, the active current of a direct sequence creates a pulsation of instantaneous power, the amplitude of which is in $2/(1+\delta_-^2)$ times less than that one generated by the active Fryze current.

The difference between the active current vectors in symmetric coordinates obtained from (10), i.e.

$$\widetilde{\boldsymbol{i}}_{\pm} = \widetilde{\boldsymbol{i}}_A - \widetilde{\boldsymbol{i}}_{A+} = \frac{P}{U_+^2+U_-^2}\begin{Vmatrix} -U_-^2/U_+ \\ \dot{U}_- \end{Vmatrix} \qquad (11)$$

defines an additional current of compensation. The active power of this current is zero:

$$P_{\pm} = \mathrm{Re}(\widetilde{\boldsymbol{u}}\,\hat{}\,\widetilde{\boldsymbol{i}}_{\pm}^*) = \left(\frac{P}{U_+^2+U_-^2}\right)^2 \begin{Vmatrix} U_+ & \dot{U}_- \end{Vmatrix}\begin{Vmatrix} -U_-^2/U_+ \\ \widetilde{U}_- \end{Vmatrix} = 0,$$

and it can be realized by PAF.

Thus, in order to realize the consumption from a three-phase current source of current active current of direct sequence, the main harmonic of the compensation current should contain the following components in symmetric coordinates:

$$\widetilde{\boldsymbol{i}}_{1C} = \boldsymbol{i}_1 - \boldsymbol{i}_{A+} = \boldsymbol{i}_{1N} + \boldsymbol{i}_{\pm}. \qquad (12)$$

In the time domain, the compensation current vector also includes a higher harmonic vector:

$$\boldsymbol{i}_{C+}(t) = \boldsymbol{i}(t) - \boldsymbol{i}_{A+}(t) = \boldsymbol{i}_{1N}(t) + \boldsymbol{i}_{\pm}(t) + \boldsymbol{i}_H(t). \qquad (13)$$

The coefficient of gain on the power loss in the formation of active current of direct sequence

$$k_{A+}^{\Delta P} = \frac{\Delta P}{\Delta P_{A+}} = \frac{I^2}{I_{A+}^2} = \frac{I_A^2+I_N^2}{I_A^2}\times\frac{I_A^2}{I_{A+}^2} = \frac{k_A^{\Delta P}}{1+\delta_-^2} \qquad (14)$$

exceeds the unit provided

$$\lambda\sqrt{1+\delta_-^2} < 1. \qquad (15)$$

Taking into account the orthogonality of the vectors $\boldsymbol{i}_{C+}(t)$, $\boldsymbol{i}_{A+}(t)$ and the limitation (15), the relative mean square value of the compensation current

$$\frac{I_{C+}^2}{I^2} = \frac{I^2-I_{A+}^2}{I^2} = 1-\frac{1}{k_{A+}^{\Delta P}} = 1-\lambda^2(1+\delta_-^2).$$

At low values of the power factor, the rms value of the compensation current increases. To reduce the power loss of the active filter, it is advisable to use PAF in combination with a passive reactive compensator [9].

**Current filtering for linear stationary load.** If the load is linear and not changeable in time, then in formula (13) $\boldsymbol{i}_H(t) = 0$, and all components of the currents are sinusoidal in the time domain, then the energy processes in the system are completely determined in the basis of symmetric coordinates. In this case, the compensation current vector corresponds to (12), and the sinusoidal inactive current can be completely generated by the reactive compensator in both the symmetric and asymmetric mode of the voltage source [5]. Therefore, in order to minimize the loss of PAF power, it is advisable to distribute the currents of the reactive compensator and the active filter in the integrated substitution circuit (Fig. 1) as follows:

$$\bar{\boldsymbol{i}}_R = \begin{Vmatrix} \dot{I}_A^R \\ \dot{I}_B^R \\ \dot{I}_C^R \end{Vmatrix} = \boldsymbol{F}_0\widetilde{\boldsymbol{i}}_{1N}; \quad \bar{\boldsymbol{i}}_F = \begin{Vmatrix} \dot{I}_A^F \\ \dot{I}_C^F \\ \dot{I}_C^F \end{Vmatrix} = \boldsymbol{F}_0\widetilde{\boldsymbol{i}}_{\pm}.$$

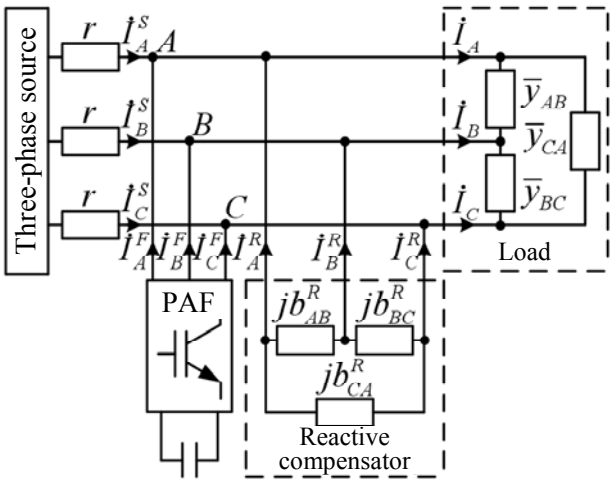


Fig. 1. The substitution circuit

This will reduce the mean square value of the PAF currents to the value

$$I_F = \sqrt{\widetilde{\boldsymbol{i}}_{\pm}\,\hat{}\,\widetilde{\boldsymbol{i}}_{\pm}^*} = \frac{PU_-}{U_+\sqrt{U_+^2+U_-^2}} = \frac{P\delta_-}{U_+\sqrt{1+\delta_-^2}}.$$

We obtain the formulas for the direct calculation of the parameters of the reactive compensator for the generation of the inactive Fryze current in the asymmetric mode of the three-phase source. Let the linear stationary load be characterized by a diagonal matrix of complex conductivities

$$\overline{\boldsymbol{Y}} = \begin{Vmatrix} \overline{y}_{AB} & 0 & 0 \\ 0 & \overline{y}_{BC} & 0 \\ 0 & 0 & \overline{y}_{CA} \end{Vmatrix} = \begin{Vmatrix} g_{AB} & 0 & 0 \\ 0 & g_{BC} & 0 \\ 0 & 0 & g_{CA} \end{Vmatrix} + j \begin{Vmatrix} b^L_{AB} & 0 & 0 \\ 0 & b^L_{BC} & 0 \\ 0 & 0 & b^L_{CA} \end{Vmatrix}.$$

In [5] it was shown that the Ohm law for input vectors of current and voltage is described by an expression in symmetric coordinates

$$\widetilde{\boldsymbol{i}} = \widetilde{\boldsymbol{Y}}\widetilde{\boldsymbol{u}} = \left( \begin{Vmatrix} g_+ & \dot{g} \\ \widetilde{g} & g_+ \end{Vmatrix} + j \begin{Vmatrix} b^L_+ & \dot{b}_L \\ \widetilde{b}_L & b^L_+ \end{Vmatrix}, \right) \widetilde{\boldsymbol{u}}, \qquad (16)$$

where

$g_+ + jb^L_+ = \overline{y}_{AB} + \overline{y}_{BC} + \overline{y}_{CA}$; $\widetilde{g} = (\dot{g})^*$; $\widetilde{b}_L = -(\dot{b}_L)^*$;

$\dot{g} = -(\dot{a}g_{AB} + g_{BC} + \tilde{a}g_{CA})$; $\dot{b}_L = -(\dot{a}b^L_{AB} + b^L_{BC} + \tilde{a}b^L_{CA})$.

Similar parameters of the jet compensator $b^R_+ = b^R_{AB} + b^R_{BC} + b^R_{CA}$; $\dot{b}_R = -\left(\dot{a}b^R_{AB} + b^R_{BC} + \tilde{a}b^R_{CA}\right)$ for realization of the compensation current vector $\widetilde{\boldsymbol{i}}_C = \left\| I^C_+ \quad I^C_+ \right\|^{\wedge}$ are determined by the matrix-vector equation [5]:

$$\begin{Vmatrix} b^R_+ \\ \dot{b}_R \end{Vmatrix} = \frac{j}{U^2_+ - U^2_-} \begin{Vmatrix} U_+ & -U_- \\ -\widetilde{U}_- & U_+ \end{Vmatrix} \begin{Vmatrix} \dot{I}^C_+ \\ -\widetilde{I}^C_- \end{Vmatrix}.$$

We show that for a compensation currents vector in the form of an inactive Fryze current

$$\widetilde{\boldsymbol{i}}_C = \widetilde{\boldsymbol{i}}_{1N} = \widetilde{\boldsymbol{Y}}\widetilde{\boldsymbol{u}} - \widetilde{\boldsymbol{i}}_A = \left( \widetilde{\boldsymbol{Y}} - \frac{P}{U^2_+ + U^2_-} \boldsymbol{I}_{2\times 2} \right) \widetilde{\boldsymbol{u}} \qquad (17)$$

the parameter $b^R_+$. will always be a real number. For this we find the expression for the active power of the given load

$$P = \mathrm{Re}\left(\widetilde{\boldsymbol{i}}^{\wedge}\widetilde{\boldsymbol{u}}^*\right) = \mathrm{Re}\left(\widetilde{\boldsymbol{u}}^{\wedge}\widetilde{\boldsymbol{Y}}^{\wedge}\widetilde{\boldsymbol{u}}^*\right) = (g_+ + \Delta g)(U^2_+ + U^2_+),$$

where $\Delta g = 2U_+ \mathrm{Re}\left(\dot{g}\dot{U}_-\right)/(U^2_+ + U^2_+) = 2\,\mathrm{Re}\left(\dot{\delta}_-\dot{g}\right)/\left(1+\delta^2_-\right)$, and substitute this expression in formula (17) and further in (16).

After the transformation we have

$$\begin{Vmatrix} b^R_+ \\ \dot{b}_R \end{Vmatrix} + \begin{Vmatrix} b^L_+ \\ \dot{b}_L \end{Vmatrix} = \frac{j}{U^2_+ - U^2_-} \begin{Vmatrix} U_+ & -\dot{U}_- \\ -\widetilde{U}_- & U_+ \end{Vmatrix} \begin{Vmatrix} U_+ & -\dot{U}_- \\ -\widetilde{U}_- & U_+ \end{Vmatrix} \begin{Vmatrix} -\Delta g \\ \dot{g} \end{Vmatrix} = \qquad (18)$$

$$= \frac{1}{1-\delta^2_-} \begin{Vmatrix} -2\,\mathrm{Im}\left(\dot{\delta}_-\dot{g}\right) \\ j\left[2\widetilde{\delta}_-\Delta g - \left(1+\delta^2_-\right)\dot{g}\right] \end{Vmatrix} = \begin{Vmatrix} b_+ \\ \dot{b} \end{Vmatrix}.$$

The first coordinates of the vectors of formula (18) are real numbers, which proves the possibility of realizing the reactive compensator of the inactive Fryze current at an arbitrary combination of linear load parameters and an asymmetric source. The reactive conductivities of the compensator are determined from the system of equations (18) in the form

$$\begin{aligned} b^R_{AB} &= \frac{b_+ - 2\,\mathrm{Re}\left(\tilde{a}\dot{b}\right)}{3} - b^L_{AB}; \\ b^R_{BC} &= \frac{b_+ - 2\,\mathrm{Re}\left(\dot{b}\right)}{3} - b^L_{BC}; \\ b^R_{CA} &= \frac{b_+ - 2\,\mathrm{Re}\left(\dot{a}\dot{b}\right)}{3} - b^L_{CA}. \end{aligned} \qquad (19)$$

**Example of simulation of currents filtration.** We consider the hybrid filtration of input currents for a three-wire linear load determined by complex conductivities

$$\overline{Y}_{AB} = \frac{G}{4+j3} = (0.16 - j0.12)G; \quad \overline{Y}_{BC} = 0;$$

$$\overline{Y}_{BC} = \frac{G}{1-j} = (0.5 + j0.5)G,$$

and the asymmetry of the source is characterized by the parameter $\dot{\delta}_- = 0.2j$.

First of all, we define the parameters of the matrix of complex conductivities in symmetric coordinates

$$g_+ = g_{AB} + g_{BC} + g_{CA} = (0.16 + 0.5)G = 0.66G;$$

$$b^L_+ = b^L_{AB} + b^L_{BC} + b^L_{CA} = (-0.12 + 0.5)G = 0.38G;$$

$$\dot{g} = -\left(\dot{a}g_{AB} + g_{BC} + \tilde{a}g_{CA}\right) = (0.33 + 0.294j)G;$$

$$\dot{b}_L = -\left(\dot{a}b^L_{AB} + b^L_{BC} + \tilde{a}b^L_{CA}\right) = (0.19 + 0.537j)G.$$

The values of the matrix of complex conductivities in accordance with (16)

$$\widetilde{\boldsymbol{Y}} = \widetilde{\boldsymbol{G}} + j\widetilde{\boldsymbol{B}}_L = \begin{Vmatrix} 0.66 + 0.38j & -0.207 + 0.484j \\ 0.867 - 0.104j & 0.66 + 0.38j \end{Vmatrix} G.$$

The load current vector

$$\widetilde{\boldsymbol{i}} = \widetilde{\boldsymbol{Y}}\widetilde{\boldsymbol{u}} = \widetilde{\boldsymbol{Y}} \begin{Vmatrix} 1 \\ 0.2j \end{Vmatrix} U_+ = \begin{Vmatrix} 0.563 + 0.339j \\ 0.791 + j0.028 \end{Vmatrix} U_+ G.$$

We determine the parameter

$$\Delta g = \frac{2\,\mathrm{Re}\left(\delta_-\dot{g}\right)}{1+\delta^2_-} = -0.113G$$

and find the Fryze active current vector:

$$\widetilde{\boldsymbol{i}}_A = \frac{P}{U^2_+ + U^2_-}\widetilde{\boldsymbol{u}} = \left(g_+ + \Delta g\right)\widetilde{\boldsymbol{u}} = \begin{Vmatrix} 0.547 \\ 0.109j \end{Vmatrix} U_+ G.$$

The value of the power factor

$$\lambda = I_A / I = \sqrt{\widetilde{\boldsymbol{i}}_A^{\wedge}\widetilde{\boldsymbol{i}}_A^* / \widetilde{\boldsymbol{i}}^{\wedge}\widetilde{\boldsymbol{i}}^*} - = 0.542$$

satisfies the condition (15):

$$\lambda\sqrt{1 + U^2_- / U^2_+} = \lambda\sqrt{1 + \delta^2_-} = 0.553 < 1.$$

Consequently, in accordance with (14), the formation of the active current of a direct sequence will bring savings in energy losses, which is estimated by the coefficient of gain

$$k^{\Delta P}_{A+} = 1/0.553^2 = 3.273.$$

Further by (18) we determine the parameters of the reactive compensator:

$$\begin{Vmatrix} b^R_+ \\ \dot{b}_R \end{Vmatrix} = \begin{Vmatrix} b_+ \\ \dot{b} \end{Vmatrix} - \begin{Vmatrix} b^L_+ \\ \dot{b}_L \end{Vmatrix} = \begin{Vmatrix} -0.137 \\ 0.272 - 0.358j \end{Vmatrix} G - \begin{Vmatrix} b^L_+ \\ \dot{b}_L \end{Vmatrix} = \begin{Vmatrix} -0.517 \\ 0.082 - 0.895j \end{Vmatrix}$$

and form a matrix of complex conductivities with elements of reactive compensation:

$$\widetilde{\boldsymbol{Y}}_R = \widetilde{\boldsymbol{Y}} + j\begin{Vmatrix} b_+^R & \dot{b}_R \\ \widetilde{b}_R & b_+^R \end{Vmatrix} = \begin{Vmatrix} 0.66-0.137j & 0.688+0.566j \\ -0.028-0.022j & -0.66-0.137j \end{Vmatrix} G.$$

The multiplication of this matrix on the vector of the input voltage gives the vector of the input current in the presence of a reactive compensator

$$\widetilde{\boldsymbol{i}}_{SR} = \widetilde{\boldsymbol{Y}}_R \widetilde{\boldsymbol{u}} = \begin{Vmatrix} 0.547 \\ 0.109 \end{Vmatrix} U_+ G,$$

which completely coincides with the previously determined vector of Fryze active current, which indicates the correctness of the calculation of the parameters of the compensator.

Generation of PAF of the vector of current determined by (11)

$$\widetilde{\boldsymbol{i}}_F = \widetilde{\boldsymbol{i}}_{\pm}(g_+ + \Delta g)\begin{Vmatrix} -0.04 \\ 0.2j \end{Vmatrix} U_+ = \begin{Vmatrix} -0.022 \\ 0.109j \end{Vmatrix} \qquad (20)$$

provides the consumption from a three-phase source of active current vector of direct sequence:

$$\widetilde{\boldsymbol{i}}_{SFR} = \widetilde{\boldsymbol{i}}_{A+} = \widetilde{\boldsymbol{i}}_A - \widetilde{\boldsymbol{i}}_{\pm} = \begin{Vmatrix} 0.569 \\ 0 \end{Vmatrix} U_+ G.$$

The joint action of PAF and reactive compensator provides a total compensation current

$$\widetilde{\boldsymbol{i}}_{C+} = \widetilde{\boldsymbol{i}} - \widetilde{\boldsymbol{i}}_{A+} = \begin{Vmatrix} -0.006+0.339j \\ 0.791+j0.028 \end{Vmatrix} U_+ G,$$

thus the relative active value of PAF currents is

$$I_F / I_{C+} = \sqrt{\widetilde{\boldsymbol{i}}_F \widehat{\widetilde{\boldsymbol{i}}}_F^* / \widetilde{\boldsymbol{i}}_{C+} \widehat{\widetilde{\boldsymbol{i}}}_{C+}^*} = 0.129 = 12.9\%.$$

The reactive conductivities of the compensator are calculated by (19):

$$b_{AB}^R = 0.371G; \quad b_{BC}^R = -0.227G;$$

Simulation of currents filtration in the time domain was carried out using the MATLAB model presented in Fig. 2

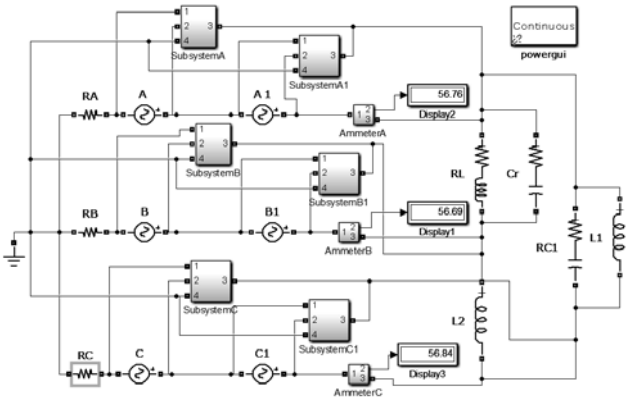


Fig. 2

Parameters of the reactive elements of the compensator for $G$ = 1 S and $\omega = 100\pi$ rad/s are, respectively, $C_{AB}$ = 1.18 mF; $L_{BC}$ = 14.02 mH; $L_{CA}$ = 4.81 mH. Asymmetry of the voltages was realized by a sequential connection of sources of symmetric sinusoidal voltages of 100 V in direct sequence and 20 V in negative sequence with values of initial phases corresponding to parameters $U_+ = 100\sqrt{3}B; \dot{\delta}_- = 0.2j.$ PAF has been simulated by dependent sources of currents controlled by source voltages. In order to generate filter currents in accordance with (11) and (20), the parameters of the dependent sources were taken equal

$$G_+ = -(g_+ + \Delta g)\delta_-^2 = 21.88\times10^{-3} G; G_- = g_+ + \Delta g = 0.547G.$$

The simulation results confirmed all calculated rms currents (Table 1) and the advantages of using a hybrid filter with the proposed currents distribution.

Table 1

| | $I^2$ | $I_{SR}^2$ | $I_{SFR}^2$ | $I_F^2$ |
|---|---|---|---|---|
| Calculated | 31751 | 9333 | 9713 | 370 |
| Measured | 31920 | 9401 | 9712 | 371 |

**Conclusions.** A principle of the distribution of compensating currents between the active filter and the reactive compensator of a three-phase three-wire power supply system with asymmetric sinusoidal voltages is proposed, which provides the consumption of symmetric sinusoidal source currents and minimizes the mean square value of the filter currents.

It is shown that the direct sequence active current provides a gain on the power of losses in accordance with (14) and creates a pulsation of power with amplitude in $2/(1+\delta_-^2)$ times less than the Fryze active current.

The possibility of compensation of inactive Friyze current by reactive elements at an arbitrary combination of linear load parameters and asymmetric sinusoidal source is proved, and direct formulas for calculating the parameters of a reactive compensator for generating Fryze inactive current are obtained.

An example of simulation of currents filtration of linear stationary load showed that the combined application of PAF and reactive compensator with the proposed distribution of currents of compensation ensured reduction of energy losses in the transmission line at 3.273 times, and the relative mean square value of PAF current was 12.9 % of the rms value of the total compensating current.

REFERENCES


***1.*** Fryze S. Active, reactive and apparent power in circuits with nonsinusoidal voltage and current. *Przegląd Elektrotechniczny*, 1931, no.7, 8, pp. 193-203.

***2.*** Shidlovskii A.K., Kuznetsov V.G. *Povysheniye kachestva elektroenergii v elektricheskikh setyakh* [Improving of the power quality in electrical networks]. Kiev: Naukova Dumka Publ., 1985. 268 p.(Rus).

***3.*** Hanzelka Z. *Mitigation of voltage unbalance*. Available at: http://www.leonardo-energy.org/chapter-5-mitigation-voltage-unbalance (accessed 22 May 2016).

***4.*** Czarnecki L.S., Haley P.M. Unbalanced Power in Four-Wire Systems and Its Reactive Compensation. *IEEE Transactions on Power Delivery*, 2015, vol.30, no.1, pp. 53-63. **doi: 10.1109/TPWRD.2014.2314599.**

***5.*** Sirotin Iu.A. Fryze's compensator and Fortescue transformation. *Przegląd Elektrotechniczny*, 2011, no.1, pp. 101-106.

***6.*** Sirotin Iu.A. Non-pulsed mode of supply in a three-phase system at asymmetrical voltage. *Przegląd Elektrotechniczny*, 2013, no.7, pp. 54-58.
***7.*** IEEE Std. 1459-2010. *Definitions for the measurement of electric power quantities under sinusoidal non-sinusoidal, balanced or unbalanced conditions*. **doi: 10.1109/IEEESTD.2010.5439063.**
***8.*** Salmerón Revuelta P., Pérez Litrán S., Prieto Thomas J. *Active power line conditioners design, simulation and implementation for improving power quality*. Elsevier Inc.: Academic Press, 2016. 436 p.
***9.*** Artemenko M.Y., Batrak L.M., Polishchuk S.Y., Mykhalskyi V.M., Shapoval I.A. Reactive compensation of non-active power in hybrid shunt filter of three-phase four-wire system at random load. *Proceedings of 2016 2nd International Conference on Intelligent Energy and Power Systems (IEPS)*. Kiev, 2016. **doi: 10.1109/IEPS.2016.7521863.**
***10.*** Artemenko M.Y., Polishchuk S.Y., Mykhalskyi V.M., Shapoval I.A. Apparent power decompositions of the three-phase power supply system to develop control algorithms of shunt active filter. *Proceedings of the IEEE First Ukraine Conference on Electrical and Computer Engineering (UKRCON)*, 2017, pp. 495-499. **doi: 10.1109/UKRCON.2017.8100537.**

*Received 13.02.2018*

*M.Yu. Artemenko*[1]*, Doctor of Technical Science, Professor,*
*L.M. Batrak*[1]*, Candidate of Technical Science,*
*S.Y. Polishchuk*[2]*, Candidate of Technical Science,*
[1] National Technical University of Ukraine «Igor Sikorsky Kyiv Polytechnic Institute»,
37, Prosp. Peremohy, Kyiv, Ukraine, 03056,
e-mail: artemenko_m_ju@ukr.net, batrakln5@gmail.com
[2] The Institute of Electrodynamics of the NAS of Ukraine,
56, prospekt Peremogy, Kiev-57, 03680, Ukraine,
e-mail: polischuk@ied.org.ua

*How to cite this article:*
Artemenko M.Yu., Batrak L.M., Polishchuk S.Y. Current filtering in a three-phase three-wire power system at asymmetric sinusoidal voltages. *Electrical engineering & electromechanics*, 2018, no.2, pp. 63-68. **doi: 10.20998/2074-272X.2018.2.11.**

UDC 621.311.1 **doi: 10.20998/2074-272X.2018.2.12**

V.G. Kuznetsov, Yu.I. Tugay, V.V. Kuchanskiy,Yu.G. Lyhovyd , V.A. Melnichuk

# THE RESONANT OVERVOLTAGE IN NON-SINUSOIDAL MODE OF MAIN ELECTRIC NETWORK

***Purpose. The resonant overvoltage arises in main electrical networks as a result of random coincidence of some parameters of circuit and its mode and it may exist for a relatively long time. Therefore, the traditional means of limitation of short duration commutation surges are not effective in this case. The study determines conditions of appearance and development of non-sinusoidal mode after switching idle autotransformer to the overhead line of extra high voltage. The purpose of the paper is to choice measures for prevention overvoltage, too. Methodology. The study has used the result of extra high voltage line testing, the methods of electric circuit theory and the simulation in the MATLAB & Simulink package. Results. The simulation model of the extra high voltage transmission line for the study of resonant non-sinusoidal overvoltage is developed. The conditions for the appearance of resonant circuits in the real power line are found and harmonic frequency in which overvoltage arises are obtained. The study proposes using the controlled switching device as a measure to prevent resonance surges and determines the appropriate settings. Originality. The expression for calculation of resonant length of extra high voltage line was derived. The special investigation of processes in the resonant circuit of the extra high voltage transmission line for higher harmonic components of voltage is carried out. The program of switching for control apparatus that prevents non-sinusoidal overvoltage has been developed at the first time. Practical value. The using of the proposed settings of controlled switchgear will prevent the occurrence of hazardous resonant surge on higher harmonic components of voltage.*** References 10, figures 4.

*Key words:* **main electric network, extra high voltage transmission line, resonant overvoltage, nonsinusoidal mode, controlled switching.**

***Резонансные перенапряжения в магистральных электрических сетях возникают вследствие случайного совпадения параметров схемы и режима и могут существовать сравнительно длительное время. Поэтому традиционные средства для их ограничения в данном случае неэффективны. Целью статьи является исследование перенапряжений, возникающих в магистральных электрических сетях на высших гармониках. Для этого было использовано имитационное и математическое моделирование в среде MATLAB&Simulink. Показано, что несинусоидальные искажения возникают при включении линии электропередачи на автотрансформатор в режиме холостого хода. Определены соответствующие частоты. Предложено использование устройства управляемой коммутации для предотвращения перенапряжения данного класса и разработана модель для определения соответствующих настроек.*** Библ. 10, рис. 4.

*Ключевые слова:* **магистральная электрическая сеть, линия электропередачи сверхвысокого напряжения, резонансные перенапряжения, несинусоидальный режим, управляемые коммутации.**

**Introduction.** Trends in the development of modern main electric networks indicate the growth of the role of super high voltage transmission lines (SHVTL) as both system-forming and inter-system. It should be noted that it is the study of overvoltage of this class of lines should be carried out particularly carefully, in particular, taking into account the influence of possible sources of distortion. This is due to the practical absence of an operating reserve of insulation, calculated for extreme parameter values, since such a reserve for extra high voltage has a high cost [1-4]. Experience of operation of AC electric networks indicates that under certain conditions in them there are stable fluctuations of currents and voltages with frequencies other than normal operating frequency. As a result, an analysis of the possibility of overvoltage in the transmission lines of the SHVTL should be performed not only for normal, but for abnormal (asymmetric and non-sinusoidal) modes.

It should also be noted that in the main electric networks of Ukraine the nominal voltage of 750 kV the replacement of the air circuit breakers into the $SF_6$ ones has been carried out. Compared to the air circuit breakers, $SF_6$ ones have certain advantages, the most important of which are the high operation speed and high ability to extinguish the arc, as well as the ability to control the switching process. The objective reason for such a modernization is also that the Ukrainian electrical engineering industry does not manufacture air switches, and in the event of their damage, proper repairs and renewals of the electricity supply becomes a complicated task.

In general, the switching time point of the air circuit breaker commutation is a random variable due to its low speed, which is why it is unrealistic to perform opening and closing at the chosen particular moment. This uncertainty of the initial conditions makes the transient process unpredictable after switching, and the appearance of internal overvoltage is unexpected. During operation it is possible to develop emergency situations, including the emergence of overvoltage in non-sinusoidal modes [2, 5, 6]. The $SF_6$ circuit breaker allows for commutation at any moment of the sinusoidal voltage change, which control device chooses according to the criterion for reducing the negative effects of transients.

**The goal of the work** is establishment of the conditions for the appearance and development of internal overvoltage that arises in main electrical networks on the higher harmonic components, as well as the choice of measures for their prevention. One of these measures is to perform controlled switching according to selected criteria, which allows to reduce the values of overvoltage to the level of effective operation of traditional protective devices, for example, nonlinear overvoltage limiters. To do this, intervals of switching angles of circuit the breaker

were determined, which allows the operation to be carried out without dangerous excess of voltage levels.

**Investigation of resonant overvoltage in SHVTL.** The main direction of previous studies of overvoltage [2-9] using mathematical modeling was focused on the development and application of mathematical models for quantitative results in order to limit overvoltage at the main frequency. They did not consider the physical processes of the development of resonance overvoltage on even harmonic components, although the occurrence of this type of overvoltage is known for a relatively long time. Therefore, it was unclear from the results obtained that the modes or commutations themselves lead to resonant overvoltage on higher harmonics and such studies can not be considered exhaustive.

**Investigation of resonant overvoltage in non-sinusoidal modes of SHVTL.** A prerequisite for the emergence of resonance overvoltage at higher harmonic frequencies is the development of an abnormal non-sinusoidal mode of the SHVTL [2-7]. Typically, sources of distortion of the shape of the curve of the voltage and currents in the transmission of SHV are ferromagnetic shunts of magnetization of transformers. It should be noted that oscillatory processes in circuits with steel require special attention in investigations of modes of main electrical networks, as linear resonances on higher harmonic components, the source of which is nonlinear inductance, and nonlinear resonances, in which this inductance is part of the resonance circuit, are possible [2, 5, 6].

A characteristic non-sinusoidal power transmission mode of the SHV is the connection of an unloaded power autotransformer (AT) to the transmission line. The physics of the process of the appearance of even harmonic components in the SHVTL with connected unloaded AT is due to the periodic change in the inductance of the magnetic shunt when the AC passes through it. This inductance varies with a double frequency in relation to the applied voltage. But it should be noted that although in theory the process of occurrence of overvoltage on even harmonic components is generally known, but the detection of factors of an abnormal mode that affect the multiplicity and duration of overvoltage of this type in practice requires additional research. It is necessary during the design and operation of main electrical networks to have means to check the possibility of not only the necessary but also sufficient conditions for the appearance of abnormal overvoltage and its possible multiplicity.

A sufficient condition for the occurrence of overvoltage on the even harmonic components is the coincidence of the parameters of the elements of the substitution circuit of the SHVTL, at which the frequency of the proper oscillations will be approximated to 100 Hz. For this it is necessary that the input impedance of the line has a capacitive character and was approximately equal to the average value of the inductive resistance of the magnetic shunt of the autotransformer at this frequency. The condition will be fulfilled only at certain lengths of the SHVTL, which can be called resonant.

Main networks operate with a grounded neutral, therefore, at simplified analysis of the resonant power transmission properties in a symmetrical non-sinusoidal mode, an one-line substitution circuit of an equivalent two-terminal network can be used. To find the critical resonance values of the transmission line lengths, the expression in the denominator of the input impedance of the equivalent two-terminal network of the TL, to which the unloaded AT connects, is extrapolated by the polynomial of the third degree and equated to zero:

$$a_1 l - a_2 l^2 - a_3 l^3 - n = 0, \quad (1)$$

where $a_1$, $a_2$, $a_3$ are the coefficients of a polynomial; $l$ is the line length; $n$ is the the number of shunt reactor (SR) groups for charging power of the SHVTL compensation.

To determine the ranges of the resonant length of the line, we vary the parameters of the elements of its substitution circuit within the limits of the existing main electrical networks. Accordingly, we obtain the ranges of changes in the values of the coefficients of the substitution polynomial:

$$a_1 = 0{,}084 \div 0{,}27; \quad (2)$$

$$a_2 = 1{,}996 \cdot 10^{-4} \div 3{,}1 \cdot 10^{-4}; \quad (3)$$

$$a_3 = 2{,}055 \cdot 10^{-7} \div 1{,}55 \cdot 10^{-6}. \quad (4)$$

After determining the ranges of changes in the values of the coefficients of the polynomial (1), we can find the resonance length of the line. Comparison of the results obtained by the expression (1) and by mathematical modeling indicates that extrapolation leads to errors of 3.3 %, which is quite acceptable to perform rapid preliminary analysis of the possible appearance of overvoltage at the higher harmonic components for the SHVTL of given length.

Let us investigate, which is the frequency at which are lengths to expect higher harmonic overvoltage when connecting a unloaded AT. We substitute the marginal value of possible parameters of the expressions (2-4) and get graphs of frequency dependence on the length of the line (Fig. 1) for the relevant parameters.

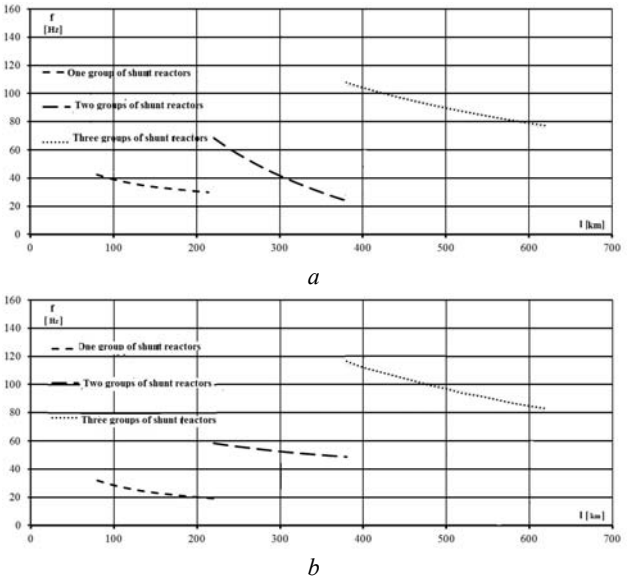


Fig. 1. Resonant length of the SHVTL:
*a* –graphs for lower values of expressions (2-4);
*b* – graphs for upper values of expressions (2-4)

The real graphs of the dependencies of the length of the line and frequency for the corresponding number of SRs will lie between the boundary ones (Fig. 1,*a* and Fig. 1,*b*). One can conclude that the harmonic overvoltage of pairwise multiplicity may arise in the SHVTL when them three groups of SR are installed on them.

**Imitation simulation of non-sinusoidal abnormal modes of SHVTL.** In the study of harmonic overvoltage, each individual factor can not be considered independent. Changing one parameter may lead to another change, in other words, in this case, there is a correlation between both the parameters of the mode of a particular network and its equipment parameters [5]. The presence of this interdependence does not allow for obtaining clear dependencies that could be used to completely correct the analysis of overvoltage on the second harmonic in the main electrical network and the choice of measures for their prevention, and in this case, as the research experience [3] shows, an effective means for modeling such undefined systems is imitation simulation [5].

In this work, an imitation model for the transmission of SHV was developed for implementation in MATLAB/&Simulink [10] environment (Fig. 2). Its peculiarity lies in the presence of models of three groups of SR, since it has been shown above that overvoltage in even harmonics arises at the lengths of lines that are required to compensate their charging power, namely, the same number of SR groups [4-6].

The poles of the circuit breakers in the model are considered separately for each of the phases: each pole is modeled by an ideal circuit breaker. This makes it possible to independently change the closing moments of each of the poles during the simulation. The overhead line is modeled by an equivalent substitution circuit with parameters corresponding to the length of the SHVTL. The electric power system is given by a three-phase voltage source and an equivalent reactance.

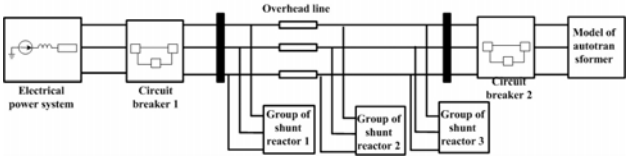


Fig. 2. The imitation model of the SHVTL

Using the model (Fig. 2), in particular, the ranges of angles of switching at which there are dangerous over-voltage are investigated. The research was carried out at a variation of the length of the line from 415 to 525 km. The moment of switching the line to an unloaded AT has changed during the complete period of the sinusoid $\delta \in [0; 360]$ in order to detect critical values for the appearance of resonant overvoltage. It is shown that the necessary condition for the occurrence of overvoltage is the coincidence of two factors: the length of the SHVTL and the angle of switching of the poles of the circuit breaker. It should be noted that the length of the SHVTL is one of the determining factors for overvoltage not only in non-sinusoidal, but also in asymmetrical modes [6-9], although the source of distortion of the mode, and the appearance of the corresponding resonant circuits in these cases are different. But the length of the line is determined when designing the track of the line, and the factor of the possibility of occurrence of overvoltage is not taken into account. Thus, for each type of overvoltage, measures for their warning on this SHVTL have to be developed and implemented separately. An event that will be effective for overvoltage in a non-sinusoidal mode will be ineffective in the asymmetric mode and vice versa [6-8]. In modern main electric networks, structural measures, which are connected with the change of the working circuit and preventing the appearance of an abnormal mode, should be used first of all. Also, if necessary, special settings may be used based on the criterion for reducing the resonance overvoltage of devices that have been installed for another purpose.

As studies have shown, overvoltage at switching of an unloaded AT significantly depends on the time point of its switching on. Thus, overvoltage can be limited by using a controlled switching unit configured to close contacts near the zero value of the idle current of the AT, which prevents the emergence of harmonic components. In general, controlled switching is a means of preventing dangerous transients by executing switching on and/or switching off operations at a predetermined time point.

Consider the choice of criteria for switching control on the example of the $SF_6$ circuit breakers widely used in the main networks of the integrated power system of Ukraine at nominal voltage 750 kV – LTB 800E4 of ABB (Asea Brown Boveri Ltd.). The Company completes circuit breakers of its production by controlled switching devices SwitchSync F236. They are intended for the issuance of commands for closing and/or opening the poles of the circuit breaker at the point of the current or voltage sinewave, which is determined by the conditions of elimination of undesirable development of transients at planned switching of sources of reactive energy, shunt reactors, autotransformers, etc. It should be noted that the recommendations for choosing the switching moment for the criterion of the prevention of overvoltage on the higher harmonic components were not available by this time.

In order to study the influence of the switching angles on the development of transients, an appropriate simulation model was developed (Fig. 3), which, unlike that developed in [6], allows us to investigate switching in both normal and abnormal modes.

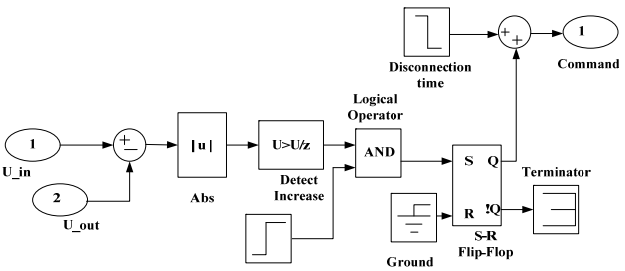


Fig. 3. Imitation model of the controlled switching device Switchsync F236

The block carries out continuous control over the module of current of AT idling. As soon as the curve of the idle current reaches zero value (in the block there are modules where the trend of changing the current value is

determined), the external command is confirmed and the output signal to the circuit breaker is fed, which, in turn, instantly closes its contacts. In the block of the controlled circuit breaker it is possible to set the moment of closing its poles, usually the closing of the contacts occurs as soon as the difference between the voltage of the source and the voltage at the end of the line reaches the minimum value, after the closing time, which is defined in the block itself.

In order to evaluate the effectiveness of the application of controlled switching to prevent overvoltage on the harmonic components of pairwise multiplicity, consider two SHVTL with the same parameters and characteristics. Each of these two lines is switched by its own circuit breaker. The first line is switched by the circuit breaker with the factory setting, and the second one by the circuit breaker with the selected on the criterion of minimizing harmonic overvoltage of dual multiplicity. The moment of switching of the first line falls into the intervals of the angles [0; 140] and [200; 240], and the second one - at intervals of angles [140; 215] and [275; 355]. In Fig. 4 graphs of voltages in the first and second SHVTL after the connection of the unloaded AT are presented (amplitude value for nominal working phase voltage of the TL 750 kV is 612 kV).

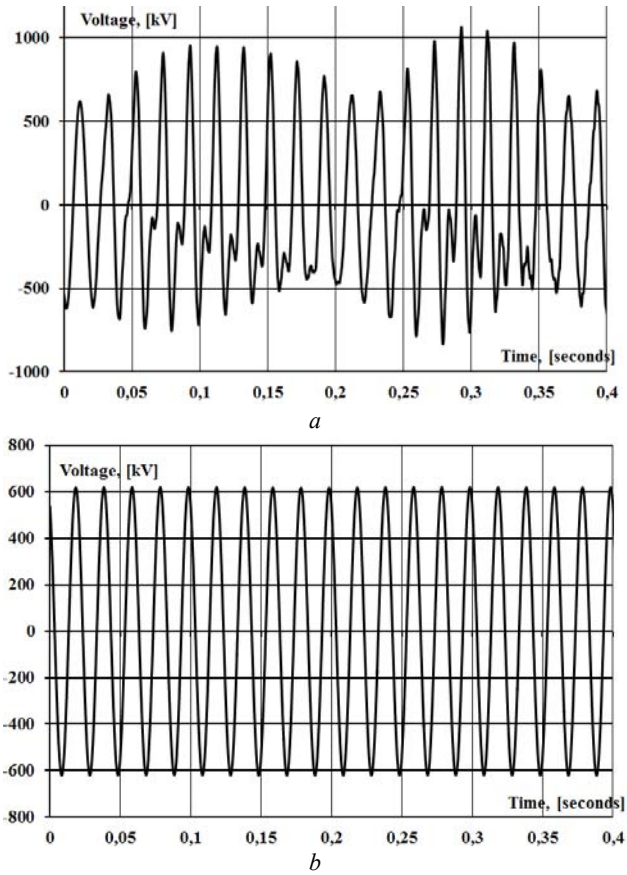


Fig. 4. Voltages of the SHVTL at the device Switchsync F236 settings:
*a* – standard setting;
*b* – setting on the non-resonant switching angles

The switching on or switching of commands supplied to the switch are performed in such a way that the contact closure takes place at a given time point in relation to the phase angle. At present, the accuracy of controlled switching is ± 2 ms, which can not be considered fully sufficient to minimize the currents when switching off the short circuit, but to prevent the emergence of harmonic components in the current of the unloaded AT, such a spread is not critical. As can be seen, the controlled by the criterion of reducing the harmonic overvoltage switching (Fig. 4,*b*) significantly limits their multiplicity compared to the standard setting, when the closing moment can fall into the range of the appearance of even harmonic components in the current of the AT.

**Conclusions.**

1. A necessary condition for the development of overvoltage in the non-sinusoidal modes of main electrical networks is the emergence of an auto-parametric source of nonlinear distortions when the unloaded autotransformer is switched on to the super high voltage transmission line, and the generation of higher harmonic components of even multiplicity characteristic.

2. Resonant adjustment of the electrical circuit of the substitution circuit of the transmission line is a sufficient condition for the overvoltage appearance on the corresponding harmonic component. The defining characteristic of this condition is the length of the transmission line.

3. According to the typical values of parameters of power transmission elements with nominal voltage of 750 kV, an expression was obtained for express analysis of the presence of sufficient conditions for the resonant overvoltage appearance. It is shown that overvoltage on the harmonic components of even multiplicity can be expected if in total three groups of shun reactors are installed in the final substations of the SHVTL.

4. To prevent resonant overvoltage or reduce them to a safe level, it is advisable to use a controlled switching device for $SF_6$ circuit breaker. Intervals of safe switching angles can be determined using developed imitation models of SHVTL.

5. If the switch-on angle of the circuit breaker falls at certain intervals, even if it is adjusted according to another criterion (for example, by the value of the aperiodic component in current), it is possible or completely prevent the occurrence of overvoltage, or to reduce their multiplicity to the levels of effective operation of traditional protective measures.

REFERENCES

***1.*** Kuznetsov V.G., Tugay Yu.I., Shpolyansky O.G. The using of controlled switching to improve the reliability of the EHV transmission lines. *Works of the Institute of Electrodynamics of the National Academy of Sciences of Ukraine*, 2012, no.32, pp. 123-128. (Ukr).

***2.*** Naumkin I., Balabin M., Lavrushenko N., Naumkin R. Simulation of the 500 kV SF6 circuit breaker cutoff process during the unsuccessful three-phase autoreclosing. *Proceedings of International Conference on Power Systems Transients*, Kyoto, Japan, 2011, pp. 5-11.

***3.*** Naumkin I.E. Emergency failures of gas-insulated circuit breakers for switching compensated lines 500-1150 kV. *Electricity*, 2012, no.10, pp. 22-32. (Rus).

***4.*** de Mattos L.M.N., Mendes A.M.P., Tavares M.C., de Lima Filho J.F. Enhanced analysis of oscillatory undamped

overvoltages in transformer energization. *Electric Power Systems Research*, 2016, vol.138, pp. 72-77. **doi: 10.1016/j.epsr.2016.03.034.**

***5.*** Kuznetsov V.G., Tugay Yu.I., Kuchansky V.V. Investigation of the effect of transposition of the extra high voltage transmission line on abnormal overvoltage. *Technical electrodynamics*, 2013, no.6, pp. 51-56. (Ukr).

***6.*** De A., Debnath D., Chakrabarti A. A study on the impact of low-amplitude oscillatory switching transients on grid connected EHV transformer windings in a longitudinal power supply system. *IEEE Transactions on Power Delivery*, 2009, vol.24, no.2, pp. 679-686. **doi: 10.1109/tpwrd.2008.2008417.**

***7.*** Kuznetsov V.G., Tugay Yu.I., Kuchansky V.V. Overvoltages in single-phase mode. *Technical electrodynamics*, 2012, no.2, pp. 40-41. (Ukr).

***8.*** Esmeraldo P.C.V., Amon F J., Carvalho F.M.S., Carvalho A.C.C., Morais S.A. Circuit-breaker requirements for alternative configurations of a 500 kV transmission system. *IEEE Transactions on Power Delivery*, 1999, vol.14, no.1, pp. 169-175. **doi: 10.1109/61.736710.**

***9.*** Morched A., Gustavsen B., Tartibi M. A universal model for accurate calculation of electromagnetic transients on overhead lines and underground cables. *IEEE Transactions on Power Delivery*, 1999, vol.14, no.3, pp. 1032-1038. **doi: 10.1109/61.772350.**

***10.*** Ketabi A., Feuillet R. New approach to harmonic overvoltages reduction during transformer energization via controlled switching. *2009 15th International Conference on Intelligent System Applications to Power Systems*, Curitiba, Brazil, 2009, pp. 1589-1595. **doi: 10.1109/isap.2009.5352837.**

*Received 14.02.2018*

*V.G. Kuznetsov*[1]*, Doctor of Technical Science, Corresponding member of NAS of Ukraine,*
*Yu.I. Tugay*[1]*, Doctor of Technical Science,*
*V.V. Kuchanskiy*[1]*, Candidate of Technical Science,*
*Yu.G. Lyhovyd*[2]*,*
*V.A. Melnichuk*[1]*,*
[1] The Institute of Electrodynamics of the NAS of Ukraine,
56, prospekt Peremogy, Kiev-57, 03680, Ukraine,
phone +380 44 2230450,
e-mail: kuznetsov@ied.org.ua; tugay@ukr.net;
skilldur@ukr.net; yit@ua.fm
[2] UKRENERGO NPC SE,
25, Symona Petliury Str, Kyiv, 01032, Ukraine,
phone +380 44 3662538,
e-mail: re_nim_tor@ukr.net

*How to cite this article:*
Kuznetsov V.G., Tugay Yu.I., Kuchanskiy V.V., Lyhovyd Yu.G., Melnichuk V.A. The resonant overvoltage in non-sinusoidal mode of main electric network. *Electrical engineering & electromechanics*, 2018, no.2, pp. 69-73. **doi: 10.20998/2074-272X.2018.2.12.**

**Матеріали приймаються за адресою:**
**Кафедра "Електричні апарати", НТУ "ХПИ", вул. Кирпичова, 21, м. Харків, 61002, Україна**
**Електронні варіанти матеріалів по e-mail: a.m.grechko@gmail.com**

**Довідки за телефонами: +38 050 653 49 82 Клименко Борис Володимирович**
**+38 067 359 46 96 Гречко Олександр Михайлович**